

# Stress Analysis of Bolted Flange Joints with Different Shell Connections

by

Mohammad CHOULAEI

THESIS PRESENTED TO ÉCOLE DE TECHNOLOGIE SUPÉRIEURE IN  
PARTIAL FULFILLMENT FOR A MASTER'S DEGREE WITH THESIS IN  
MECHANICAL ENGINEERING  
M.A.Sc.

MONTREAL, AUGUST 17, 2022

ÉCOLE DE TECHNOLOGIE SUPÉRIEURE  
UNIVERSITÉ DU QUÉBEC



Mohammad Choulaei, 2022



This Creative Commons license allows readers to download this work and share it with others as long as the author is credited. The content of this work can't be modified in any way or used commercially.

**BOARD OF EXAMINERS  
THIS THESIS HAS BEEN EVALUATED  
BY THE FOLLOWING BOARD OF EXAMINERS**

Mr. Abdel-Hakim Bouzid, Thesis Supervisor  
Department of Mechanical Engineering, École de technologie supérieure

Mr. Lucas Hof, President of the Board of Examiners  
Department of Mechanical Engineering, École de technologie supérieure

Mr. Anh Dung Ngo, Member of the jury  
Department of Mechanical Engineering, École de technologie supérieure

**THIS THESIS WAS PRESENTED AND DEFENDED  
IN THE PRESENCE OF A BOARD OF EXAMINERS AND PUBLIC  
ON AUGUST 17, 2022  
AT ÉCOLE DE TECHNOLOGIE SUPÉRIEURE**



## **ACKNOWLEDGMENT**

Dr. Abdel-Hakim Bouzid, my advisor, deserves my sincerest appreciation. I was blessed to have an adviser who offered me the flexibility to explore on my own while still guiding me in the proper direction. Throughout my master's study, I am grateful for his patience, wisdom, inspiration, and unwavering support.

Special thanks to my parents, Khadijeh and Parviz, for their patience, and encouragement through the years.

I would really like to convey my heartfelt appreciation to my spouse, Negar, for her assistance and support.

Thank you, my beloved daughter, Nellie Rose, for all the time I could have spent with you but did not.



# **Analyse des contraintes des joints à brides boulonnées avec différentes connexions de coque**

Mohammad CHOULAEI

## **RESUME**

Les composants de tuyauterie des récipients sous pression sont largement utilisés dans une variété d'industries, y compris le pétrole et le gaz, l'énergie nucléaire et les centrales électriques. En raison des conditions de haute pression et de haute température, le problème le plus critique concernant leurs applications est la sécurité de fonctionnement. Différentes coques sont reliées de manière permanente par des joints soudés ou temporairement par des raccords à brides boulonnées, également appelés assemblages à brides boulonnées, dans les récipients sous pression et les systèmes de tuyauterie. Une tâche critique dans le processus de conception consiste à déterminer le niveau de concentration de contraintes au point où la coque rencontre l'anneau de la bride. L'une des tâches les plus difficiles consiste à déterminer l'intégrité de cette jonction. Dans le processus de conception, il est avantageux d'employer des techniques d'analyse analytique et numérique par éléments finis pour modéliser le comportement général de l'assemblage à brides boulonnées sous diverses conditions de chargement. Les résultats générés par la solution analytique seront utilisés et validés la technique des éléments finis. De plus, les performances de diverses configurations de raccordement à bride ne sont pas bien comprises. Cependant, la conception actuelle des brides du code ASME BPV n'intègre pas de critères de fuite ni d'analyse de flexibilité pour fournir une évaluation précise des différents paramètres. L'objectif de cette recherche est d'évaluer l'intégrité et l'étanchéité de différents types de coques reliées à la couronne de la bride.

Cette étude examine divers paramètres tels que la rotation de la bride, la contrainte de contact sur le joint et la répartition des contraintes à la jonction bride-coque en utilisant plusieurs théories de coque selon la forme et la géométrie. Plusieurs formes de connexions de coque ont été comparées, notamment cylindriques, sphériques, bombées et coniques. Toutes les coquilles sont directement reliées à l'anneau de bride à face surélevée sans la présence de la collerette.

## VIII

De plus, les connexions de coque ont été simulées à l'aide du logiciel d'éléments finis à usage général pour soutenir la méthode analytique et valider l'étude. Un autre objectif important de cette étude est d'examiner l'influence des dimensions des brides sur les résultats en examinant différentes tailles d'assemblage à brides boulonnées. À cette fin, trois tailles différentes de la bride, à savoir NPS 26, 48 et 60 ASME B16.47 series A, ont été modélisées et simulées par le logiciel ANSYS pour faire une comparaison entre les résultats numériques et analytiques. Il convient de noter que les résultats numériques et analytiques sont très concordants.

**Mots-clés:** Assemblages à brides boulonnées, assemblages de coques, analyse des contraintes, rotation des brides, contraintes aux jonctions et sur le joint

## **Stress analysis of bolted flange joints with different shell connections**

Mohammad CHOULAEI

### **ABSTRACT**

Pressure vessel piping components are widely utilized in a variety of industries, including oil and gas, as well as nuclear power and power plants. Due to the high-pressure and high-temperature conditions, the most critical issue concerning their applications is operational safety. Different shells are joined permanently by welded joints or temporarily by bolted flange connections, also known as bolted flange joints, in pressure vessels and piping systems. A critical task in the design process is to determine the stress concentration level at the point where the shell meets the flange ring. One of the most challenging tasks is the determination of the flange integrity of this junction. In the design process, it is beneficial to employ analytical and finite element techniques to model the general behavior of the bolted flange joint under various loading conditions. The results generated from the analytical solution will be validated by the finite element technique. Furthermore, the performance of various flange connection configurations is not comprehended well. However, the present ASME BPV Code flange design does not incorporate the leakage criteria or flexibility analysis to provide an accurate assessment of various parameters. The purpose of this research is to assess the integrity and leakage tightness of various types of shells connected to the flange ring.

This investigation examines various parameters such as flange rotation, gasket contact stress, and stress distribution at the flange-shell junction using multiple shell theories depending on the form and geometry. Several forms of shell connections have been compared together, including cylindrical, spherical, dished, and conical. All shells are directly connected to a raised-face flange ring without a hub. Furthermore, the shell connections have been simulated using a general-purpose finite element software to support the analytical method and validate the study. Another significant purpose of this study is to look into the influence of flange dimensions on the results by examining various sizes of flange connections. For this purpose, three different sizes of the flange, namely NPS 26, 48, and 60 ASME B16.47 series A, were

modeled and simulated by the ANSYS software to make comparison between numerical and analytical results. It is worth noting that the numerical and analytical results compared well.

**Keywords:** Bolted flange joints, shell connections, stress analysis, flange rotation, flange and shell stresses

## TABLE OF CONTENTS

	Page
INTRODUCTION .....	1
CHAPTER 1 LITERATURE REVIEW .....	5
1.1 Introduction.....	5
1.2 Bolted Flange Joints.....	5
1.3 Analytical Studies .....	8
1.3.1 The Theories of Shells of Revolution .....	9
1.3.1.1 Membrane Theory.....	9
1.3.1.2 Bending Moment Theory .....	11
1.3.2 Beam on the Elastic Foundation .....	15
1.3.3 Plate Theories.....	17
1.3.4 Discontinuity Analysis.....	20
1.4 Design Codes, Standards and the other References.....	21
1.5 Numerical Finite Element Studies .....	26
1.6 Experimental Research .....	33
1.7 Research Project Objectives .....	39
CHAPTER 2 FEM MODELLING AND STRESS ANALYSIS METHODOLOGY ....	41
2.1 Introduction.....	41
2.2 Proposed Model of Bolted Flange Joint.....	41
2.3 Analytical Method .....	42
2.3.1 Bolt Load .....	44
2.3.2 Gasket Modelling.....	45
2.3.3 Flange Ring.....	46
2.3.4 Shell Stress Analysis.....	47
2.3.4.1 Cylindrical Shell .....	48
2.3.4.2 Spherical Shell .....	50
2.3.4.3 Dished Shell.....	51
2.3.4.4 Conical Shell.....	54
2.4 Finite Element Modelling .....	56
CHAPTER 3 GASKET CONTACT STRESS AND TIGHTNESS .....	61
3.1 Introduction.....	61
3.2 Flange Rotation.....	61
3.3 Gasket Contact Stress .....	65
3.4 Tightness Criteria of Gasket .....	69
CHAPTER 4 EFFECT OF SHELL GEOMETRY ON THE STRESSES DISTRIBUTION AT THE JUNCTION WITH BOLTED FLANGE CONNECTIONS .....	71
4.1 Abstract.....	71

4.2	Introduction .....	72
4.3	Analytical Methods .....	75
4.3.1	Bolt Stiffness .....	77
4.3.2	Gasket Modeling .....	78
4.3.3	Flange Ring .....	79
4.3.4	Shell Stress Analysis .....	80
4.3.4.1	Cylindrical shell .....	80
4.3.4.2	Spherical Shell .....	83
4.3.4.3	Dished Shell .....	84
4.3.4.4	Conical Shell .....	86
4.4	Finite Element Modelling .....	88
4.5	Result and Discussion .....	90
4.5.1	Flange Rotation .....	90
4.5.2	Stress Distribution in the Different Shells .....	95
4.6	Conclusion .....	112
	CONCLUSION .....	113
	RECOMMENDATIONS .....	114
	BIBLIOGRAPHY .....	117

## LIST OF TABLES

		Page
Table 2.1	FEM model properties .....	58
Table 3.1	The analytical and numerical results of the flange rotation for various shell connections in bolt-up and pressurization .....	65
Table 4.1	Geometry properties and input data of the FEM model for different flange sizes.....	89
Table 4.2	The analytical and numerical results of the flange rotation of the various shell connections in bolt-up and pressurization .....	94



## LIST OF FIGURES

		Page
Figure 0.1	Flange-to-shell connections: a) cylindrical, b) conical, c) dished, and d) spherical. ....	2
Figure 1.1	Bolted flange joint model.....	6
Figure 1.2	Flange rotation schematic .....	7
Figure 1.3	Various types of bolted flange joint configurations.....	8
Figure 1.4	Surface of revolution model.....	10
Figure 1.5	a) Egg-shaped shell of revolution, and b) variation of membrane stresses over the three regions of the eggshell .....	11
Figure 1.6	Shell-to-conical head connection .....	12
Figure 1.7	Free body diagram of the shell of revolution in bending moment theory .	12
Figure 1.8	Element of the shell with acting forces, stress resultants and couples.....	13
Figure 1.9	Shell parameters of a) conical, b) ellipsoidal, and c) spherical heads .....	14
Figure 1.10	Multiple stages egg-shape pressure vessel.....	14
Figure 1.11	Various applications of beam on elastic foundation theory .....	16
Figure 1.12	Beam on elastic foundation theory .....	16
Figure 1.13	Two plate theories: a) Waters and Taylor model, and b) Timoshenko model.....	17
Figure 1.14	Analytical model of integrated bolted flange joint .....	18
Figure 1.15	Acting forces and moments on the circular plate with a central hole .....	19
Figure 1.16	FEM modeling and results for the flange rotation and leakage rate .....	20
Figure 1.17	Causes of discontinuities at the shell of the pressure vessel .....	21
Figure 1.18	Various flange-to-shell connections .....	22
Figure 1.19	Principal dimensions of typical heads.....	23

Figure 1.20	Working pressure by flange classes .....	24
Figure 1.21	Dimensional flange characteristics based on NPS .....	25
Figure 1.22	Bolt dimensions based on the nominal size .....	26
Figure 1.23	Spring modeling and finite element simulation of the flange.....	27
Figure 1.24	a) 3D model and meshing, and b) stress variation for combined loading..	28
Figure 1.25	a) Bolted flange model, b) 3D finite element model, and c) gasket displacement .....	29
Figure 1.26	3D finite element model of bolted flange joint.....	29
Figure 1.27	Finite element mesh of bolted flange joint .....	30
Figure 1.28	Characteristics of a) asbestos, b) graphite, and c) PTFE based gaskets ....	31
Figure 1.29	Flange rotation and axial bolt force variation vs. internal pressure .....	31
Figure 1.30	Finite element model of L-shape bolted flange joint.....	32
Figure 1.31	Contour graphs of the axial stresses in the bolt and the A through E locations .....	33
Figure 1.32	Normalized axial stresses and the plastic strains vs. tensile shell segment force .....	33
Figure 1.33	Experimental set-up of bolted flange joint.....	34
Figure 1.34	Experimental set-up performed by Kobayashi .....	35
Figure 1.35	Bolted joint modeling, bolt force reduction and leak rate in creep conditions.....	36
Figure 1.36	FEM model for the bolted flange joint .....	37
Figure 1.37	Positioning of TekScan sensors and strain gauges .....	38
Figure 1.38	a) Measured contact pressure immediately after bolt tightening, and b) measured contact pressure 10 minutes after bolt tightening for the flat face flange.....	38
Figure 2.1	Bolted flange model.....	43
Figure 2.2	Bolt parameters .....	45

Figure 2.3	Nonlinear unloading–loading curve of gasket .....	46
Figure 2.4	Flange ring and cylindrical shell.....	48
Figure 2.5	Flange ring and spherical shell .....	51
Figure 2.6	Flange ring and dished shell .....	53
Figure 2.7	Flange ring and conical shell .....	56
Figure 2.8	FEM bolted flange joint model in ANSYS.....	59
Figure 3.1	Flange rotation for shell connections during bolt-up (NPS 26 class 300).....	62
Figure 3.2	Flange rotation for shell connections during pressurization (NPS 26 class 300).....	62
Figure 3.3	Flange rotation for shell connections during bolt-up (NPS 48 class 300).....	63
Figure 3.4	Flange rotation for shell connections during pressurization (NPS 48 class 300).....	63
Figure 3.5	Flange rotation for shell connections during bolt-up (NPS 60 class 300).....	64
Figure 3.6	Flange rotation for shell connections during pressurization (NPS 60 class 300).....	64
Figure 3.7	Gasket stress for shell connections during bolt-up (NPS 26 class 300).....	66
Figure 3.8	Gasket stress for shell connections during pressurization (NPS 26 class 300).....	67
Figure 3.9	Gasket stress for shell connections during bolt-up (NPS 48 class 300).....	67
Figure 3.10	Gasket stress for shell connections during pressurization (NPS 48 class 300).....	68
Figure 3.11	Gasket stress for shell connections during bolt-up (NPS 60 class 300).....	68
Figure 3.12	Gasket stress for shell connections during pressurization (NPS 60 class 300).....	69

Figure 4.1	Bolted flange model.....	77
Figure 4.2	Unloading-loading curve for the implemented gasket.....	78
Figure 4.3	Flange rings and different shell types: .....	81
Figure 4.4	FEM bolted flange joint model in ANSYS.....	88
Figure 4.5	Flange rotation of shell connections during bolt-up (NPS 26 class 300).....	91
Figure 4.6	Flange rotation of shell connections during pressurization (NPS 26 class 300).....	92
Figure 4.7	Flange rotation of shell connections during bolt-up (NPS 48 class 300).....	92
Figure 4.8	Flange rotation of shell connections during pressurization (NPS 48 class 300).....	93
Figure 4.9	Flange rotation of shell connections during bolt-up (NPS 60 class 300).....	93
Figure 4.10	Flange rotation of shell connections during pressurization (NPS 60 class 300).....	94
Figure 4.11	Tangential stress at IR of shell connections during bolt-up (NPS 26 class 300).....	96
Figure 4.12	Tangential stress at IR of shell connections during bolt-up (NPS 48 class 300).....	96
Figure 4.13	Tangential stress at IR of shell connections during bolt-up (NPS 60 class 300).....	97
Figure 4.14	Tangential stress at OR of shell connections during bolt-up (NPS 26 class 300).....	97
Figure 4.15	Tangential stress at OR of shell connections during bolt-up (NPS 48 class 300).....	98
Figure 4.16	Tangential stress at OR of shell connections during bolt-up (NPS 60 class 300).....	98
Figure 4.17	Tangential stress at IR of shell connections during pressurization (NPS 26 class 300).....	99

Figure 4.18 Tangential stress at IR of shell connections during pressurization (NPS 48 class 300).....99

Figure 4.19 Tangential stress at IR of shell connections during pressurization (NPS 60 class 300).....100

Figure 4.20 Tangential stress at OR of shell connections during pressurization (NPS 26 class 300).....100

Figure 4.21 Tangential stress at OR of shell connections during pressurization (NPS 48 class 300).....101

Figure 4.22 Tangential stress at OR of shell connections during pressurization (NPS 60 class 300).....101

Figure 4.23 Longitudinal stress at IR of shell connections during bolt-up (NPS 26 class 300).....103

Figure 4.24 Longitudinal stress at IR of shell connections during bolt-up (NPS 48 class 300).....103

Figure 4.25 Longitudinal stress at IR of shell connections during bolt-up (NPS 60 class 300).....104

Figure 4.26 Longitudinal stress at OR of shell connections during bolt-up (NPS 26 class 300).....104

Figure 4.27 Longitudinal stress at OR of shell connections during bolt-up (NPS 48 class 300).....105

Figure 4.28 Longitudinal stress at OR of shell connections during bolt-up (NPS 60 class 300).....105

Figure 4.29 Longitudinal stress at IR of shell connections during pressurization (NPS 26 class 300).....106

Figure 4.30 Longitudinal stress at IR of shell connections during pressurization (NPS 48 class 300).....106

Figure 4.31 Longitudinal stress at IR of shell connections during pressurization (NPS 60 class 300).....107

Figure 4.32 Longitudinal stress at OR of shell connections during pressurization (NPS 26 class 300).....107

Figure 4.33 Longitudinal stress at OR of shell connections during pressurization (NPS 48 class 300).....108

Figure 4.34	Longitudinal stress at OR of shell connections during pressurization (NPS 60 class 300).....	108
Figure 4.35	Comparison of maximum stresses of shells during bolt-up (NPS 26 class 300).....	109
Figure 4.36	Comparison of maximum stresses of shells during bolt-up (NPS 48 class 300).....	110
Figure 4.37	Comparison of maximum stresses of shells during bolt-up (NPS 60 class 300).....	110
Figure 4.38	Comparison of maximum stresses of shells during pressurization (NPS 26 class 300).....	111
Figure 4.39	Comparison of maximum stresses of shells during pressurization (NPS 48 class 300).....	111
Figure 4.40	Comparison of maximum stresses of shells during pressurization (NPS 60 class 300).....	112

## LIST OF ABBREVIATIONS

ASME	American Society of Mechanical Engineers
BPVC	Boiler and Pressure Vessel Code
CPU	Central processing unit
FEM	Finite element method
IR	Inner surface
NPS	Nominal pipe sizes
OR	Outer surface
PTFE	Polytetrafluoroethylene
ROTT	Room Temperature Tightness Test



## LIST OF SYMBOLS

$\alpha$	Cone angle (rad)
$\beta_s$	Shell flexural rigidity ( $\text{mm}^{-1}$ )
$\theta_f$	Flange rotation (deg)
$\nu$	Poisson's ratio
$\sigma_l, \sigma_t$	Longitudinal and tangential stresses (MPa)
$A_r$	Root stress area of the bolt ( $\text{mm}^2$ )
$A_s$	Tensile stress area of the bolt ( $\text{mm}^2$ )
$A_p$	Pressurized area ( $\text{mm}^2$ )
$D_b$	Nominal diameter of the bolt (mm)
$E$	Young's modulus (MPa)
$E_g$	Gasket compression modulus (MPa)
$H_B$	Bolt force (N)
$H_G$	Gasket force (N)
$k$	Ratio of outside to inside diameter of flange
$K$	stiffness, (N/mm)
$M_f$	Twisting moment of flange ring (N.mm/mm)
$M_\theta, M_\phi, M_s$	Bending moments around $\theta, \phi, s$ directions respectively (N.mm/mm)
$N_\theta, N_\phi, N_s$	Normal forces in $\theta, \phi, s$ directions (N/mm)
$p_b$	Pitch of the bolt threads (mm)
$P$	Internal pressure (MPa)

$Q$	Shear force (N/mm)
$r_b$	Bolt circle radius (mm)
$r_g$	Average radius of gasket (mm)
$R$	Internal radius of flange (mm)
$S_g$	Gasket stress (MPa)
$t$	thickness (mm)
$t_f$	Flange thickness (mm)
$U$	axial displacement (mm)
$w$	Radial displacement (mm)
$w_{M_0}, w_p, w_{Q_0}$	Displacement due to edge moment, internal pressure, and edge load (at the junction) mm
$y_s$	Yield stress (MPa)
$Y$	Factor involving K

## INTRODUCTION

Bolted flange joints are widely used in various industries, particularly oil and gas, as well as industries related to power and nuclear facilities, food processing, and so on. Because they are used to connect pressurized components, bolted flange joints must be comprehensively evaluated in terms of their integrity and their mechanical behavior under operating conditions. Generally, a bolted flange joint consists of a pipe (or the head of a pressure vessel), bolts, a flange body, and a gasket. The gasket is trapped between the flanges and prevents fluid from leaking out from the pipe or the pressure vessel. Initial tightening of the bolts may provide the required load before pressurization to ensure the integrity of the bolted flange joint. Any failure in the bolted joint can have drastic consequences on the environment, health and safety, and industrial installations. For this reason, the research conducted for this thesis investigated the mechanical integrity of bolted flange joints to determine their safe use under real operating conditions. The simplest method to achieve this goal was to use computational modeling to simulate various realistic load conditions. The results of this investigation could reduce operating costs by diminishing the likelihood of an unplanned shutdown and preventing negative environmental impacts.

The four most common shell connections listed below and shown in Figure 0.1 have a wide range of applications and are connected to the flange ring of bolted flange connections in different industry applications:

- cylindrical,
- spherical,
- conical, and
- dished.

Due to the discontinuity at the junction, bolted flange joints are susceptible to failure in the presence of high stresses and unexpected deformation. Therefore, a stress analysis of bolted flange joints is necessary to determine the integrity of the complex structure, particularly at the junction. It should be noted that each type of head connection creates a unique set of stress,

flange rotation, and gasket reaction conditions. Furthermore, the shape and geometry of the flange ring and the shell that form the junction have a considerable impact on the load redistributions and high stresses created in the bolted joint.

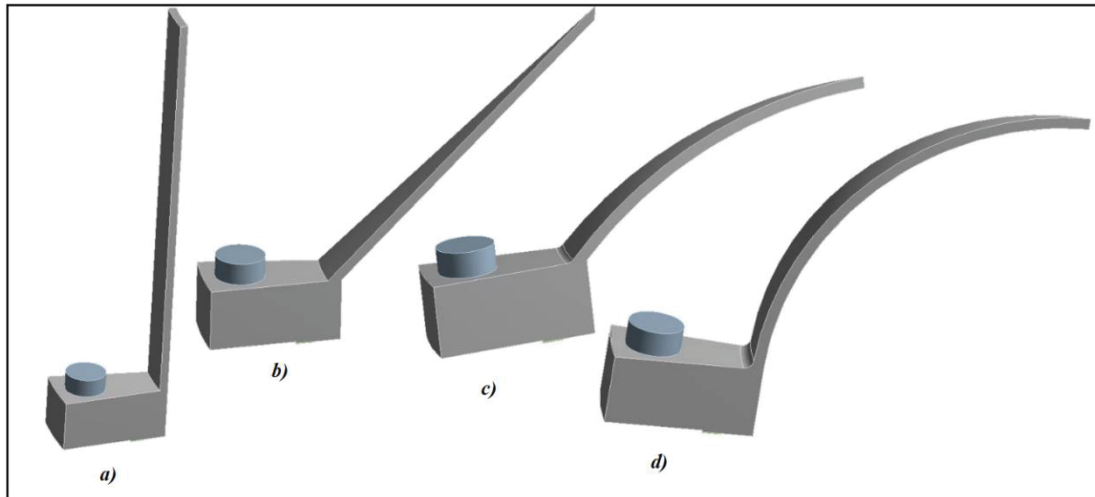


Figure 0.1 Flange-to-shell connections: a) cylindrical, b) conical, c) dished, and d) spherical.

Shell stresses occurring during the bolt-up and pressurization stages are split into longitudinal and tangential stress components. To these stresses one can superpose the thermal stresses that occur during high temperature operating conditions. In the case of narrow shell thickness, the radial stress component may be negligible. The highest values of stress often occur at the junction and as the distance from the discontinuity location increases, the stress values gradually decrease. Of particular interest is the amount of stress at the inner and outer surfaces of the shell. Another essential issue to consider in the stress analysis of bolted flange joints is the contact stress distribution and its relationship to flange rotation.

To achieve a safe design of the bolted flange joints, all the acting forces and moments on the flange must be modeled in the presence of the different shell connections listed above to determine a precise estimate of the stresses involved. Furthermore, accurate flange rotation prediction, bolt load change, and gasket contact pressure during operation are also critical design factors.

The rotation of the flange has a significant impact on gasket integrity and leakage. Excessive flange rotation can cause high stresses that produce sheet gasket rupture failure or gasket lift-off. On the one hand, bolt stress controls flange rotation, and a high value of it may cause the above-mentioned repercussions on the gaskets. On the other hand, small values of bolt stress may not provide the adequate sealing required for the bolted flange joint application. As a result, it is critical to establish a flange rotation limit, which has been set by the American Society of Mechanical Engineers (ASME) to 0.3 degrees for non-hubbed flanges and 0.2 degrees for hubbed flanges. The amount of flange rotation for four different types of shell connections used with three different flange sizes is investigated herein.

Gaskets play an important role in sealing and maintaining tightness in bolted flange joints (Diany, Bouzid & Derenne, 2005). To prevent fluid discharge, the bolt force compresses the gasket located between two flanges, which causes leak paths at the interface to close. The contact stress generated at the contact surfaces between the gasket and the flange body is not uniform across the gasket width due to the rotational flexibility of the flange ring. Instead, it increases gradually from the inner to the outer radius. In essence, the gasket is used to form a static seal between two flanges and to keep the seal in place during operation, even if the internal pressure and loads change (Do, 2012).

Generally, gaskets are available in a variety of materials, including metallic and nonmetallic, as described in ASME B16.20 and ASME B16.21, respectively. However, they can also be made of a mixture of the two. In terms of mechanical behavior, to obtain more reliable results, the nonlinear loading and unloading characteristics were taken into consideration in the numerical finite element analysis conducted for this thesis, while in the analytical model the gasket was modeled as a linear spring.

This introduction provided an overview of the characteristics and challenges of bolted flange joints. It also described the context and presented general information about the research conducted for this thesis in order to fully understand the problem.

Chapter 1 presents the results from the literature review that was conducted to help determine this project's objectives.

In Chapter 2, the effect of distinct shell connections on bolted flange joint characteristics is discussed. It should be noted that the results of Chapter 2, which form a cornerstone of this investigation, were presented at the 2021 ASME International Mechanical Engineering Congress and Exposition (IMECE 2021) as Technical Paper No IMECE2021-72063. The conference paper has been extended and supplemented by the addition of different flange sizes, and will be submitted to the Journal of Pressure Vessel Technology as a journal paper.

In Chapter 3, the results of the gasket contact stress and flange rotation for four different types of heads and three different flange sizes (NPS 26, 48, and 60) are provided.

In Chapter 4, the complete study, including the methodology and the results, of the effect of four different shell connections and three sizes of flanges on bolted flange joint characteristics is presented in the format of a journal paper, which has been submitted to the Journal of Pressure Vessel Technology.

Finally, in the conclusion, the key results of the research conducted for this thesis are presented and discussed, along with several recommendations for potential future research in this field of study.

## CHAPTER 1

### LITERATURE REVIEW

#### 1.1 Introduction

Most research on bolted flanged joints concentrates on the leakage behavior of gaskets under various operating conditions, such as high pressure and high temperature. Moreover, most studies pertain to different metallic gaskets and very few focus on nonmetallic gaskets. For this chapter, an extensive review of current scholarly articles and publications was conducted, and the results of this literature review are divided into the following sections:

- bolted flange joints,
- analytical studies,
- numerical studies, and
- experimental research.

This chapter presents an overview of the literature on bolted flange joints, as well as materials and corresponding codes and standards. However, before looking at these standards in more depth, particularly the ASME Boiler and Pressure Vessel Code (BPVC), Section VIII, it is important to first introduce the many features of bolted flange joints. After that, the analytical investigations on bolted flange joints are discussed, followed by an in-depth review of codes, standards, and other references. Next, studies on the use of numerical finite element models to simulate the behavior of the flanges are presented. Finally, experimental investigations and test methodologies are discussed, and the objectives of this research project are presented.

#### 1.2 Bolted Flange Joints

Bolted flange joints have a wide range of applications in piping and pressure vessels due to their ability to produce reliable connections when assembling multiple pressure vessels and

pipng components (Figure 1.1). Moreover, they are an excellent alternative to welding because they can be rapidly dismantled, removed, and reassembled for inspection, maintenance, and replacement (Bouzid & Derenne, 2001). The flanges (with or without a hub), gasket, and bolts constitute the bolted flange joint. These components form an integrated complex structure that allows two pressure vessels and pipe components to be connected. Despite their substantial capacity to provide reliable connections, bolted flange joints face various challenges during operation.

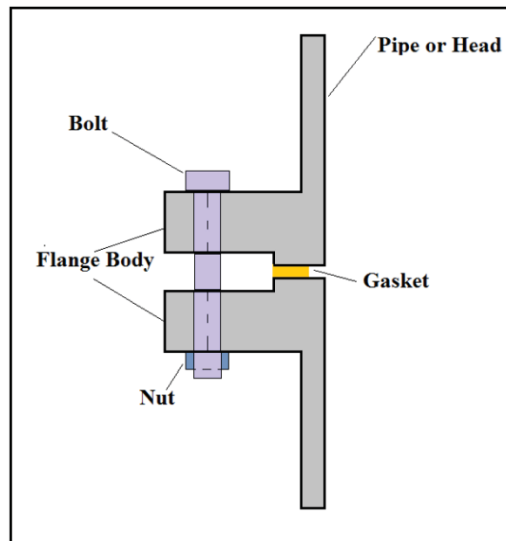


Figure 1.1 Bolted flange joint model

The possibility of leakage due to the effects of high pressure and high temperature loading is a major concern (Figure 1.2) for bolted flange joints. During operation, there are numerous potential causes for failure and rupture, including high stresses, stress concentration, improper gasket selection, and so on. The gasket's nonlinear behavior and its tendency to become permanently deformed during loading and unloading cycles is another complexity that must be considered when bolted flange joint failures are investigated. The effects of the bolt preload and internal pressure on flange rotation and changes in the amount of contact stress have been explored in several studies. Excessive flange rotation, as shown in Figure 1.2, can alter the contact stress between the flange's raised face and the gasket, which can lead to leakage. Excessive rotation may also cause high localized stresses, thereby resulting in gasket crushing and failure or gasket lift-off in the presence of a guide ring, such as that found in spiral wound

gaskets. As a result, the ASME code restricts non-hubbed flange rotations to 0.3 degrees and hubbed flanges to 0.2 degrees (Choulai & Bouzid, 2021).

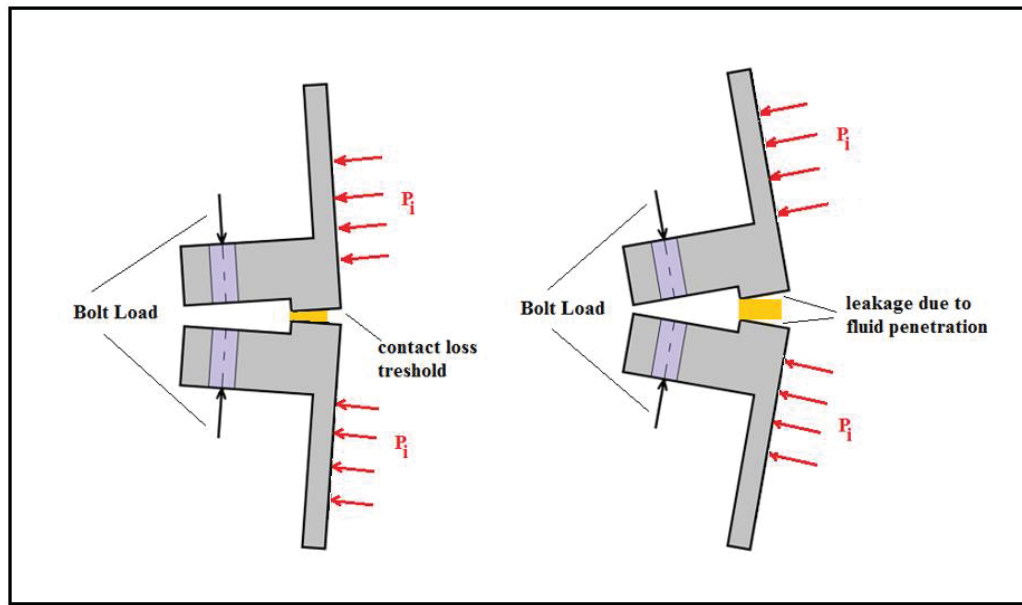


Figure 1.2 Flange rotation schematic

Bolted flange joints may have various configurations, depending on their applications. They may be distinguished by the diversity of the flange types, as well as by the gaskets. To seat the sealing gasket material, different types of flange faces are used as contact surfaces, such as raised faces and flat faces. ASME B16.5 and B16.47 provide an excellent reference for different types of flanges and fittings, based on size and class, that can be specified by the operating pressure and temperature. Materials, dimensions, tolerances, and fabrication of different types of metallic and nonmetallic gaskets are addressed in ASME B16.20 and B16.21, respectively. Additionally, ASME B18.2.1 covers a diverse range of bolts used in bolted flange joints. Figure 1.3 shows a few types of bolted flange joints (with or without hub) used with different flange facings and gasket types.

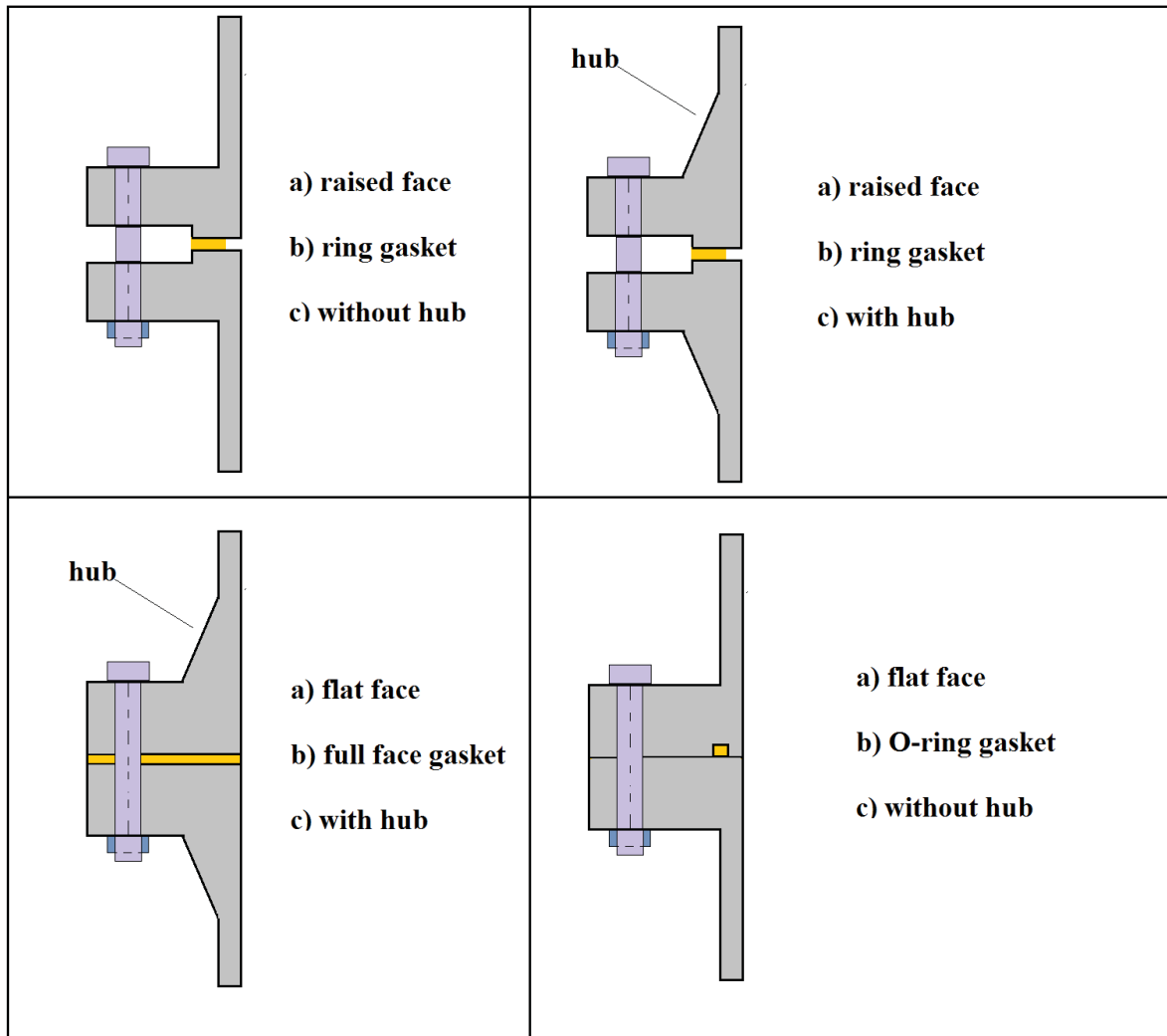


Figure 1.3 Various types of bolted flange joint configurations

### 1.3 Analytical Studies

As previously stated, a bolted flange joint is made up of several components, including the shell or head, flange ring, gasket, and bolts. This multiplicity of components necessitates the application of various theories to fully comprehend the behavior of a bolted flange joint. Theories corresponding to the shell and flange ring have been separated in the following subsections to examine the effects of discontinuity, applied forces, and moments on the integrity of the bolted flange joint. To do this, shell theory and beam on elastic foundation theory are used to treat the behavior of the shell. Plate theory, particularly circular plate with a

central hole, is used to model the behavior of the flange ring for small flange sizes, and ring theory is used to model large diameter flanges.

### **1.3.1 The Theories of Shells of Revolution**

In order to develop an adequate mathematical model, it is necessary to examine several shell theories. Membrane theory and bending theory are the two main shell theories used to study the forces and moments acting on the pressure vessel shell. The key difference between these two methods is in the consideration of the twisting and bending moments. Both approaches, which are examined in the following subsections, have been widely used in previous research to examine the behavior of shells, particularly in pressure vessel applications.

#### **1.3.1.1 Membrane Theory**

Membrane theory considers the deformation of shells without taking bending and twisting effects into consideration. This is because membrane elements cannot withstand any bending moment on account of not having flexural stiffness. This simplification of shell theory was theoretically formulated by Truesdell and Goldenweiser in 1945. When the loads are distributed across a large area of the shell, such as those produced by internal pressure and wind loads, the method gives accurate results. However, it can also be used to achieve a rough estimate of stresses at the intersection of two shells with different geometries. To obtain more reliable results, a more accurate analysis can be achieved using bending moments theory to determine the discontinuity stresses of the attached parts at their junction (Jawad, 2017). This method was implemented by Jawad and Farr (2019) to design pressurized equipment such as pressure vessels, heat exchangers, and elevated water towers.

Figure 1.4 shows a free body diagram of the revolution surface. Membrane theory is derived using the following fundamental assumptions (Gibson, 1965):

- The shell is isotropic and homogeneous;
- The thickness of the shell is small in comparison to its curvature radius;

- The bending effects are negligible and only the middle-surface strains are examined; and
- The shell deflection is small compared to the thickness of the shell.

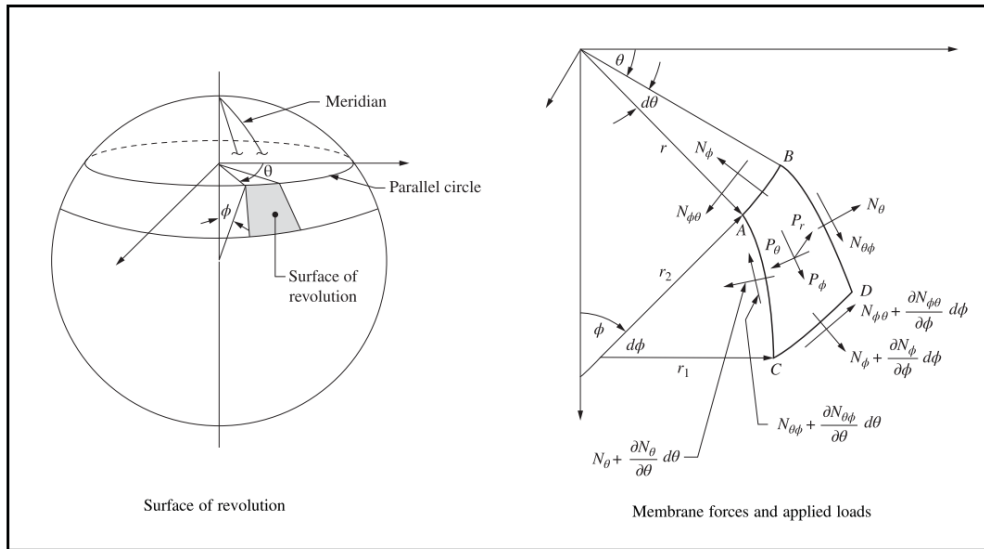


Figure 1.4 Surface of revolution model  
Taken from Jawad (2017, p. 3)

Zingoni (2001) derived the corresponding amount of stress and deformation in an egg-shaped sludge digester based on membrane theory of the shells of revolution. The stresses obtained were satisfactory throughout the structure except at the location of discontinuities, as expected. He calculated the amount of stress as a function of the angle variation across the shell (Figure 1.5). The sudden change of stresses indicated at the discontinuities shown in Figure 1.5 correlates with the abrupt variation of the shell curvature radius.

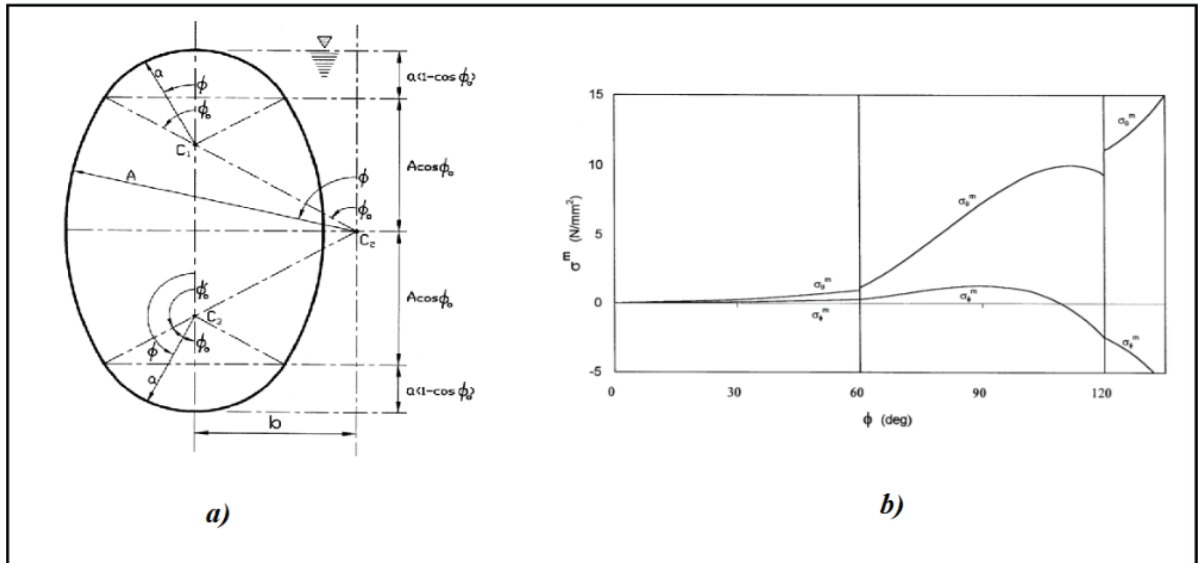


Figure 1.5 a) Egg-shaped shell of revolution, and b) variation of membrane stresses over the three regions of the eggshell

Taken from Zingoni (2001, p. 1366)

### 1.3.1.2 Bending Theory

The bending theory of shells is a more reliable method for investigating stress and deformation in shell structures. In fact, it provides more accurate results, especially at the discontinuity zones, by taking local edge effects into account. Watts and Lang (1952 & 1953) performed some analytical pressure vessel evaluations for three types of heads, namely conical, flat, and hemispherical, using the linear bending theory. They adopted the existing bending theory solutions for two different geometries and imposed continuity at the junction in terms of radial displacement and tangential rotation to evaluate the required transverse shear and meridional bending moments developed at the junction. They concluded that the highest amount of stress occurs at the junction of the cylindrical shell with a conical head (Figure 1.6). They conducted some additional experiments to validate their findings.

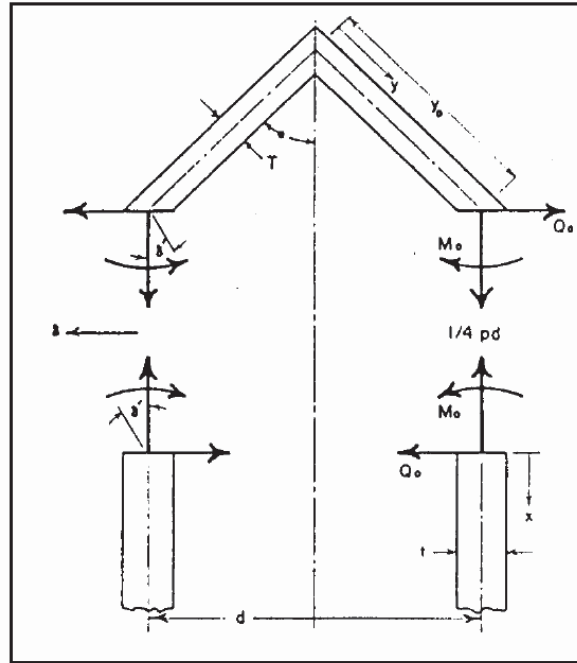


Figure 1.6 Shell-to-conical head connection  
Taken from Watts and Lang (1952, p. 208)

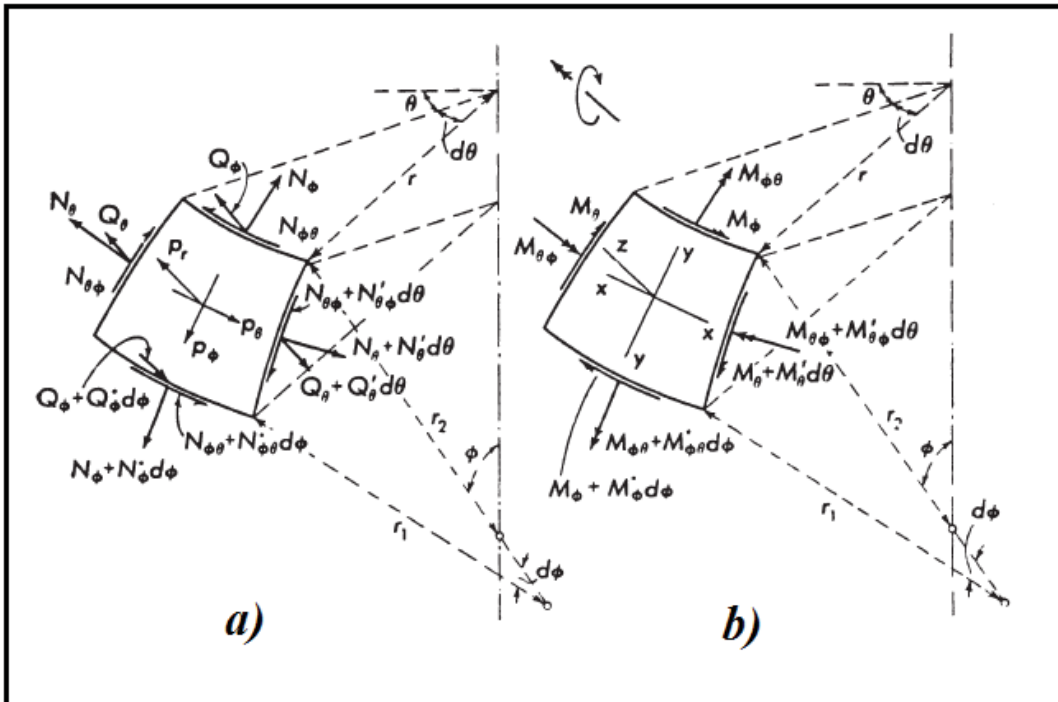


Figure 1.7 Free body diagram of the shell of revolution in bending moment theory  
Taken from Flugge (1973, p. 317)

Flügge (1973) also provided detailed solutions for several forms of shell-to-head connections, including spherical, dished, and conical, based on the bending theory of shells (Figure 1.7). His findings were complemented by various numerical approaches.

Uddin (1986a,b,c) employed two linear theories, one based on small deformation and the other on Reissner's nonlinear theory for large deformation, to analyze the behavior of the shell with three types of heads, namely spherical, ellipsoidal, and conical. For the shell-to-head discontinuities (Figures 1.8 and 1.9), he derived the corresponding formulations for the meridional and circumferential bending moments. Moreover, he compared the results of stresses due to bending at the inside and outside surfaces of the shell using linear and nonlinear shell theories.

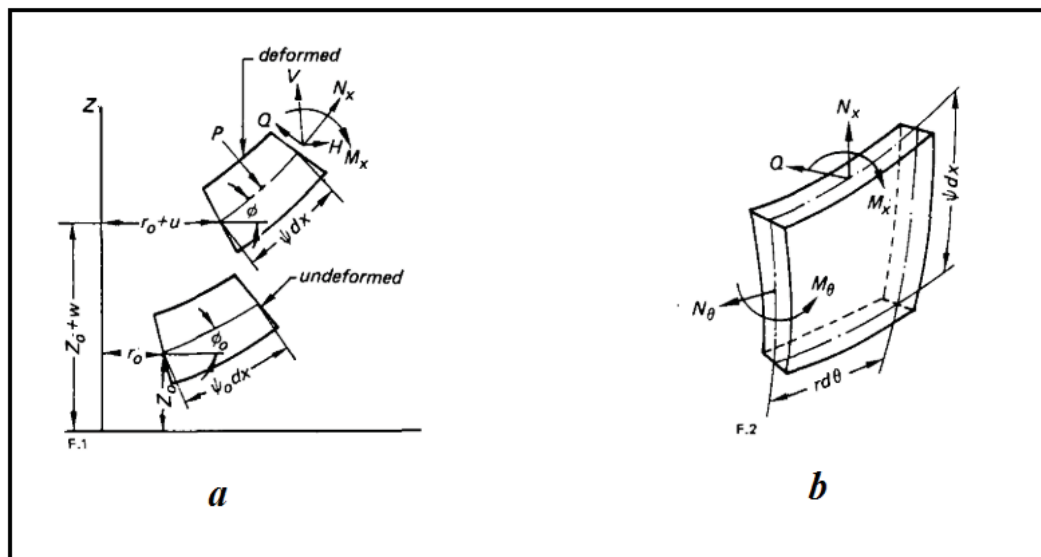


Figure 1.8 Element of the shell with acting forces, stress resultants and couples  
Taken from Uddin (1986, p. 488)

Zingoni, Mokhothu and Enoma (2015) improved on Zingoni's earlier model on the effect of edge loads on deformations and stresses at the discontinuity locations using bending theory of shells. Consequently, the results near the discontinuity were much more accurate in comparison to results from the previous model. They successfully evaluated the meridional and hoop stresses at the inner and outer surfaces of a large thin-walled, liquid-filled vessel in

the shape of multi-segmented spherical shells using the new bending moment formulation (Figure 1.10) (Zingoni et al., 2015). Furthermore, the analytical results indicated excellent agreement with the numerical data from the finite element method (FEM).

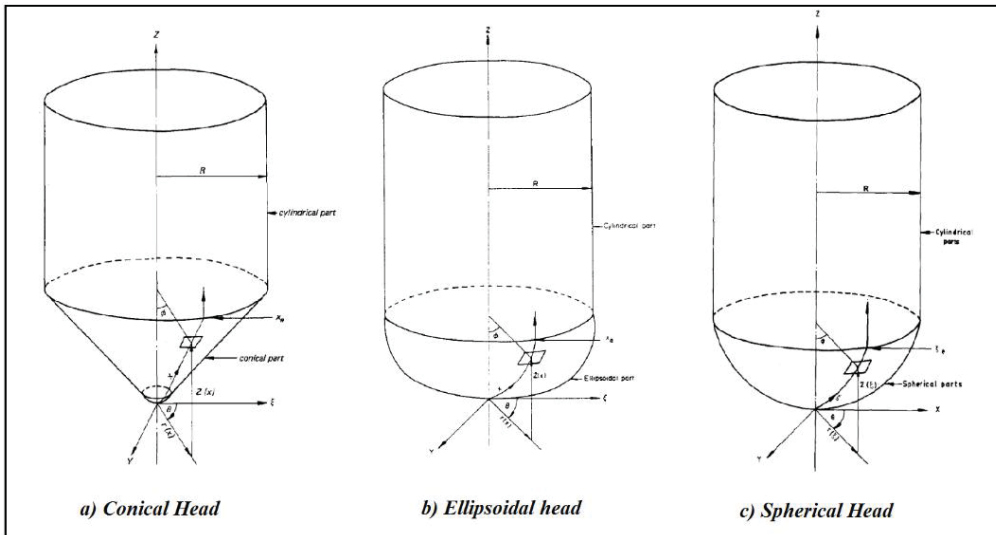


Figure 1.9 Shell parameters of a) conical, b) ellipsoidal, and c) spherical heads  
Adapted from Uddin (1986, p. 488)

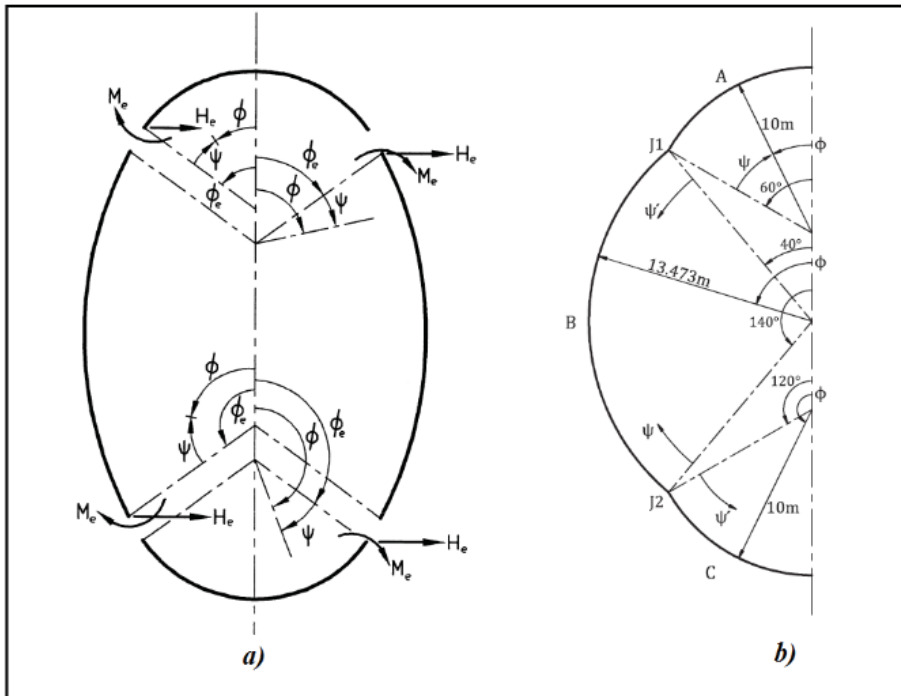


Figure 1.10 Multiple stages egg-shape pressure vessel  
Taken from Zingoni et.al (2015, p. 22)

### 1.3.2 Beam on Elastic Foundation Theory

Since the radial displacement of a cylindrical vessel with uniform thickness exposed to symmetric loading may be considered to be the deflection of a longitudinal element of the unit width, the element serves as a beam on the elastic foundation (Huang & Shi, 1998). Hetenyi (1979) and Harvey (1980) investigated the application of the governing equations of a beam on the elastic foundation for the symmetric circumstances with a uniform thickness of pressure vessels. Their results demonstrated the reliability of this theory. The primary idea of the beam on elastic foundation theory can be used to derive the applied stresses acting on the pressure vessel shell, as well as the shell deflection, as shown in Figure 1.11. When the thickness of two sides is unequal, using this approach may also be advantageous for estimating the discontinuity loads at the junction. The acting loads on the pressure vessel shell may include:

- external pressure,
- internal pressure,
- thermal flux,
- bending moments,
- torsional moments, and
- axial loads.

The simple governing equation of beam on elastic foundation theory (Figure 1.12) is given by:

$$EI \frac{d^4 y}{dx^4} + ky = p \quad (1.1)$$

A general solution for this equation, to determine the shell deflection by considering the constant amount of  $k$ , leads to the following equation:

$$y = e^{\beta x} (A \cos \beta x + B \sin \beta x) + e^{-\beta x} (C \cos \beta x + D \sin \beta x) \quad (1.2)$$

Where  $\beta$  is defined by:

$$\beta = \sqrt[4]{\frac{k}{4EI}} \tag{1.3}$$

Coefficients  $A$  to  $D$  can also be found based on the boundary condition definitions.

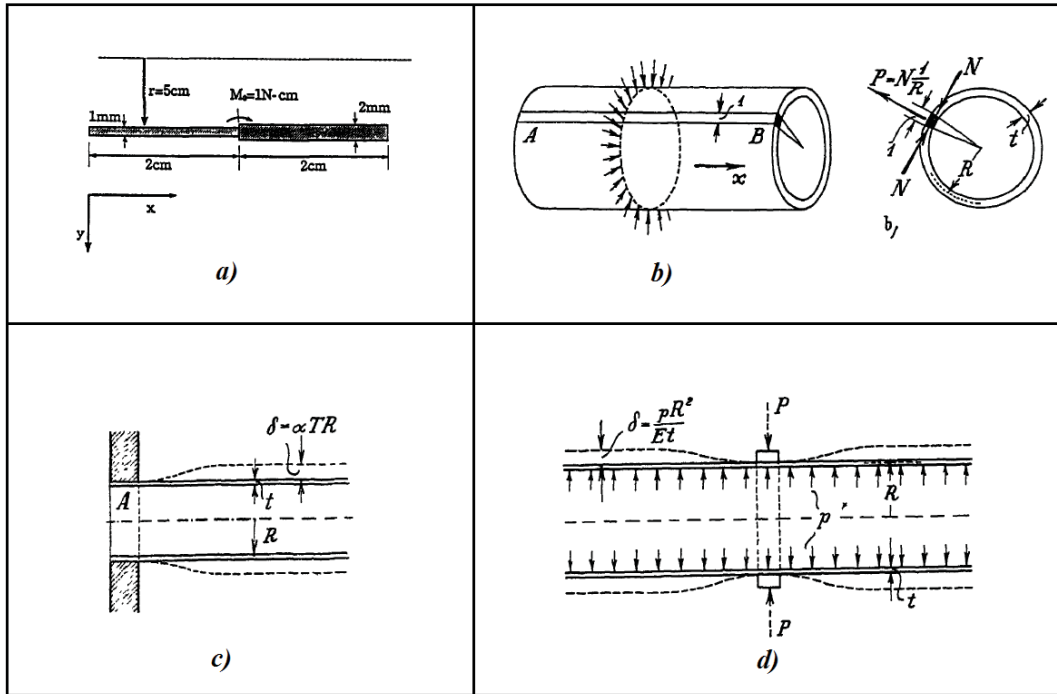


Figure 1.11 Various applications of beam on elastic foundation theory  
 Taken from Hetenyi (1979, p. 30)

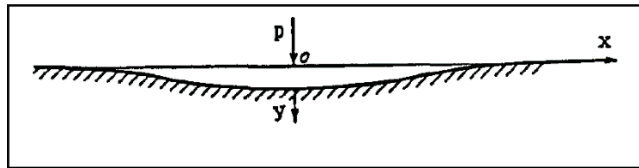


Figure 1.12 Beam on elastic foundation theory  
 Taken from Huang and Shi (1998, p. 294)

Huang and Shi (1998) proposed a finite element formulation that uses a precise displacement as the shape function. They employed a line element with two nodes. They also proved that the FEM can be used to tackle problems involving non-uniform thickness and the varying material characteristics

### 1.3.3 Plate Theories

In 1927, Waters and Taylor made a first attempt to determine a precise approach based on the idea of a beam on the elastic foundation and the deflection of flat circular plates. They conducted a discontinuity analysis between a cylindrical shell and a flat circular plate with a central hole. In 1951, Waters et al. conducted a study on flange behavior, based on the shell and plate theory. These two studies formed the cornerstones of the approach in the current ASME code. After Waters and Taylor, Timoshenko (1927) applied a simplified version of the primary concept based on the principle of the ring theory, founded on the assumption that the flange thickness is substantially greater than the connecting hub thickness. In other words, Timoshenko simplified the complicated plate bending formulation into the rotation of a circular ring. Szilard developed some classical and numerical approaches to treat the plate analysis (Szilard, 1974; 2004), and Naser conducted a three-directional stress analysis of the shell to derive the tangential, radial, and axial components at the shell-to-flange junction (Naser, 1995).

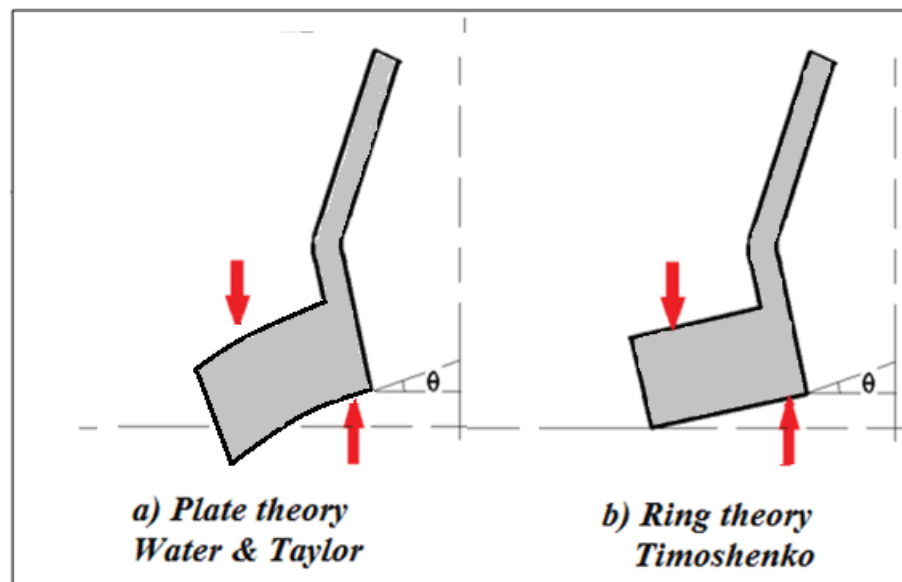


Figure 1.13 Two plate theories: a) Waters and Taylor model, and b) Timoshenko model

The most effective method of predicting leakage is to consider the flange structural system interaction. This means that the flexibility of the flange, gaskets, and bolts must be determined to properly predict the gasket and bolt stresses resulting from both the internal pressure and the external loads (Koves, 1996) and then verify for the leakage tightness.

This approach has been used in various research. For example, Nechache and Bouzid (2008) investigated the load relaxation in bolted flange joints that were subjected to creep. To develop an analytical approach, they split the complete bolted flange joint in several sections. Linear springs are considered to model the bolts and gaskets and predict their behavior using equilibrium and compatibility equations (Figure 1.14). They examined the tightness of a bolted flange junction while it was subjected to creep. They also compared the behavior of the bolted flange joints using the theory of rings and that of a circular plate with a central hole, and the proposed analytical approach (Figure 1.15).

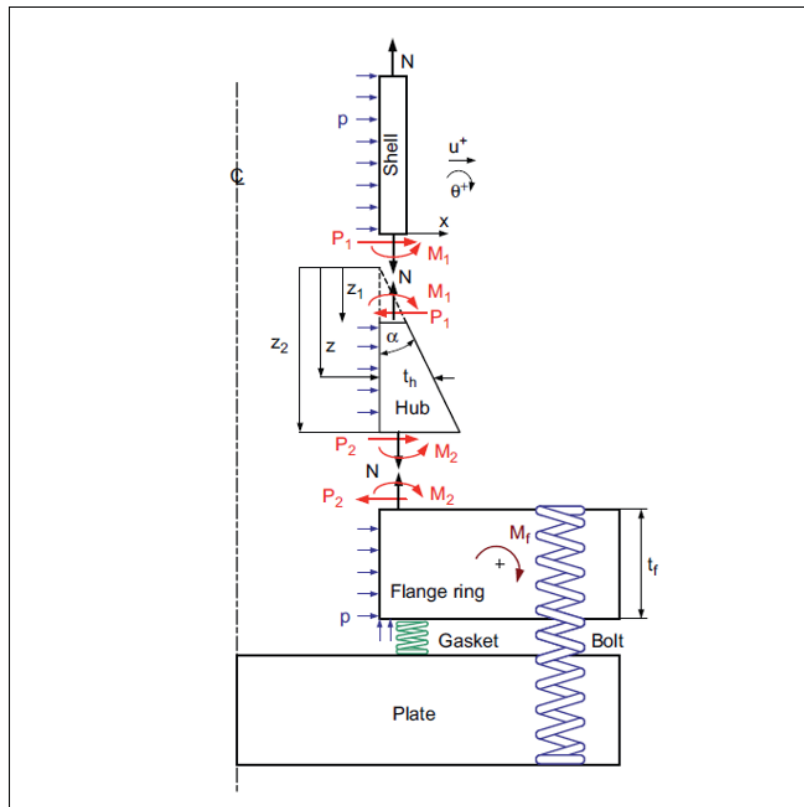


Figure 1.14 Analytical model of integrated bolted flange joint  
Taken from Nechache and Bouzid (2008, p. 488)

Cao and Bell (1992) presented two generic solutions to treat the circular flat plate with and without a central hole based on plate theory in the presence of transverse loads and bending moments. Currently, their approach can practically be applied to circular flange analysis.

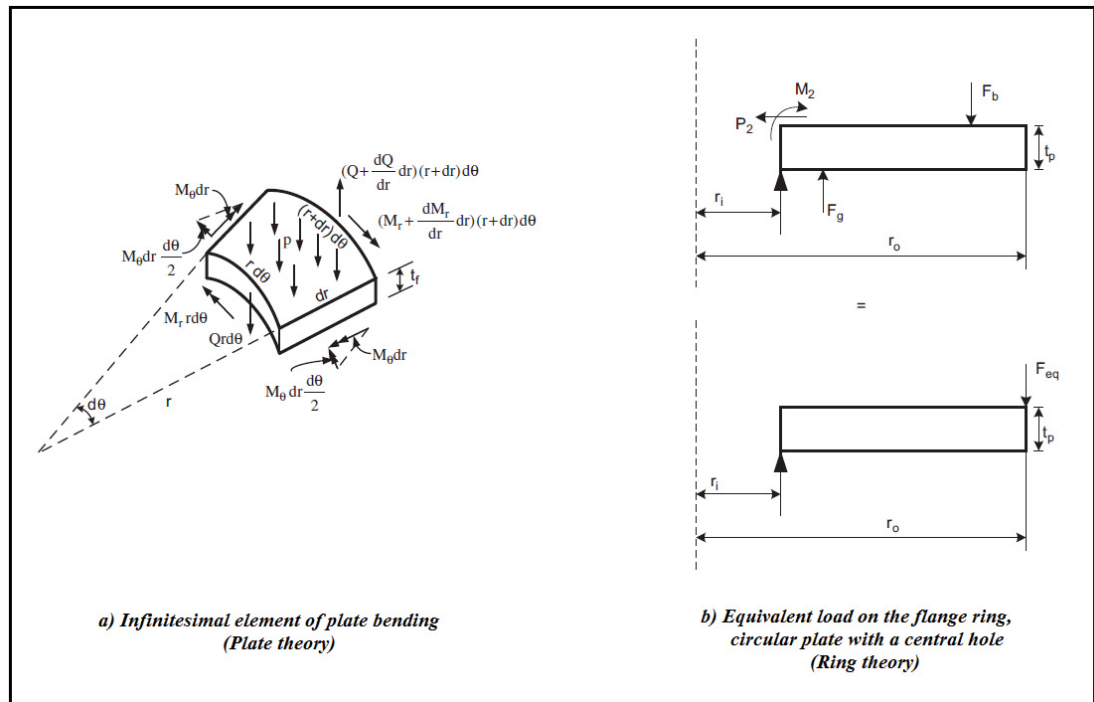


Figure 1.15 Acting forces and moments on the circular plate with a central hole  
Adapted from Nechache and Bouzid (2008, p. 488)

Koves (1996) proposed an analytical approach to analyze the behavior of the bolted flange joint under external loads. His research was grounded on the approach developed by Waters et al. (1951) in the shell and plate theory. His analytical model comprised the flange joint flexibility, and his predictions were compared to leakage data. In addition to implementing an analytical approach, Koves made an important comparison between the results extracted from a ring subjected to a twisting couple and the experiment to predict the leakage rate based on the amount of flange rotation and pipe bending moment (Figure 1.16).

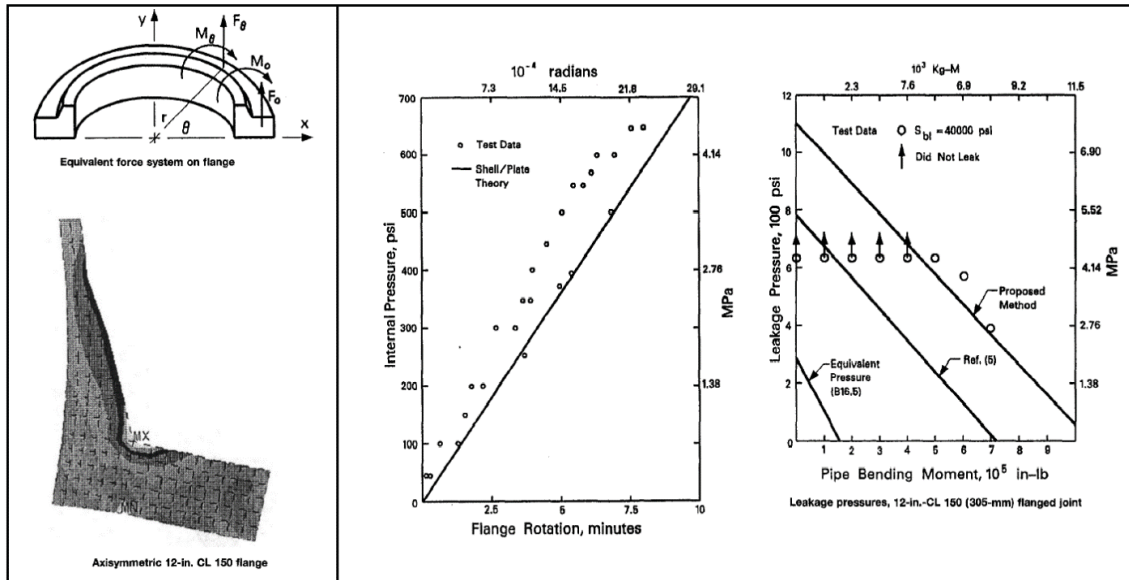


Figure 1.16 FEM modeling and results for the flange rotation and leakage rate  
Adapted from Koves (1996, p. 61)

### 1.3.4 Discontinuity Analysis

Sudden changes in shape, material characteristics, or stress can occur in metallic pressure vessels. These are referred to as discontinuity areas, and the stresses associated with them are referred to as discontinuity stresses. To analyze pressure vessel discontinuities, both theoretical and experimental stress evaluations are used (NASA, 1971).

Discontinuities in a pressure vessel can occur due to a variety of reasons, including (Figure 1.17):

- variations of thickness,
- changes in material,
- variations of shape, and
- changes in temperature.

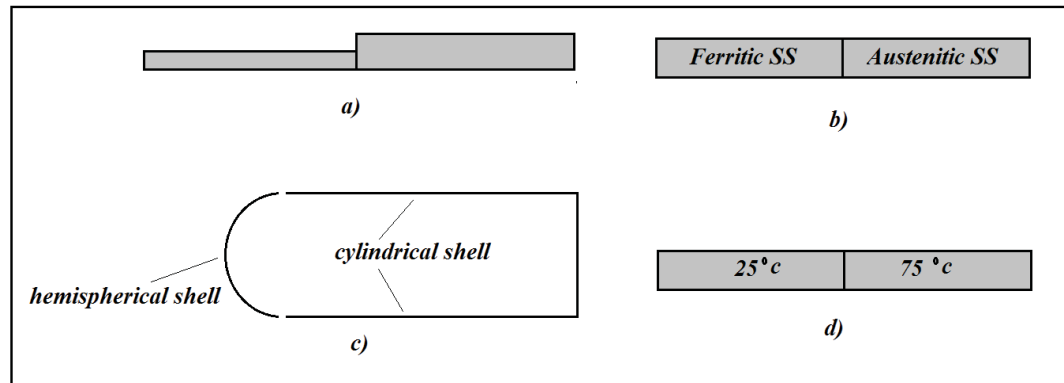


Figure 1.17 Causes of discontinuities at the shell of the pressure vessel

The ASME BPVC has comprehensively addressed discontinuity analysis for numerous types of connections, including cylindrical, spherical, torispherical, ellipsoidal, and flat heads (ASME BPVC, Sec VIII, Div 2, Appendix 4, 1998). In addition, Flugge (1973) introduced the discontinuity analysis for conical and dished connections.

#### 1.4 Design Codes, Standards and Other References

Bolted flange joint design references can be classified based on the following components:

- general design,
- flange body,
- gasket, and
- bolt.

##### General Design

The design rules for pressure vessels are covered by the ASME BPVC, Section VIII (Divisions 1 and 2). The general and welding-related regulations for pressure vessel components are presented in the UG and UW parts of Division 1. Furthermore, the mandatory appendix 1 (Division 1) elaborates on the supplementary design calculations for various types of heads, including hemispherical, torispherical, ellipsoidal, and conical (Figures 1.18 and 1.19). Megyesy (1972) offered the same design calculations for several types of heads based on the internal and external pressures of the pressure vessels. The thickness calculations for various

load cases were published in his handbook. Moreover, Moss (2004) provided a thorough reference for designing pressure vessel components with diverse geometries.

Additionally, the mandatory appendix 2 of ASME BPVC, Division 1, contains the rules for bolted flange connections with ring-type gaskets. It also includes bolt load estimations, gasket requirements, and flange stresses. The general design rules for flanged joints in the scope of Division 2 can be found in Section 4.16 (2017), in addition to the calculations provided in some earlier versions of the ASME codes.

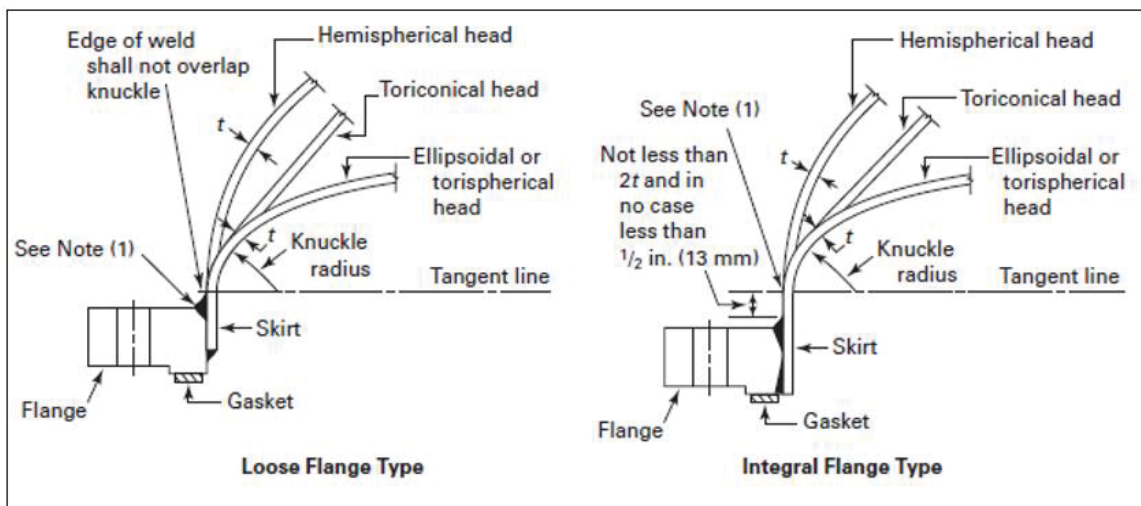


Figure 1.18 Various flange-to-shell connections  
Taken from ASME BPVC, Sec VIII, Div 1 (2017, p. 366)

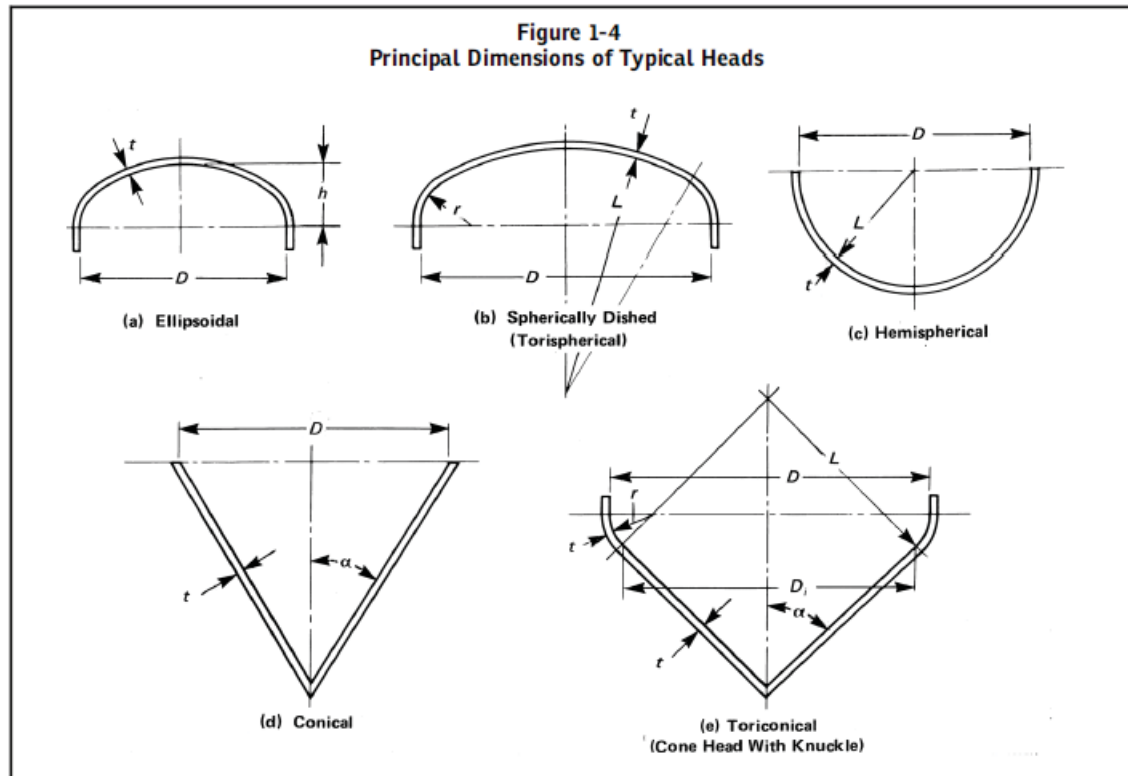


Figure 1.19 Principal dimensions of typical heads  
Taken from ASME BPVC, Sec VIII, Div 1 (2017, p. 361)

### Flange Body

For pipe flanges and flanged fittings, ASME B16.5 and B16.47 provide a comprehensive reference for the handling of many types of flange specifications, such as pressure-temperature ratings, materials, dimensions, tolerances, labeling, testing, and methodologies for identification. Specifically, ASME B16.5 covers flanges with nominal pipe sizes (NPS) ranging from 0.5 to 24 (inches), whereas ASME B16.47 covers flanges with NPS ranging from 26 to 60 (inches). The class rating is determined by the operating pressure and temperature that correlate to the base material of the flange (Figure 1.20).

Nominal Designation	Forgings	Castings	Plates			
C-Si	A105 [Note (1)]	A216 Gr. WCB [Note (1)]	A515 Gr. 70 [Note (1)]			
C-Mn-Si	A350 Gr. LF2 [Note (1)]	...	A516 Gr. 70 [Notes (1), (2)]			
C-Mn-Si	...	...	A537 Cl. 1 [Note (3)]			
C-Mn-Si-V	A350 Gr. LF6 Cl. 1 [Note (4)]	...	...			
3½Ni	A350 Gr. LF3	...	...			
Working Pressure by Classes, bar						
Temperature, °C	75	150	300	400	600	900
-29 to 38	9.8	19.6	51.1	68.1	102.1	153.2
50	9.6	19.2	50.1	66.8	100.2	150.4
100	8.8	17.7	46.6	62.1	93.2	139.8
150	7.9	15.8	45.1	60.1	90.2	135.2
200	6.9	13.8	43.8	58.4	87.6	131.4
250	6.0	12.1	41.9	55.9	83.9	125.8
300	5.1	10.2	39.8	53.1	79.6	119.5
325	4.6	9.3	38.7	51.6	77.4	116.1
350	3.1	8.4	37.6	50.1	75.1	112.7
375	...	7.4	36.4	48.5	72.7	109.1
400	...	6.5	34.7	46.3	69.4	104.2
425	...	5.5	28.8	38.4	57.5	86.3
450	...	4.6	23.0	30.7	46.0	69.0
475	...	3.7	17.4	23.2	34.9	52.3
500	...	2.8	11.8	15.7	23.5	35.3
538	...	1.4	5.9	7.9	11.8	17.7

Figure 1.20 Working pressure by flange classes  
Taken from ASME B16.47 (2017, p. 13)

For the purposes of this investigation, Figure 1.21 shows the essential dimensional information for the flange class 300, series A, based on ASME B16.47.

### Gasket

ASME B16.20 provides a comprehensive set of requirements for metallic gaskets (e.g., spiral wound gaskets) that can be used to estimate their dimensions. ASME B16.21, provides comparable categories for the nonmetallic flat gaskets of pipe flanges.

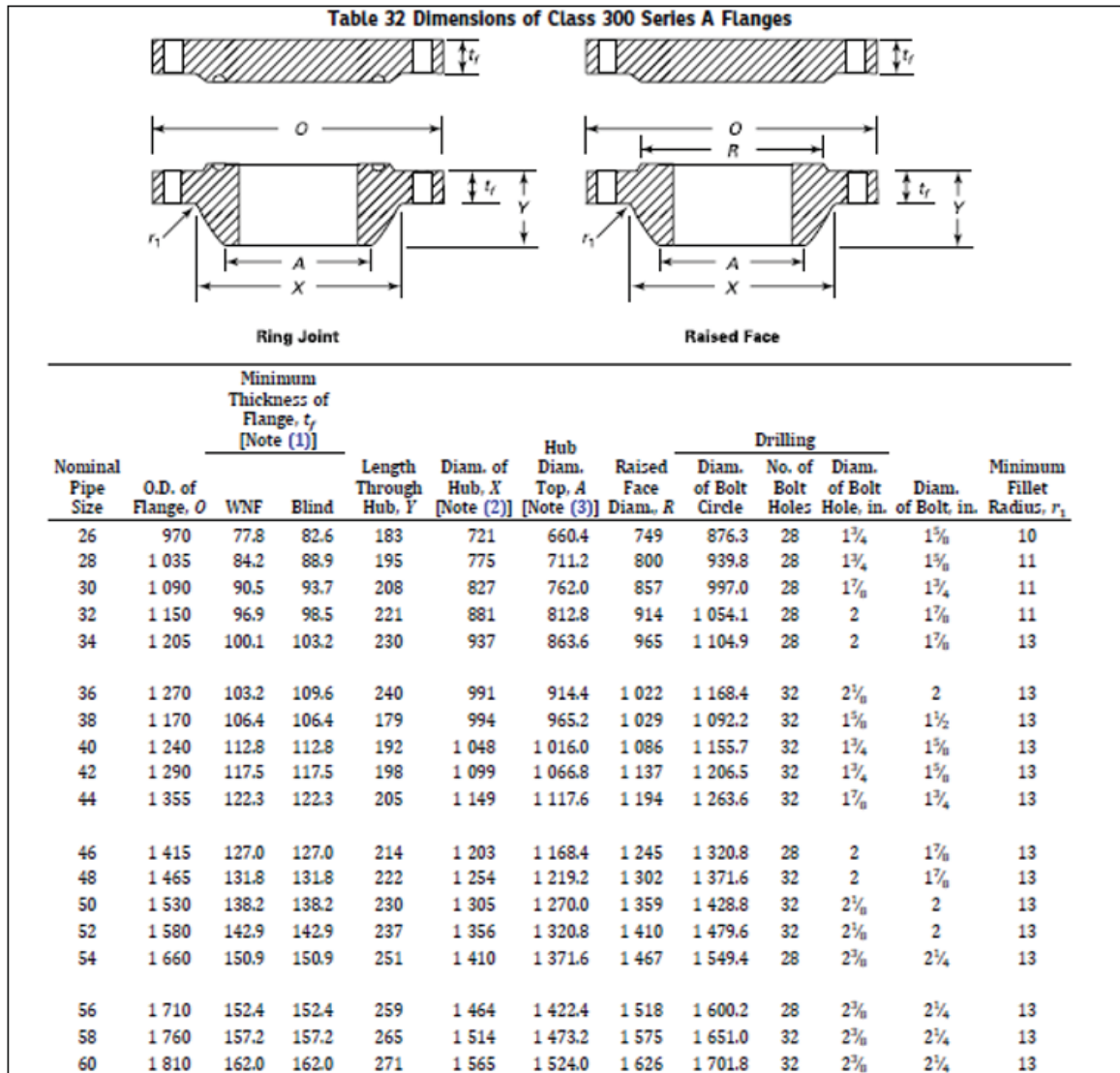


Figure 1.21 Dimensional flange characteristics based on NPS  
Taken from ASME B16.47 (2017, p. 41)

**Bolt**

Earlier standards, ANSI B1.1 (1974) and ASME B18.3.1 (1978), specified the dimensions of screw threads and socket head cap screws, respectively, and served as a reference for other handbooks, such as Shigley’s Mechanical Engineering Design (Budynas & Nisbett, 2011). ASME B18.2.1 (2012) provides a set of widely applicable requirements for several types of bolts, which may be used as a guide to determine the dimensions of industrial bolts (Figure 1.22). Furthermore, Bickford’s (2008) book on the design and behavior of bolted joints is a

good resource for estimating the bolt preload based on the compression stress and bolt dimensions.

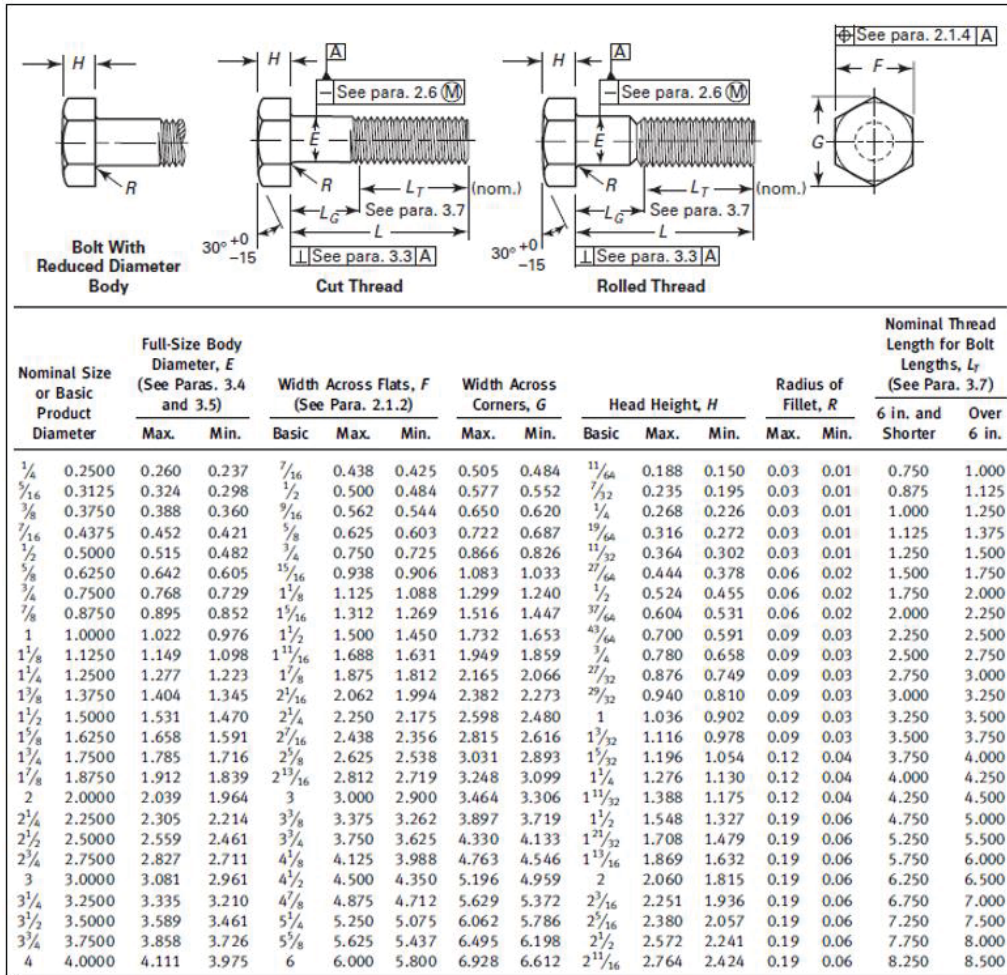


Figure 1.22 Bolt dimensions based on the nominal size  
Taken from ASME B18.2.1 (2012, p. 6)

### 1.5 Numerical Finite Element Studies

Beghoul (2003) proposed a new approach to study the behavior of bolted flange joints by simulating bolt and gasket flexibility with a spring element model (Figure 1.23). He used FEM software to conduct a numerical study on the effect of several forms of mechanical and thermal load cases, including internal pressure, thermal expansion, external loads, and creep, on the leakage rate of the bolted flange joint.

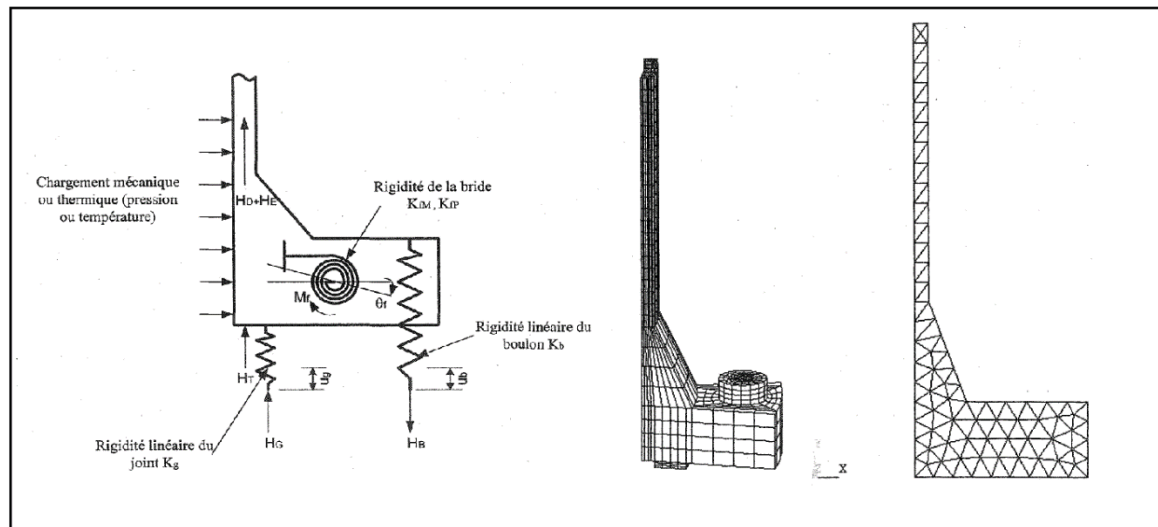


Figure 1.23 Spring modeling and finite element simulation of the flange  
Adapted from Beghoul (2003, p. 74)

Another study explored the performance of gasketed flange joints in the presence of a combined form of pressure and temperature (Abid, 2006). It also simultaneously examined the strength and sealing capability variables, as they were key criteria for the assessment of the bolted flange joint conformity. Pressurization and steady-state temperature conditions were both taken into consideration in Abid's research. He utilized ANSYS software to create an integral flange to simulate his three-dimensional (3D) model of the bolted flange joint shown in Figure 1.24. He also specified the stress intensity under different temperature settings, ranging from 100°C to 400°C, using ANSYS software.

Nechache and Bouzid (2007) explored the impact of creep on the bolt load in bolted flange joints. They used a flexible model to investigate the creep-relaxation behavior of the bolted flange joints. The flange flexibility is addressed using linear and rotational spring components. They also presented a 3D ANSYS model (Figure 1.25) that can be used to simulate the interaction between the gasket and the bolted flange joint. Moreover, they used two gasket models (corrugated metal sheet and compressed asbestos) to establish a relationship between the gasket contact stress and displacement. In another study, Nechache and Bouzid (2008) investigated the load relaxation in bolted flange joints subjected to creep. They evaluated the tightness of a bolted flange joint when subjected to the creep phenomenon using a plate theory-

based analytical method. They then compared the FEM results with those derived from the theory to validate their analytical model (Figure 1.26).

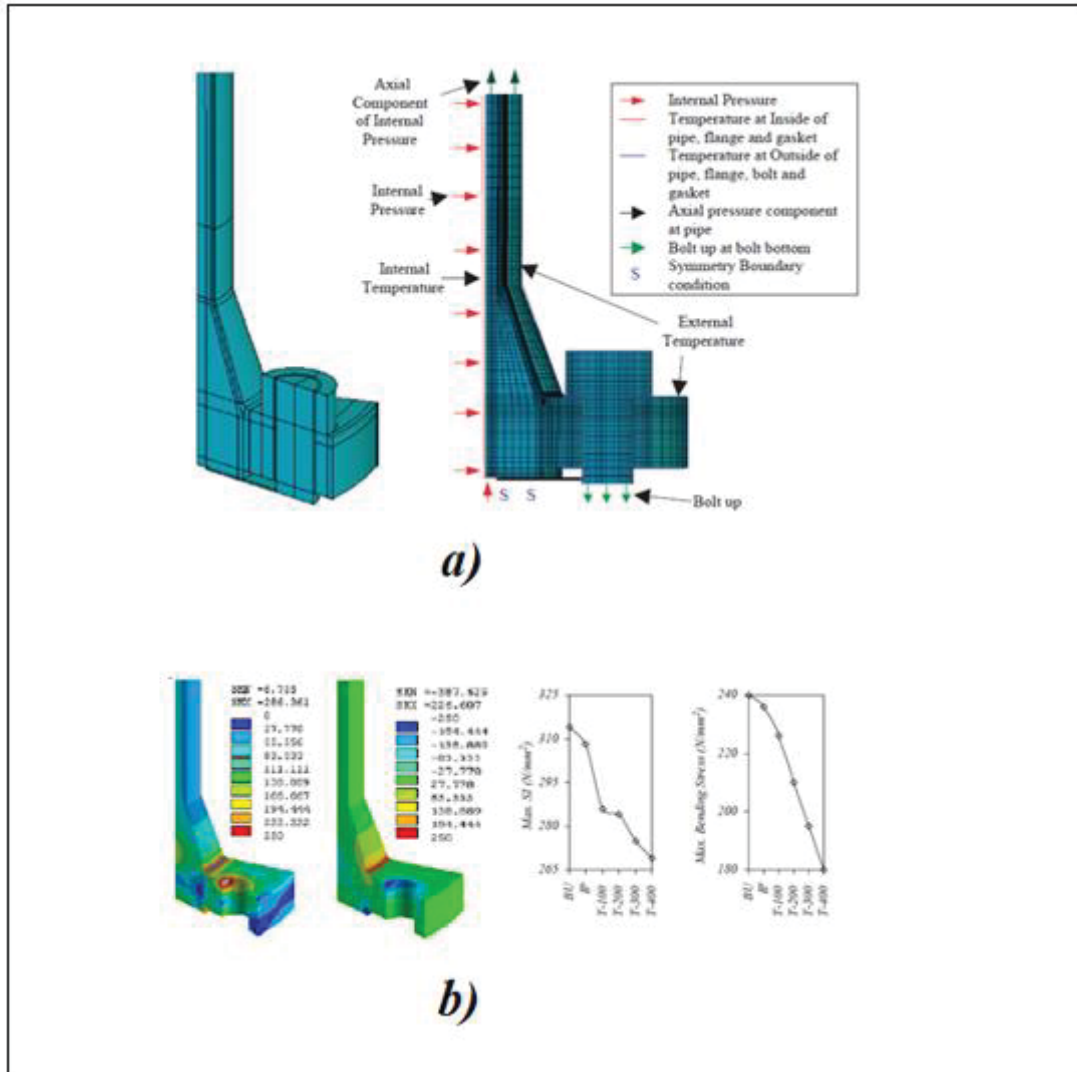


Figure 1.24 a) 3D model and meshing, and b) stress variation for combined loading  
Adapted from Abid (2006, p. 437)

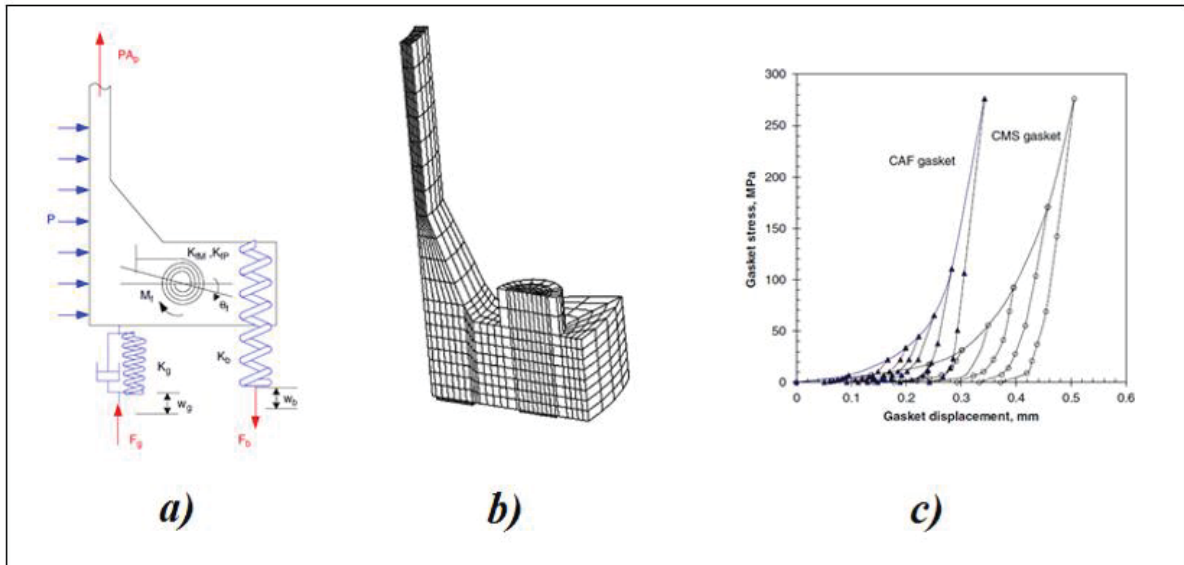


Figure 1.25 a) Bolted flange model, b) 3D finite element model, and c) gasket displacement  
Taken from Nechache and Bouzid (2007, p. 187)

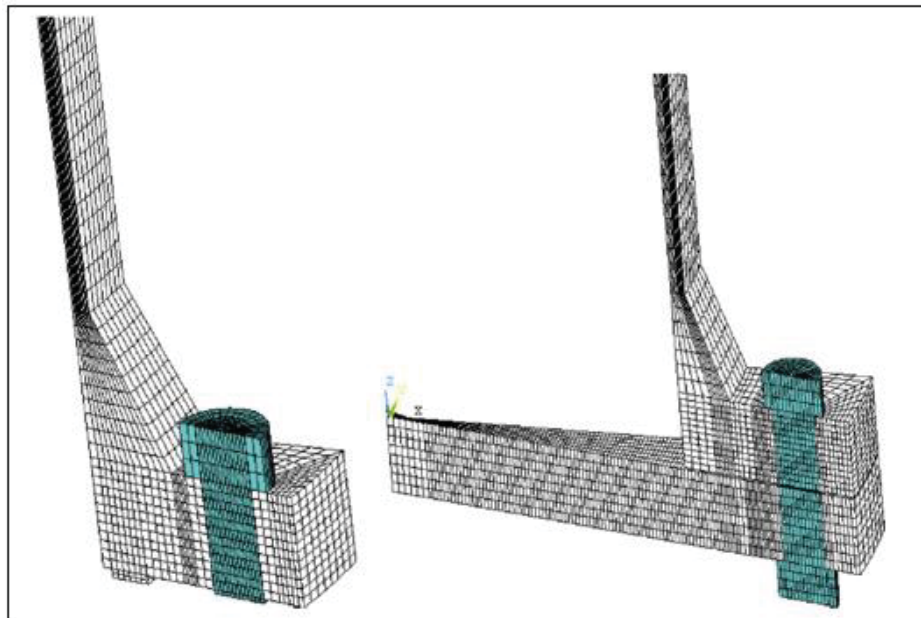


Figure 1.26 3D finite element model of bolted flange joint  
Taken from Nechache and Bouzid (2008, p. 491)

Krishna, Shunmugam and Prasad (2007) used the experimental results of the loading characteristics of gaskets to perform a 3D finite element analysis of the bolted flange joint to check its leak tightness (Figure 1.27). They investigated the nonlinear behavior of gaskets with respect to the internal pressure (Figure 1.28) in various loading and unloading conditions with

three distinct types of sheet gasket materials, namely asbestos, graphite, and polytetrafluoroethylene (PTFE).

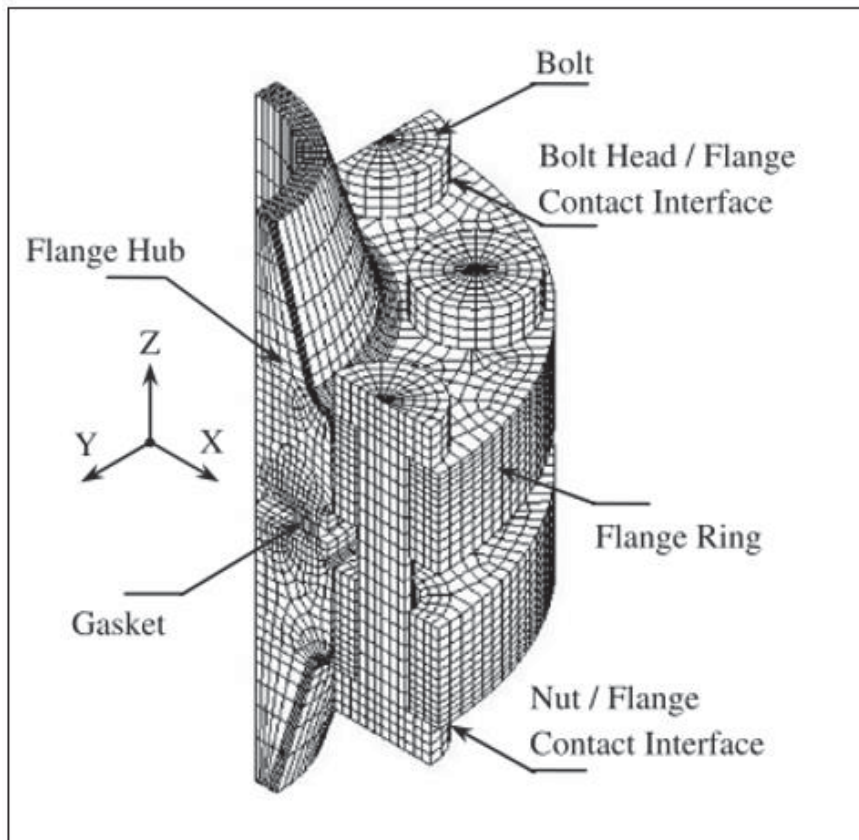


Figure 1.27 Finite element mesh of bolted flange joint  
Taken from Krishna et al. (2007, p. 351)

Krishna et al. (2007) also showed the relationship between the internal pressure and the flange rotation (Figure 1.29a), as well as the axial bolt force (Figure 1.29b). As shown in the diagrams, increasing the internal pressure causes a linear rise in the amount of flange rotation as well as in the bolt force. Furthermore, they estimated the maximum flange rotation for three different types of gasket materials in order to establish an upper limit to avoid leakage.

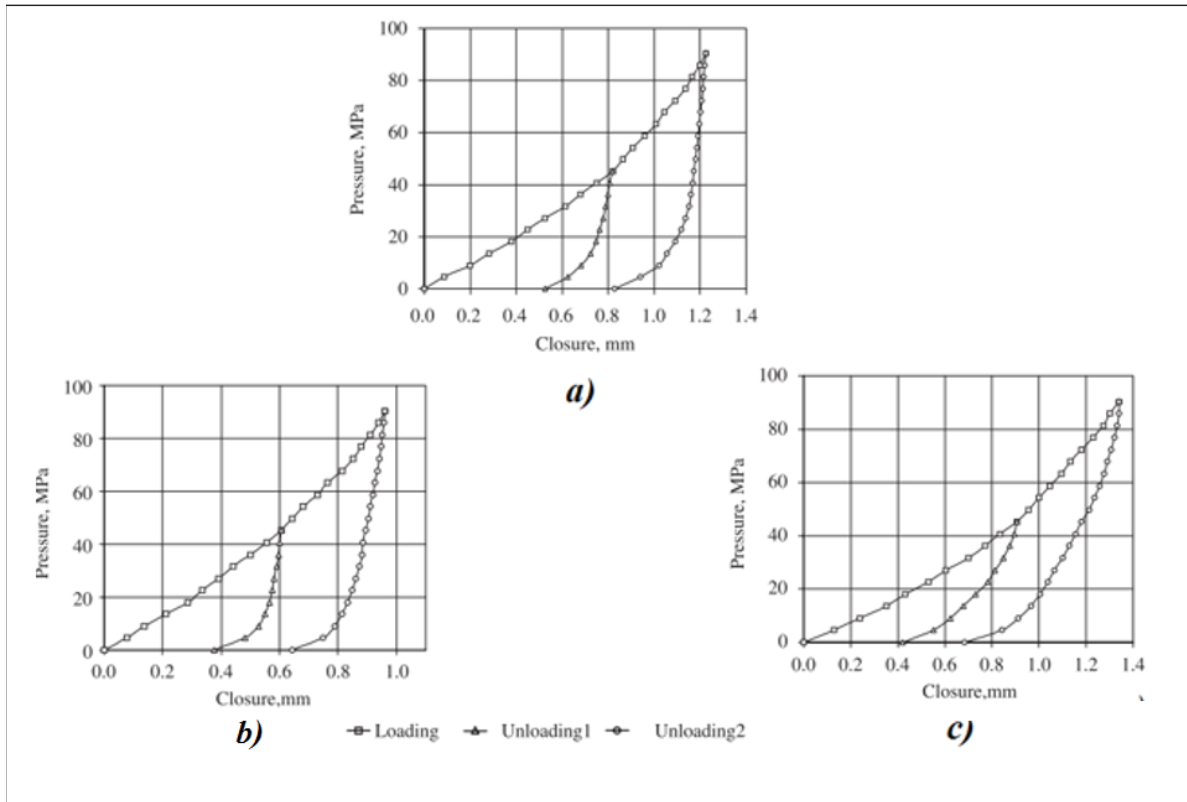


Figure 1.28 Characteristics of a) asbestos, b) graphite, and c) PTFE based gaskets  
 Taken from Krishna et al. (2007, p. 351)

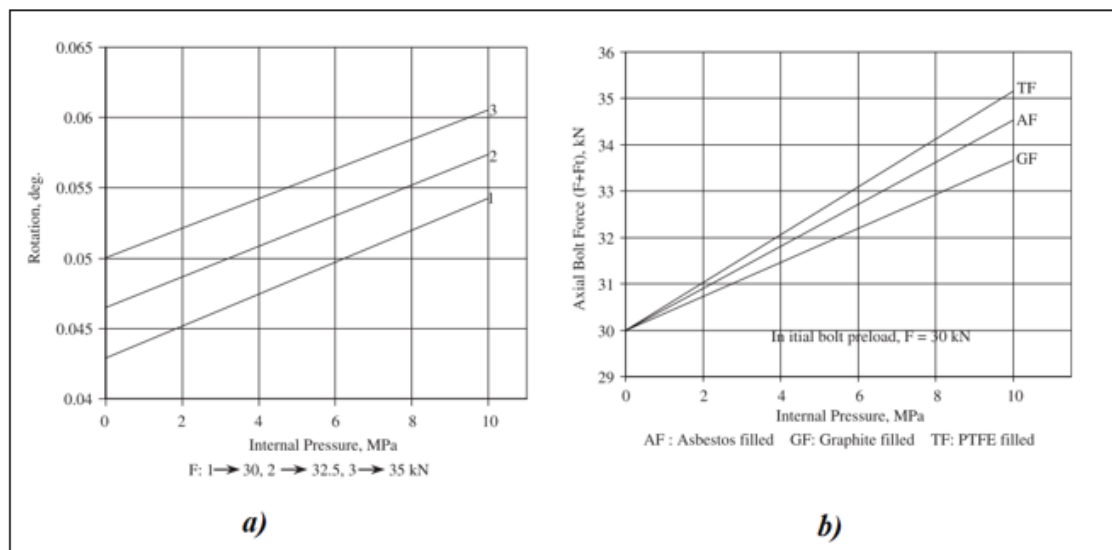


Figure 1.29 Flange rotation and axial bolt force variation vs. internal pressure  
 Taken from Krishna et al. (2007, p. 353)

A study by Madsen, Kragh-Poulsen, Thage and Andreassen (2017) investigated an analytical and a numerical method for determining the plastic strain of the bolt and shell of a bolted flange joint used in offshore wind turbine foundations. Although their study concentrated on the stress analysis of L-shaped flanges, it is included in the literature review because their goal was to identify high-stress zones near the flange-shell junction. Madsen et al. presented a finite element model, including the flange ring, shell, bolt, nut and washers with the appropriate boundary conditions and the applied loads (Figure 1.30). As shown in Figure 1.31, they investigated the rate of stresses at several locations on the bolt and the shell to determine the rate of plastic strain. First, they derived the ultimate resistance of the elements, and then they determine the axial load limit. Contour graphs in Figure 1.31 show the predicted axial stresses in the bolt and flange segments when the axial load was close to the ultimate resistance. Figure 1.32 gives the stresses and plastic strains as a function of segment shell force for the locations A through E shown in Fig. 1.31.

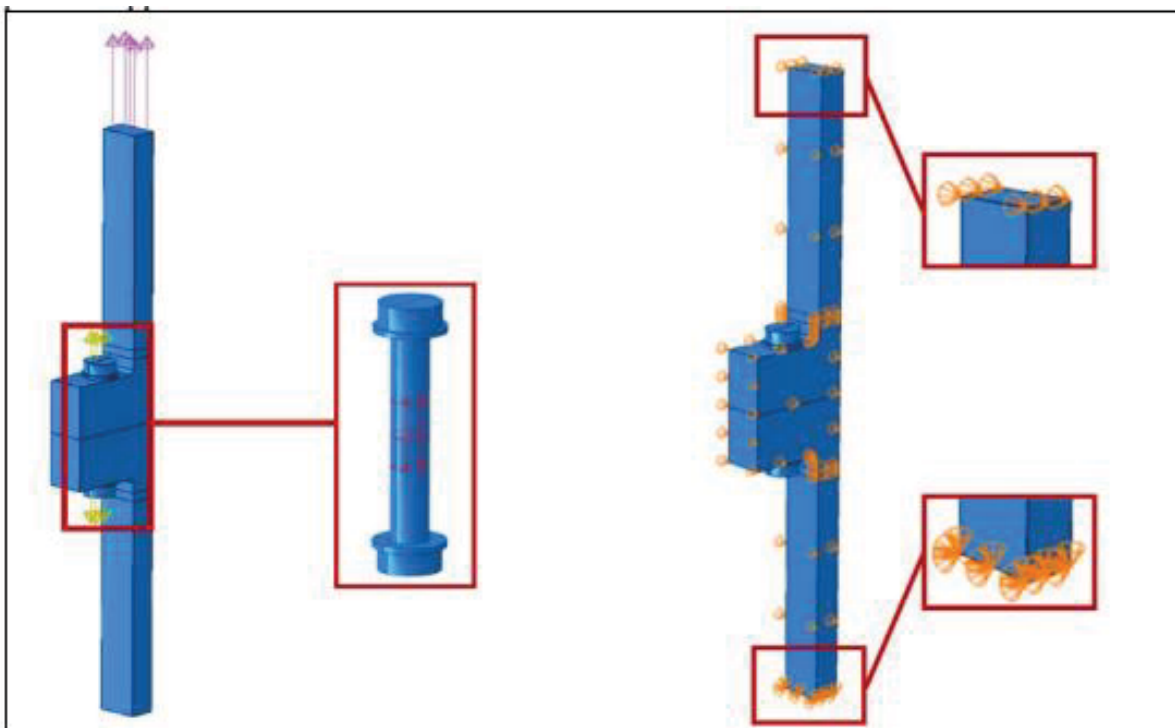


Figure 1.30 Finite element model of L-shape bolted flange joint  
Adapted from Madsen et al. (2017, p. 7)

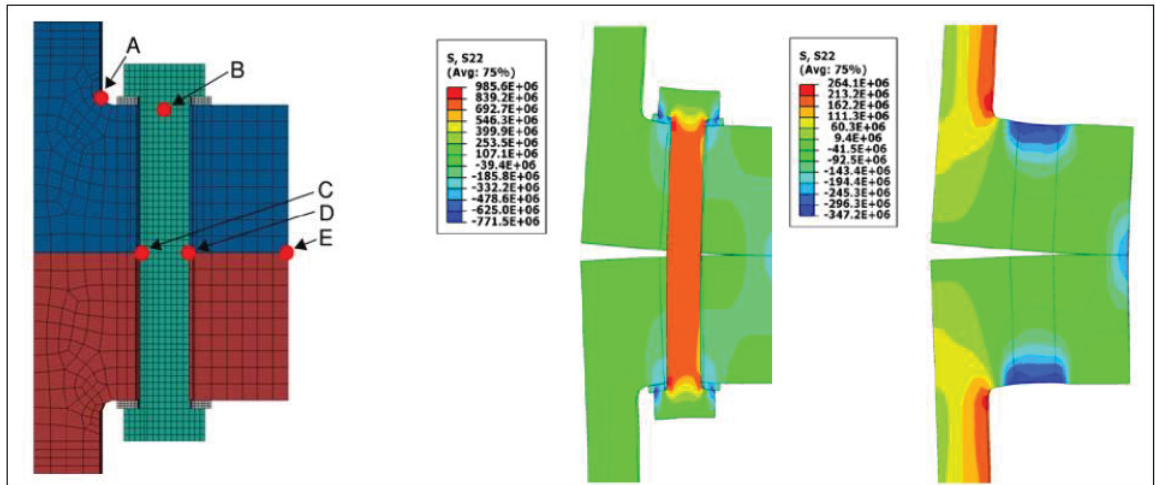


Figure 1.31 Contour graphs of the axial stresses in the bolt and the A through E locations  
 Taken from Madsen et al. (2017, p. 13)

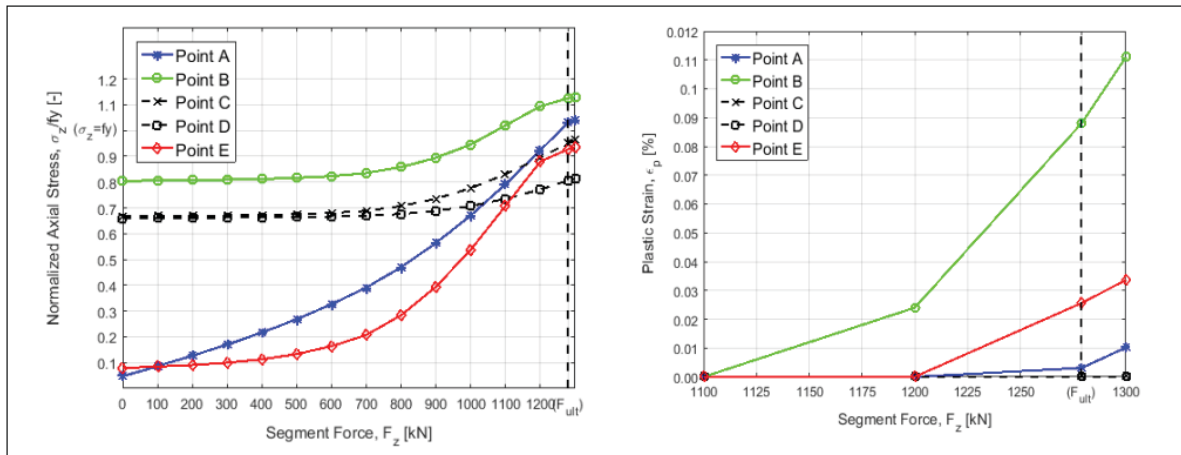


Figure 1.32 Normalized axial stresses and the plastic strains vs. tensile shell segment force  
 Taken from Madsen et al. (2017, p. 13)

## 1.6 Experimental Research

Abid and Nash (2006) focused on gasketed and non-gasketed flange joints under bolt-up and operational conditions (Figure 1.33). They used different gasketed and non-gasketed flange joint assemblies in a series of studies to investigate flange behavior during joint preloading, operating conditions, and retightening. They discovered that all stresses in a non-gasketed joint are confined within the yield strength during the bolt-up and pressurization. They also showed

that in the gasketed joint, the allowable stress is close to the design pressure during the bolt-up, whereas during the proof test and higher pressures, the allowable stress is larger than the acceptable stress at certain locations. Abid and Nash also investigated the structural strength of bolted flange connections, highlighted the problem with gasketed joints, and performed a comparative analysis of non-gasketed joints under bolt-up and operating circumstances to decrease stress variation and increase the joint strength.

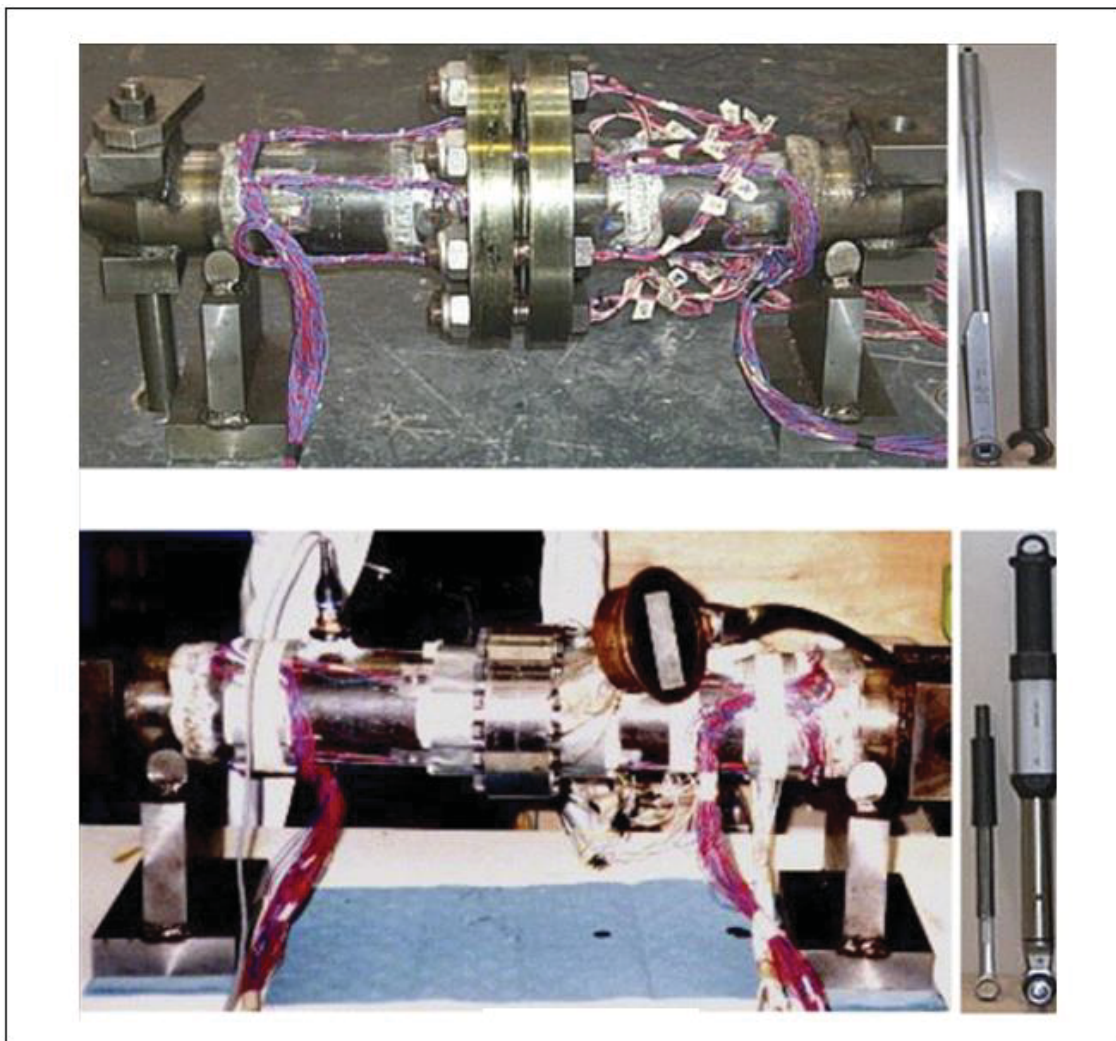


Figure 1.33 Experimental set-up of bolted flange joint  
Taken from Abid and Nash (2006, p. 3)

Kobayashi (2014) experimentally investigated the viscoelastic behavior of the gasket and its deformation under the influence of stress (Figure 1.34). Kobayashi has authored or co-authored

several papers in this research area (Kobayashi, 2014; Kobayashi & Hamano, 2004; Kobayashi, 2008; Kobayashi, Hagiri, Nishiura, Hiratshuka, & Itoi, 2012). Kobayashi (2014) used springs to model all components of the gasketed flange connection (Figure 1.35). Furthermore, by setting up the experimental rig, he was practically been able to measure several parameters, such as leak rate, bolt load, and gasket deflection (Figure 1.35). These parameters were measured with time as creep was taking place.

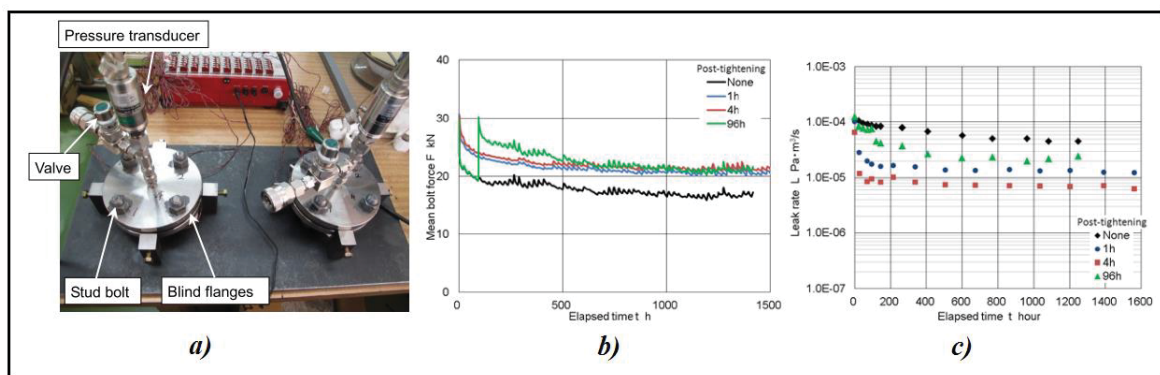


Figure 1.34 Experimental set-up performed by Kobayashi  
Taken from Kobayashi (2014, p. 2)

Kobayashi (2014) also used the flexibility method to model the bolted flanged connection. He proposed an approach based on the Maxwell model to evaluate the relaxation of the bolt load and its effect on the leakage tightness in bolted joints. He observed that the compression of the gasket makes the gasket material less porous, which increases the sealing ability of the gasket even when the bolt load is reduced (Figure 1.35). Finally, he validated his suggested approach by demonstrating that the theoretical and experimental results related to the bolt force reduction and tightness were in agreement.

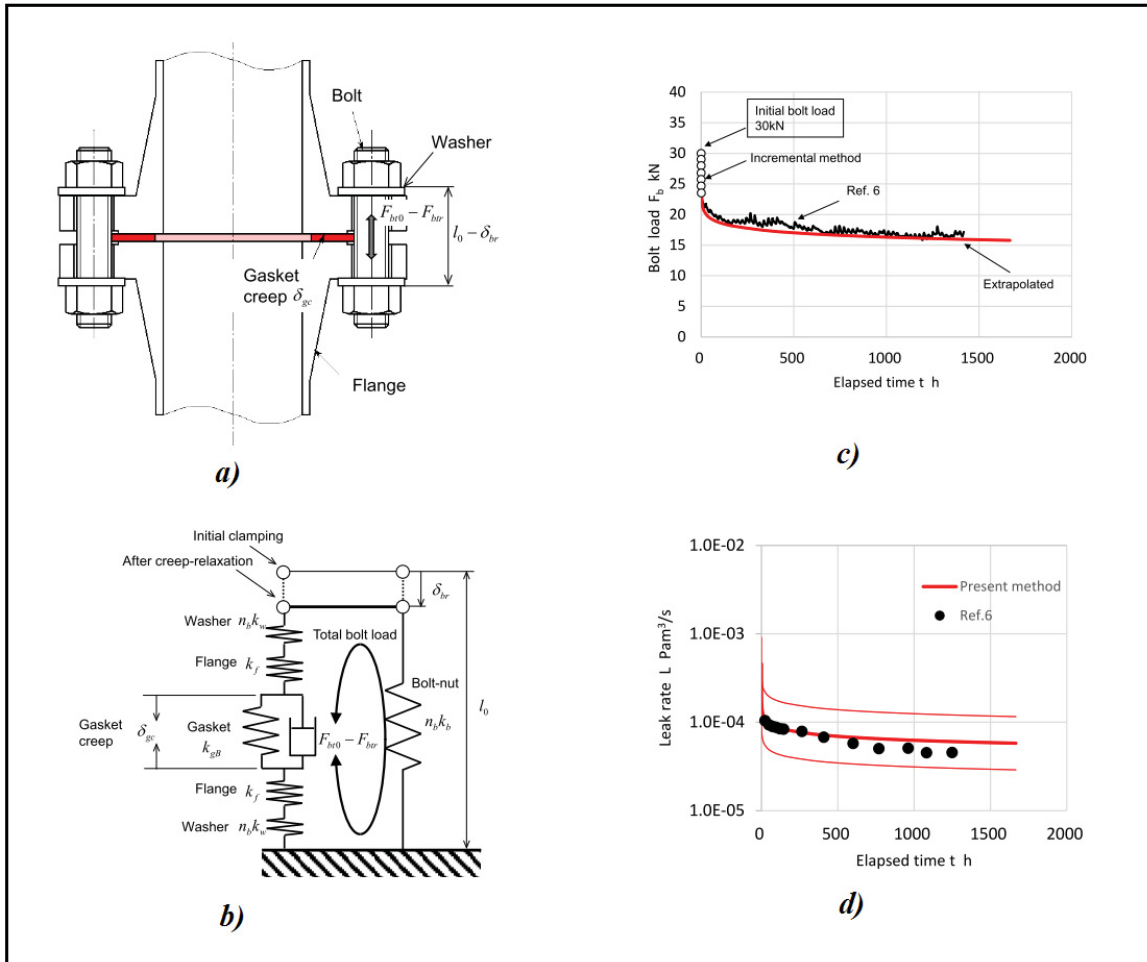


Figure 1.35 Bolted joint modeling, bolt force reduction and leak rate in creep conditions  
Taken from Kobayashi (2014, p. 2)

Luyt, Theron and Pietra (2017) used nonlinear finite element modeling to investigate the impact of gasket creep-relaxation on circular bolted flange connections. They looked at the contact pressure between the gasket and the flange face because it is an important aspect in the bolted flange joint leakage assessment. They also compared the performance of two types of flanges: one flat and one raised face (class PN10, size DN50), both with non-asbestos compressed fiber ring gaskets with aramid and a nitrile rubber binder. They used ANSYS to simulate the bolted flange joint behavior and compare the experimental results (Figure 1.36). Luyt et al. found that the number of bolt tightening increments and the time interval between bolt tightening increments have a substantial impact on gasket creep-relaxation.

In their study, Luyt et al. used TekScan sensor equipment to measure the contact pressure between the gasket surface and the flange faces in order to obtain more reliable results (Figure 1.37). They also installed strain gauges on the flanges and bolts (Figure 1.37). Furthermore, they generated 2D and 3D FE models to analyze the deflections and contact pressure using the crisscross pattern for bolt tightening (Figure 1.38).

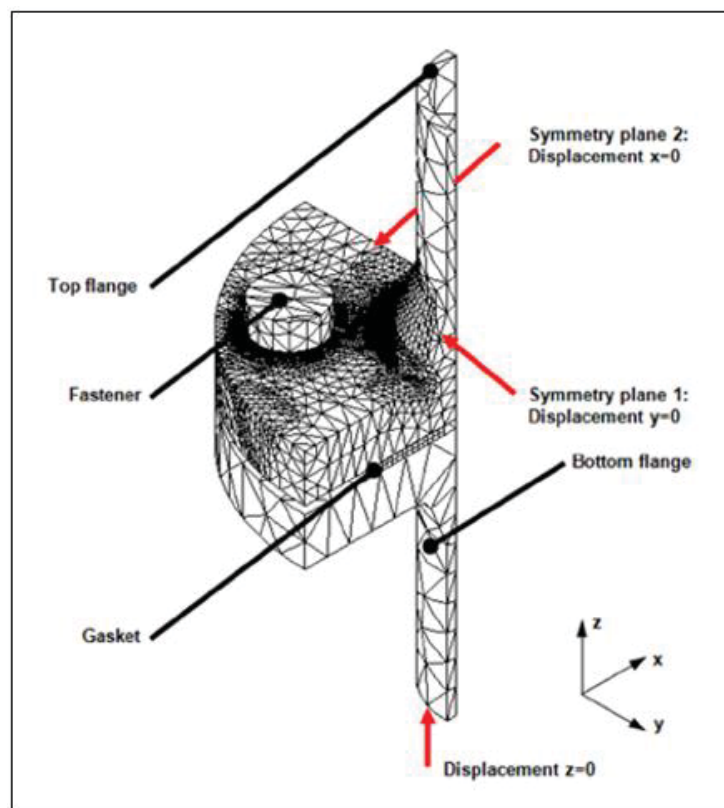


Figure 1.36 FEM model for the bolted flange joint  
Adapted from Luyt et al. (2017, p. 53)

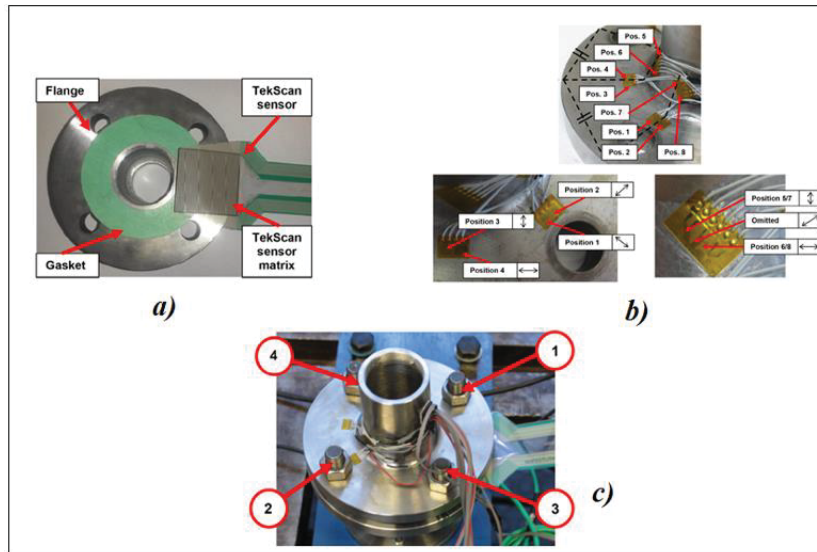


Figure 1.37 Positioning of TekScan sensors and strain gauges  
Adapted from Luyt et al. (2017, p. 54)

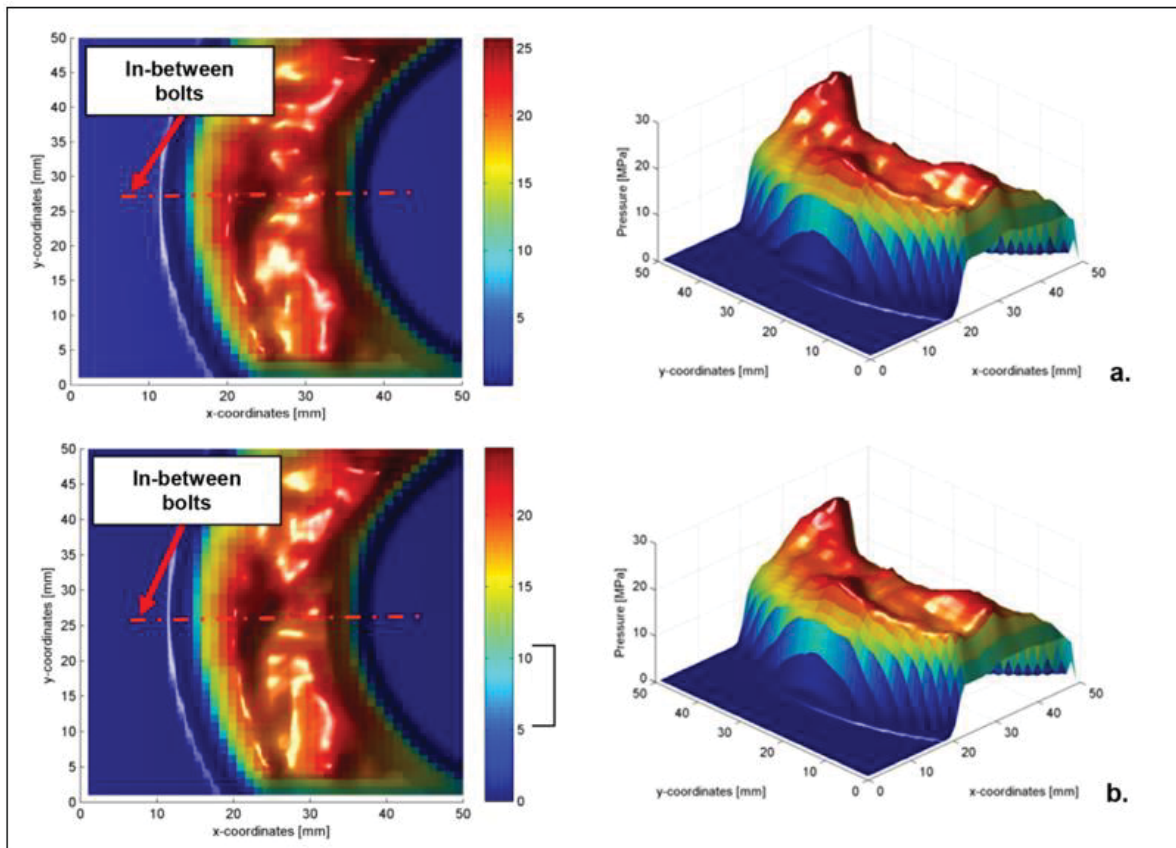


Figure 1.38 a) Measured contact pressure immediately after bolt tightening, and b) measured contact pressure 10 minutes after bolt tightening for the flat face flange  
Taken from Luyt et al. (2017, p. 57)

## 1.7 Research Project Objectives

The literature review revealed a scarcity of comparative research and publications on bolted flange joints that examine a variety of shell connections and their influence on underlying characteristics, such as bolt load, gasket contact pressure, flange rotation, and flange stresses. In addition, the effects of the flange size on stress distributions in the flange has not been examined. This investigation intends to address these challenges and provide an integrated concept for analytically and numerically analyzing the stresses and strains in bolted flange joints subjected to the two operating conditions of the bolt-up and pressurization. The research objectives are:

- Develop an analytical approach to determine the stresses and strains in bolted flange joints by considering different shell connections, including spherical, cylindrical, conical, and dished;
- Investigate the impact of flange geometry on the stress distributions by considering different flange sizes;
- Assess the effect of the nonlinear gasket characteristics by considering the nonlinearity in the numerical analysis and compare with the analytical model.



## **CHAPTER 2**

### **FEM MODELING AND STRESS ANALYSIS METHODOLOGY**

#### **2.1 Introduction**

The integrated complex of the bolted flange joint is exposed to higher stresses at the junction of the shell and the flange ring. Furthermore, increased flange rotation leads to increased gasket contact pressure, which may jeopardize the integrity of the bolted flange joint. Accordingly, an investigation of the acting loads on the bolted flange joint during the bolt-up and pressurization stages is required. A more reliable analysis may also be required that considers numerous challenging operating situations, such as high pressure, high temperature, vibration, and external loads (Wagner, Huehne & Niemann, 2018).

In some cases, unpredicted high stresses at the shell-to-flange junction can be responsible for leakages and the release of dangerous substances into the atmosphere. Load redistributions and high stresses generated at the junctions depend significantly on the shape and geometry of the flange ring and the shell type. The pressure vessel shells of cylindrical, spherical, conical, and dished shapes tend to be used without any comparison to optimize their use. To ensure a safe design of bolted joints, it is essential to model all the acting forces and stresses on the flange in the presence of different shell connections to create an accurate prediction of the stresses. In addition, accurate prediction of the flange rotation and bolt and gasket loads during operation are key parameters for a successful design.

#### **2.2 Proposed Model of Bolted Flange Joint**

This study evaluated the integrity and leakage tightness of different types of shells connected to the flange ring, using the different shell theories to analyze the different parameters, including flange rotation, gasket contact stress, and stress distribution at the flange-to-shell junction. To do this, several types of shell connections, namely cylindrical, spherical, dished,

and conical are compared to evaluate the effect of the size and geometry of the shells on the behavior of the bolted flange joint. Hence, all types of shells are directly connected to the raised-face flange ring. To support the analytical approach and validate the study, these shell connections are modeled using general-purpose finite element software (Choulaei & Bouzid, 2021).

This chapter describes the analytical method developed to evaluate the behavior of the bolted flange joint by estimating the flange rotation, various stress components, and gasket contact stress. It also describes the numerical models used for validation. ANSYS software was used to build the numerical finite element bolted flange joint models.

### **2.3 Analytical Method**

This section summarizes the different theories used to obtain the analytical solution of the stresses in the shell-to-flange ring junction. Different types of connections with an overview of the flange rotation and bolt load are considered. The flange ring and the shell are the two main components of the flange. For simplicity, the hub section depicted in Figure 2.1 is not considered. FEM analysis is applied to validate the method and verify the gasket contact stress and leakage characteristics.

Continuity and equilibrium equations generated from the bolted joint analysis were used during both bolt-up and pressurization to evaluate the bolt and gasket loads changes, discontinuity edge loads, and stresses.

The continuity conditions of radial displacement and tangential rotation of the shell and ring require that:

$$w_f = w_s \quad (2.1)$$

And

$$\theta_f = \theta_s \quad (2.2)$$

The gasket force can be determined during bolt-up as follows:

$$H_G^i = H_B^i \quad (2.3)$$

And during pressurization:

$$H_G^f = H_B^f - pA_p \quad (2.4)$$

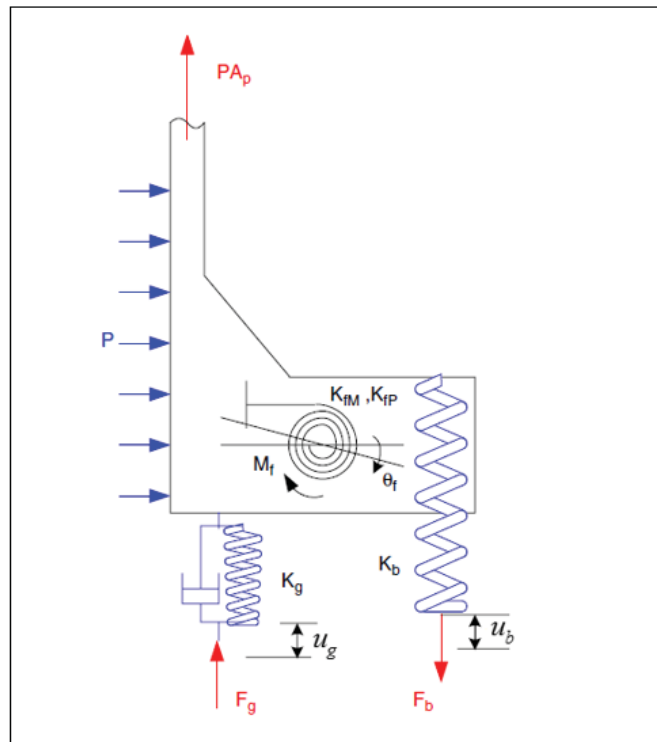


Figure 2.1 Bolted flange model

Taken from Nechache and Bouzid (2007, p. 187)

The bolted joint shown in Figure 2.1 is a complex structure with a statistically indeterminate system that requires an additional equation to solve the problem. The compatibility of the axial displacement of the flange joint elements described in previous papers (Bouzid & Chaaban, 1993; Bouzid & Nechache, 2005) was used to overcome this situation, which states that the nut traveling axial distance  $\Delta_e$  remains the same, and is given as follows:

$$\Delta_e = u_b^i + u_g^i + u_f^i = u_b^f + u_g^f + u_f^f \quad (2.5)$$

And in terms of the linear stiffnesses and ring rotation:

$$\frac{H_B^i}{K_b} + \frac{H_G^i}{K_g} + 2\theta_f^i (r_b - r_g) = \frac{H_B^f}{K_b} + \frac{H_G^f}{K_g} + 2\theta_f^f (r_b - r_g) \quad (2.6)$$

### 2.3.1 Bolt Load

The stress area is a cross-sectional area used to determine the stiffness of the bolt. The tensile stress area of the bolt, by considering the standard 60° thread, is given by (Bickford, 2008):

$$A_s = \frac{\pi}{4} (D_b - 0.938 p_b)^2 \quad (2.7)$$

By implementing the equation for the stress area, the bolt load may be obtained as follows:

$$H_B = \sigma_b A_s \quad (2.8)$$

Where  $\sigma_b$  is the applied bolt stress and  $H_b$  is the resulting bolt load.

The root area is a more conservative stress area, and is extensively used in ASME B31.1. Because the root area is dependent on the root of threads or minor diameter, it has a lower stress area than the tensile stress area. In fact, its purpose is to add a margin of safety to thread strength estimations.

To ensure that the rod is not overstressed in service, the designer uses a *root stress area* that is less than the *actual tensile stress area* (Figure 2.2).

The bolt root area is given by:

$$A_r = \frac{\pi}{4}(D_b - 1.22687p_b)^2 \quad (2.9)$$

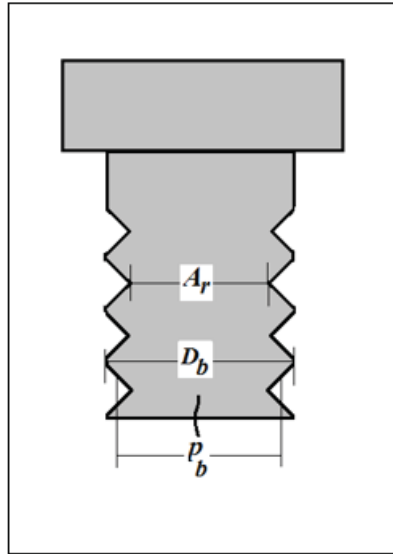


Figure 2.2 Bolt parameters

### 2.3.2 Gasket Modeling

The modeling of the gasket is a key factor for predicting leakage by estimating the reaction load and contact pressure during service with reasonable accuracy. The gasket is sufficiently compressed to seal the flange connection. The gasket material behavior during the bolt-up or seating stage is nonlinear, while during unloading or pressurization, it behaves rather linearly.

Figure 2.3 shows the typical load compression curves for the corrugated metal sheet gasket with a flexible graphite layer. These curves were obtained experimentally in the Static and Dynamic Sealing Laboratory of the ETS University, using the Room Temperature Tightness Test (ROTT) (ASTM F2836, 2018). The ROTT rig was conducted on a real pair of NPS 4, class 900 flanges (ASME B16.5, 2016). It is assumed that the mechanical behavior will be the same as the sizes of the gaskets used in this investigation.

The bolted flange joints in this study are made of NPS 26, 48, and 60, class 300, series A flanges of ASME B16.47 (2017). In the analytical model, the gasket unloading was assumed to be linear, and the slope of the unloading was used in the evaluation of the gasket compression modulus as follows (Bouzid & Chaaban, 1993):

$$E_g = \frac{\Delta S_g}{\Delta D_g} \times (t_g - D_s) \quad (2.10)$$

Where  $t_g$  is the initial gasket thickness and  $D_s$  is the displacement corresponding to the seating stress (Choulaei & Bouzid, 2021).

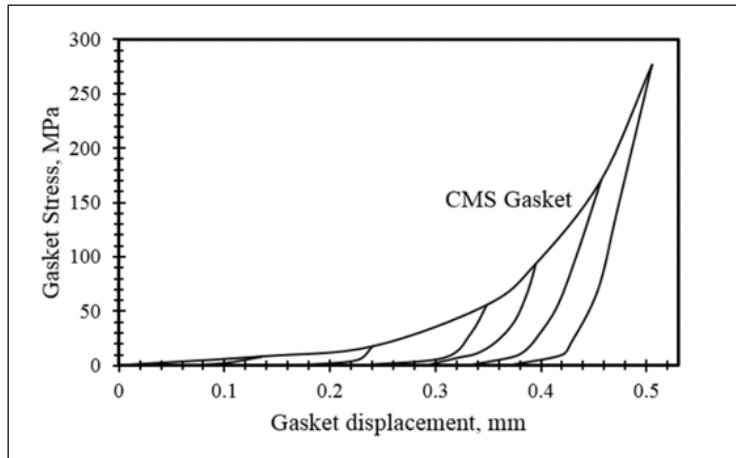


Figure 2.3 Nonlinear unloading–loading curve of gasket

### 2.3.3 Flange Ring

The flange ring rotation is an important parameter, and the ASME code limits the rotation to 0.2 degrees for flanges with a hub and 0.3 degrees for flanges without a hub. The flange rotation always increases by exerting the bolt preload and applying internal pressure. However, excessive rotation has a major influence on the gasket contact stress and can cause lift-off with certain gasket types that have a limit stop to control compression, such as spiral wound gaskets. The applicable theory for flange ring rotation was chosen based on the width-to-thickness ratio of the flange.

The theory of circular plate with the central hole can be replaced with ring theory by using the above-mentioned ratio to obtain the rotation (Timoshenko & Woinowsky-Krieger, 1989):

$$\theta_f = \frac{2RY}{Et_f^3} M_f \quad (2.11)$$

Where  $Y$  for a flange considered as a ring is given by:

$$Y = \frac{6}{\ln k} \quad (2.12)$$

And for a flange considered as a circular plate with a central hole:

$$Y = \frac{3}{k-1} \left[ (1-\nu) + 2(1+\nu) \frac{k^2 \ln k}{k^2 - 1} \right] \quad (2.13)$$

The radial displacement of the flange at the junction with the shell is given by:

$$w_f = \left( p + Q_o \frac{t_f}{2} \right) \frac{R}{E} \left[ \frac{k^2 + 1}{k^2 - 1} + \nu \right] + \theta_f \frac{t_f}{2} \quad (2.14)$$

### 2.3.4 Shell Stress Analysis

The evaluation of the high local shell stress requires an analysis of the discontinuity effect at the junction of the shell and the flange ring in the absence of a hub. In this investigation, the different types of shells, including cylindrical, spherical, conical, and dished, were connected directly to the ring. It should be noted that a small hub or a fillet is usually considered to attenuate the stress concentration. However, this study sought to investigate the discontinuity effect and its influence on the bolted flange joint behavior (Jawad & Farr, 2019; Moss, 2014).

### 2.3.4.1 Cylindrical Shell

Figure 2.4 shows the different applied forces and moments acting on the long cylinder, including the discontinuity loads generated at the junction.

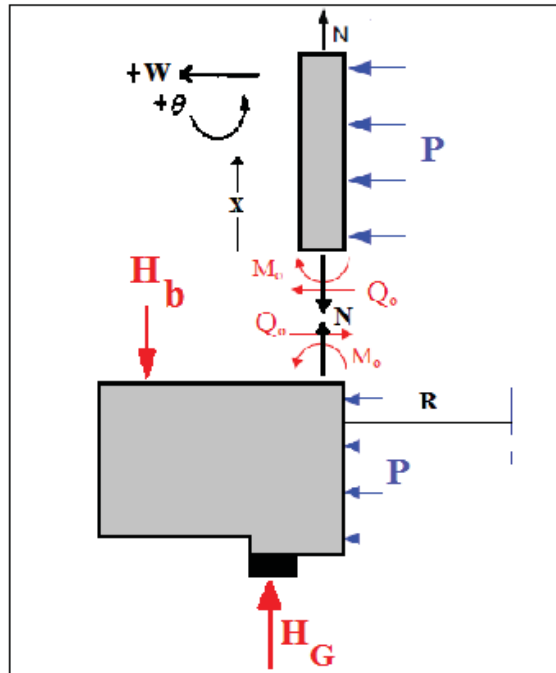


Figure 2.4 Flange ring and cylindrical shell

The radial displacement and rotation are given by:

$$w_c = w_p + w_{Q_0} + w_{M_0} \quad (2.15)$$

$$w_c = \frac{pR^2}{Et_s} \left(1 - \frac{\nu}{2}\right) + \frac{Q_0}{2\beta_s^3 D_s} + \frac{M_0}{2\beta_s^2 D_s} \quad (2.16)$$

And

$$\theta_c = -\theta_{Q_0} - \theta_{M_0} \quad (2.17)$$

$$\theta_c = -\frac{2Q_0\beta_s^2}{k_s} - \frac{4M_0\beta_s^3}{k_s} \quad (2.18)$$

Where  $D_s$  and  $\beta_s$  are defined as below:

$$D_s = \frac{Et_s^3}{12(1-\nu^2)}, \quad \beta_s = \frac{\sqrt[4]{3(1-\nu^2)}}{\sqrt{Rt_s}}, \quad k_s = \frac{Et_s}{R^2} \quad (2.19)$$

In the bolt-up step, there is no internal pressure or hydrostatic force. The bolt and gasket forces  $H_b$  and  $H_g$ , as well as the edge loads  $M_0$  and  $Q_0$ , can be determined for each working condition.

The stresses, displacement, rotation, bending moment, and shear force created by the edge loads  $M_0$  and  $Q_0$  as a function of the axial distance are obtained as follows:

$$w_s(x) = \frac{Q_0}{2\beta_s^3 D_s} f_1(\beta_s x) + \frac{M_0}{2\beta_s^2 D_s} f_2(\beta_s x) \quad (2.20)$$

$$\theta_s(x) = \frac{-Q_0}{2\beta_s^2 D_s} f_3(\beta_s x) - \frac{M_0}{\beta_s^3 D_s} f_1(\beta_s x) \quad (2.21)$$

$$M(x) = \frac{Q_0}{\beta_s} f_4(\beta_s x) + M_0 f_3(\beta_s x) \quad (2.22)$$

$$Q(x) = Q_0 f_2(\beta_s x) - 2M_0 \beta_s f_4(\beta_s x) \quad (2.23)$$

Where:

$$f_1(\beta_s x) = e^{-\beta_s x} \cos \beta_s x \quad (2.24)$$

$$f_2(\beta_s x) = e^{-\beta_s x} (\cos \beta_s x - \sin \beta_s x) \quad (2.25)$$

$$f_3(\beta_s x) = e^{-\beta_s x} (\cos \beta_s x + \sin \beta_s x) \quad (2.26)$$

$$f_4(\beta_s x) = e^{-\beta_s x} \sin \beta_s x \quad (2.27)$$

The longitudinal and tangential stresses of the cylindrical shell at the inner and outer surfaces are given as a function of axial distance from the junction:

$$\sigma_l(x) = \frac{pR}{2t_s} \pm \frac{6M(x)}{t_s^2} \quad (2.28)$$

$$\sigma_t(x) = \frac{pR}{t_s} + \frac{Ew_s(x)}{R} \pm \frac{6\nu M(x)}{t_s^2} \quad (2.29)$$

### 2.3.4.2 Spherical Shell

Figure 2.5 shows the geometry of a spherical shell subjected to the internal pressure and edge loads. For this type of head, the equations of the displacement and rotation at the junction are given by:

$$w_s = \frac{pR^2}{2Et_s}(1-\nu_s) + \frac{Q_0}{2\beta_s^3 D_s} + \frac{M_0}{2\beta_s^2 D_s} \quad (2.30)$$

$$\theta_s = -\frac{2Q_0\beta_s^2}{k_s} - \frac{4M_0\beta_s}{k_s} \quad (2.31)$$

The displacement, rotation, moment, and shear force at any angle  $\phi$  from the junction are as follows:

$$w_s(x) = \frac{Q_0 \sin^2 \phi}{2\beta_s^3 D_s} f_1(\beta_s x) + \frac{M_0 \sin \phi}{2\beta_s^2 D_s} f_2(\beta_s x) \quad (2.32)$$

$$\theta_s(x) = \frac{Q_0 \sin \phi}{2\beta_s^2 D} f_3(\beta_s x) + \frac{M_0}{\beta D} f_1(\beta_s x) \quad (2.33)$$

$$M(x) = \frac{Q_0 \sin \phi}{\beta} f_4(\beta x) + M_0 f_3(\beta x) \quad (2.34)$$

$$Q(x) = Q_0 \sin \phi f_2(\beta x) - 2\beta M_0 f_4(\beta x) \quad (2.35)$$

Where:

$$x = \alpha R = \left(\frac{\pi}{2} - \phi\right)R \quad (2.36)$$

The functions  $f$  are given by Equations 2.24 to 2.27. Therefore, the longitudinal and tangential stresses for the spherical shell can be obtained as follows:

$$\sigma_r(x) = \frac{pR}{2t_s} \pm \frac{6M(x)}{t_s^2} \quad (2.37)$$

$$\sigma_r(x) = \frac{pR}{2t_s} + \frac{Ew_s(x)}{R} \pm \frac{6\nu M(x)}{t_s^2} \quad (2.38)$$

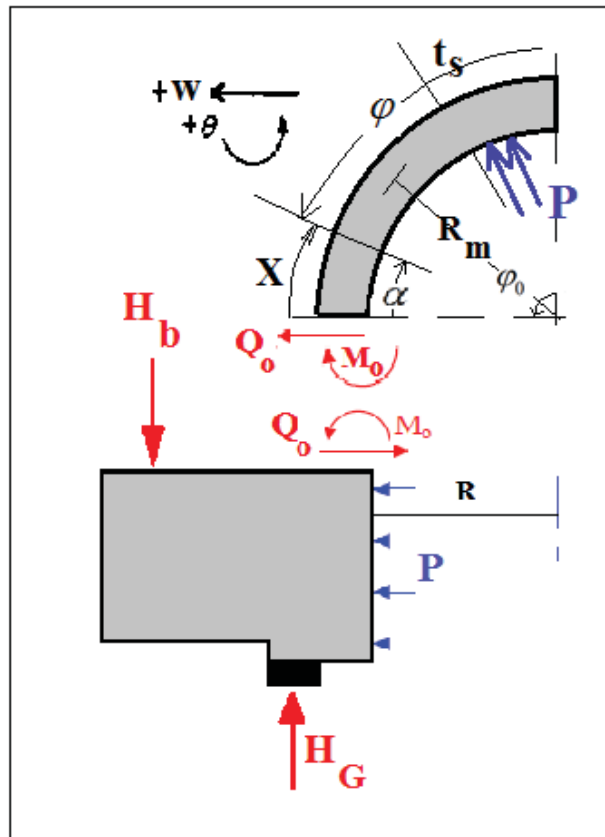


Figure 2.5 Flange ring and spherical shell

### 2.3.4.3 Dished Shell

The displacement and rotation at angle  $\phi$  from the dished shell axis can be presented as follows (Flügge, 1973):

$$\begin{aligned}
w_s &= \frac{R\zeta\sqrt{2}}{Et_s} [A_1(\text{beix} + x^{-1}(1+\nu)\text{ber}'x) \\
&\quad - A_2(\text{berx} + x^{-1}(1+\nu)\text{bei}'x) + B_1(\text{keix} + x^{-1}(1+\nu)\text{ker}'x) \\
&\quad - B_2(\text{kerx} + x^{-1}(1+\nu)\text{kei}'x)]
\end{aligned} \tag{2.39}$$

And

$$\begin{aligned}
\lambda_s(1-\nu^2)\theta_s &= A_1(2\zeta^2\text{bei}'x - \nu\text{ber}'x) \\
&\quad - A_2(2\zeta^2\text{ber}'x + \nu\text{bei}'x) + B_1(2\zeta^2\text{kei}'x - \nu\text{ker}'x) \\
&\quad - B_2(2\zeta^2\text{ker}'x + \nu\text{kei}'x)
\end{aligned} \tag{2.40}$$

Where:

$$x = \zeta_s \phi \sqrt{2} \tag{2.41}$$

$$\zeta_s = \left[ 3(1-\nu^2) \frac{R^2}{t_s^2} - \frac{\nu^2}{4} \right]^{1/4} \tag{2.42}$$

$$\lambda_s = \frac{Et_s}{1-\nu^2} \tag{2.43}$$

The general equations for shear forces,  $Q_\phi$ , membrane forces ( $N_\phi$ ,  $N_\theta$ ) and bending moments ( $M_\phi$ ,  $M_\theta$ ) are given by:

$$Q_\phi = A_1\text{ber}'x + A_2\text{bei}'x + B_1\text{ker}'x + B_2\text{kei}'x \tag{2.44}$$

$$N_\phi = -\phi^{-1}Q_\phi \tag{2.45}$$

$$\begin{aligned}
N_\theta &= \zeta_s \sqrt{2} [A_1(\text{beix} + x^{-1}\text{ber}'x) \\
&\quad - A_2(\text{berx} - x^{-1}\text{bei}'x) + B_1(\text{keix} + x^{-1}\text{ker}'x) \\
&\quad - B_2(\text{kerx} - x^{-1}\text{kei}'x)]
\end{aligned} \tag{2.46}$$

$$\begin{aligned}
M_\phi &= \frac{D_s\zeta\sqrt{2}}{\lambda R(1-\nu^2)} \{ A_1[2\zeta_s^2(\text{berx} - \frac{1-\nu}{x}\text{bei}'x) + \nu(\text{beix} + \frac{1-\nu}{x}\text{ber}'x)] \\
&\quad + A_2[2\zeta_s^2(\text{beix} + \frac{1-\nu}{x}\text{ber}'x) - \nu(\text{berx} - \frac{1-\nu}{x}\text{bei}'x)] \\
&\quad + B_1[2\zeta_s^2(\text{kerx} - \frac{1-\nu}{x}\text{kei}'x) + \nu(\text{keix} + \frac{1-\nu}{x}\text{ker}'x)] \\
&\quad + B_2[2\zeta_s^2(\text{keix} + \frac{1-\nu}{x}\text{ker}'x) - \nu(\text{kerx} - \frac{1-\nu}{x}\text{kei}'x)] \}
\end{aligned} \tag{2.47}$$

$$\begin{aligned}
M_\theta = & \frac{D_s \zeta_s \sqrt{2}}{\lambda_s a (1-\nu^2)} \left\{ A_1 \left[ 2\zeta_s^2 \nu \text{ber}x + \frac{1-\nu}{x} \text{bei}'x \right] + \nu \left( \nu \text{bei}x - \frac{1-\nu}{x} \text{ber}'x \right) \right. \\
& + A_2 \left[ 2\zeta_s^2 \left( \nu \text{bei}x - \frac{1-\nu}{x} \text{ber}'x \right) - \nu \left( \nu \text{ber}x + \frac{1-\nu}{x} \text{bei}'x \right) \right] \\
& + B_1 \left[ 2\zeta_s^2 \left( \nu \text{ker}x + \frac{1-\nu}{x} \text{kei}'x \right) + \nu \left( \nu \text{kei}x - \frac{1-\nu}{x} \text{ker}'x \right) \right] \\
& \left. + B_2 \left[ 2\zeta_s^2 \left( \nu \text{kei}x - \frac{1-\nu}{x} \text{ker}'x \right) - \nu \left( \nu \text{ker}x + \frac{1-\nu}{x} \text{kei}'x \right) \right] \right\}
\end{aligned} \tag{2.48}$$

It should be noted that in Equations 2.44 to 2.48,  $A_2$  and  $B_2$  are equal to zero when the shell extends from the junction to  $\phi = 0$  (Figure 2.6).

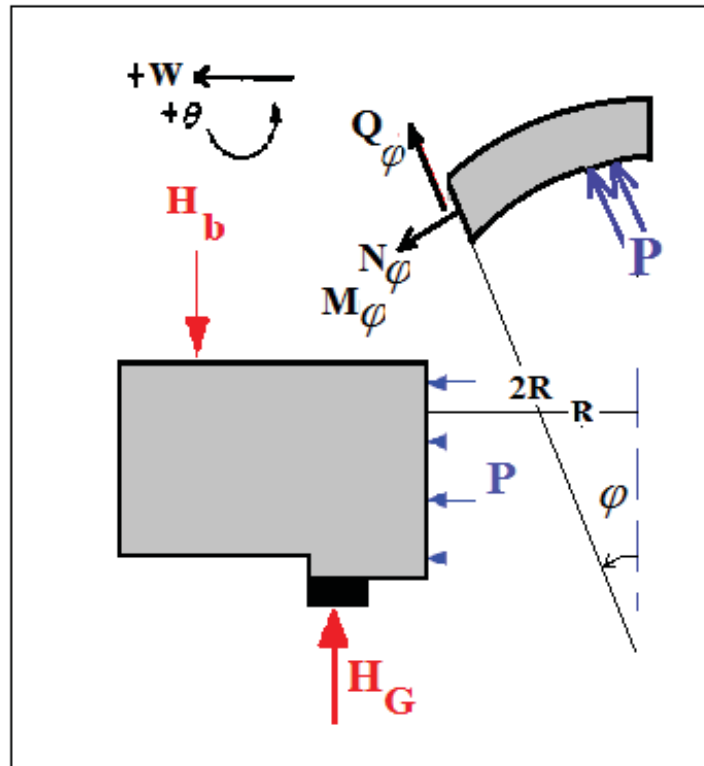


Figure 2.6 Flange ring and dished shell

The longitudinal and tangential stresses are given by:

$$\sigma_l(x) = \frac{pR}{2t_s} + \frac{N_\phi(x)}{t_s} \pm \frac{6M_\phi(x)}{t_s^2} \quad (2.49)$$

$$\sigma_\theta(x) = \frac{pR}{2t_s} + \frac{N_\theta(x)}{t_s} \pm \frac{6M_\theta(x)}{t_s^2} \quad (2.50)$$

#### 2.3.4.4 Conical Shell

Similarly, the displacement and rotation at any position on the conical shell, shown in Figure 2.7, can be obtained as follows (Flugge, 1973):

$$\begin{aligned} w_s = & -\frac{\sin \alpha \tan \alpha}{2Et_s} [A_1(-x\text{ber}'x + 2(1+\nu)\text{ber}x - 4(1+\nu)x^{-1}\text{bei}'x) \\ & -A_2(x\text{bei}'x - 2(1+\nu)\text{beix} - 4(1+\nu)x^{-1}\text{ber}'x) \\ & -B_1(x\text{ker}'x - 2(1+\nu)\text{ker}x + 4(1+\nu)x^{-1}\text{kei}'x) \\ & +B_2(x\text{kei}'x - 2(1+\nu)\text{keix} - 4(1+\nu)x^{-1}\text{ker}'x)] \end{aligned} \quad (2.51)$$

And

$$\begin{aligned} \theta = & \frac{2 \cot \alpha \sqrt{3(1-\nu^2)}}{Et^2} [A_1(\text{beix} + 2x^{-1}\text{ber}'x) \\ & -A_2(\text{ber}x - 2x^{-1}\text{bei}'x) + B_1(\text{keix} + 2x^{-1}\text{ker}'x) \\ & -B_2(\text{ker}x - 2x^{-1}\text{kei}'x)] \end{aligned} \quad (2.52)$$

Where:

$$x = \chi_s \sqrt{s} \quad (2.53)$$

And

$$\chi_s = 2[3(1-\nu^2)]^{1/4} \sqrt{\frac{2 \cot(\alpha)}{t_s}} \quad (2.54)$$

The general equations for shear forces,  $Q_s$ , membrane forces ( $N_s$ ,  $N_\theta$ ) and bending moments ( $M_s$ ,  $M_\theta$ ) are given by:

$$Q_s = \frac{1}{s} [A_1(\text{ber}x - 2x^{-1}\text{bei}'x) + A_2(\text{beix} + 2x^{-1}\text{ber}'x) + B_1(\text{ker}x - 2x^{-1}\text{kei}'x) + B_2(\text{keix} + 2x^{-1}\text{ker}'x)] \quad (2.55)$$

$$N_s = -Q_s \cot \alpha \quad (2.56)$$

$$N_\theta = -\frac{\cot \alpha}{2s} [A_1(x\text{ber}'x - 2\text{ber}x + 4x^{-1}\text{bei}'x) + A_2(x\text{bei}'x - 2\text{beix} - 4x^{-1}\text{ber}'x) + B_1(x\text{ker}'x - 2\text{ker}x + 4x^{-1}\text{kei}'x) + B_2(x\text{kei}'x - 2\text{keix} - 4x^{-1}\text{ker}'x)] \quad (2.57)$$

$$M_s = 2x^{-2} \{A_1[x\text{bei}'x - 2(1-\nu)(\text{beix} + 2x^{-1}\text{ber}'x)] - A_2[x\text{ber}'x - 2(1-\nu)(\text{ber}x - 2x^{-1}\text{bei}'x)] + B_1[x\text{kei}'x - 2(1-\nu)(\text{keix} + 2x^{-1}\text{ker}'x)] - B_2[x\text{ker}'x - 2(1-\nu)(\text{ker}x - 2x^{-1}\text{kei}'x)]\} \quad (2.58)$$

$$M_\theta = 2x^{-2} \{A_1[\nu x\text{bei}'x + 2(1-\nu)(\text{beix} + 2x^{-1}\text{ber}'x)] - A_2[\nu x\text{ber}'x + 2(1-\nu)(\text{ber}x - 2x^{-1}\text{bei}'x)] + B_1[\nu x\text{kei}'x + 2(1-\nu)(\text{keix} + 2x^{-1}\text{ker}'x)] - B_2[\nu x\text{ker}'x + 2(1-\nu)(\text{ker}x - 2x^{-1}\text{kei}'x)]\} \quad (2.59)$$

It should be noted that  $A_2$  and  $B_2$  are equal to zero when the shell extends from the junction to the apex of the cone,  $s = 0$  (Figure 2.7). As a result, the longitudinal and tangential stresses of the conical shell can be obtained as follows:

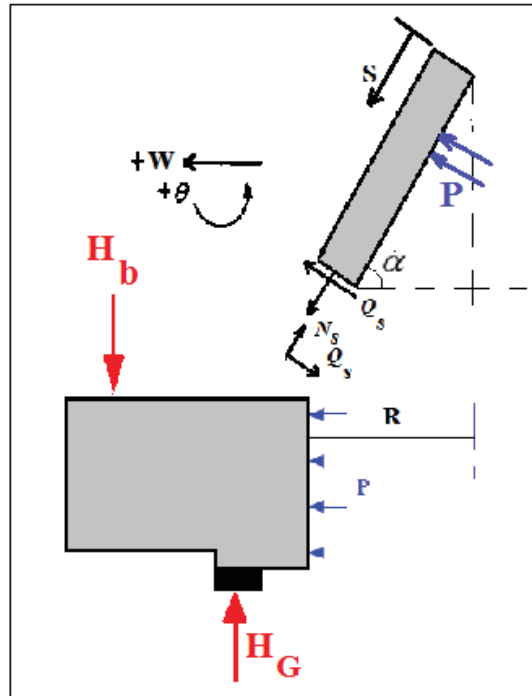


Figure 2.7 Flange ring and conical shell

$$\sigma_l(x) = \frac{ps \tan \alpha}{2t_s} + \frac{N_s(x)}{t_s} \pm \frac{6M_s(x)}{t_s^2} \quad (2.60)$$

$$\sigma_\theta(x) = \frac{ps \tan \alpha}{t_s} + \frac{N_\theta(x)}{t_s} \pm \frac{6M_\theta(x)}{t_s^2} \quad (2.61)$$

## 2.4 Finite Element Modeling

To validate the analytical results, finite element modeling of the bolted flange joint, including the shell or head, flange ring, gasket, and bolts, was conducted for the different types of shell connections, namely cylindrical, spherical, dished, and conical. The bolted flange joint was composed of two identical flanges and therefore was used in a symmetrical configuration with respect to the gasket di thickness plan for simplification.

In order to compare the stresses at the junction under the same conditions, it was essential to use the same materials and geometric parameters for the different shell connections of the bolted flange joint. Table 2.1 shows the specifications and data used in the simulations. Three different sizes of bolted flange joints were modeled and simulated, namely NPS 26, 48, and 60 (class 300, series A), to investigate the effect of flange size variation. It should be noted that the hub was not included in the analytical or numerical modeling. In addition, for the above-mentioned flange sizes, the corresponding results of the flange rotation and stress analysis are reported in Chapter 4.

ANSYS Workbench software was utilized to model and simulate the different types of shells with the flange ring. Due to the axial symmetry, and in order to simplify the analysis and decrease the simulation central processing unit (CPU) time, a half portion model of the bolted flange joint was simulated (Figure 2.8). In the case of the cylindrical shell, a sufficient length of the shell was modeled to attenuate the stress effects. Because of the axial symmetry, there was neither axial displacement nor rotation at the gasket mid-plane passing through the mid-length of the bolt. Moreover, the cyclic boundary condition was considered at the two cut sections between bolts in the axial direction.

Additionally, to obtain more precise stress measurements, SOLID186 elements (20 nodes per element) were applied, and the mesh was refined to reach the convergence criterion of less than 1% in the shell equivalent stress at the junction. PRETS179 elements were used to model the pretension load of the bolts. CONTA174 elements were used to define the type of contact between the flange ring and the gasket and between the bolts and the flange ring, with the friction coefficients of 0.7 and 0.15, respectively.

Table 2.1 Specifications and data used in the FEM model for different flange sizes

<b>Model Properties</b>			
<b>Flange size (in.)</b>	<b>26</b>	<b>48</b>	<b>60</b>
Outer diameter of flange (mm)	970	1465	1810
Inner diameter of flange (mm)	635	1193.8	1498.6
Bolt circle diameter (mm)	876.3	1371.6	1701.8
Head radius (mm)	317.5	596.9	749.3
Head thickness (mm)	12.7	12.7	12.7
Raised face height (mm)	2	2	2
Flange thickness (mm)	77.8	131.8	162
Bolt diameter (mm)	41.275	47.63	57.15
Number of bolts (mm)	32	32	32
Gasket height (mm)	2	2	2
Gasket width (mm)	22.15	20.7	25.5
Inner diameter of the gasket (mm)	704.7	1235.2	1575
Outer diameter of gasket (mm)	749	1276.6	1626
Bolt preload (kN)	104.6	204.6	380.32
Internal pressure (MPa)	2.07	2.07	2.07
Cone angle (deg)	45	45	45

Internal pressure of 300 psi was applied to the internal surfaces of the connected shell. In terms of the cylindrical shell, an axial surface load was added to the cylindrical shell end, in addition to lateral pressure to simulate the hydrostatic end effect. The resulting pull-out stress on the cylindrical shell was implemented based on the different flange internal radius and shell thicknesses for each flange size. The material of the flanges was ASTM A105 and the bolts were made of ASTM A193 B7. Young's Modulus and Poisson's ratio were 207 GPa and 0.3, and yield stress was 400 MPa.

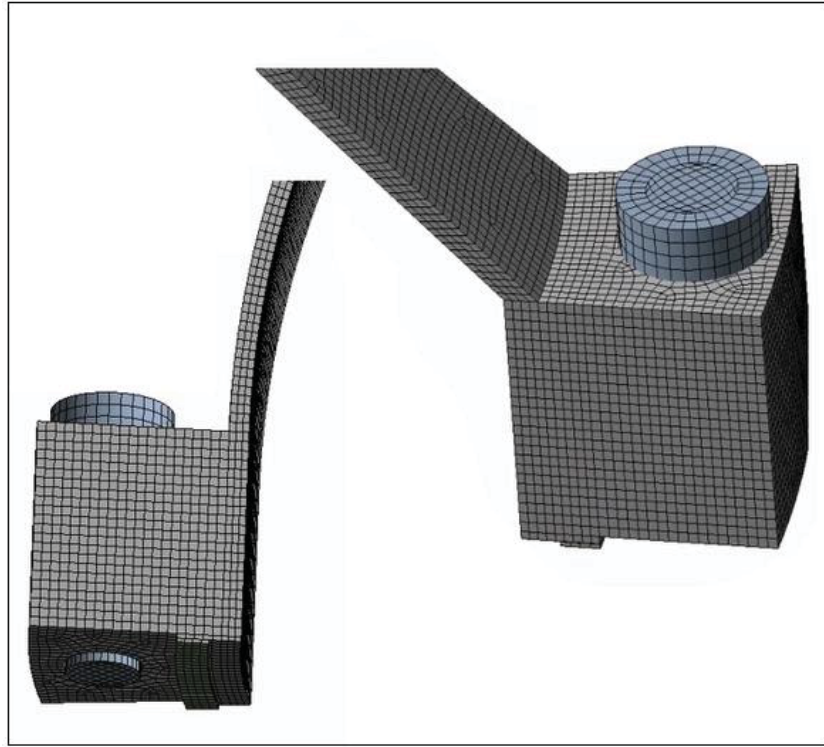


Figure 2.8 FEM bolted flange joint model in ANSYS



## CHAPTER 3

### GASKET CONTACT STRESS AND TIGHTNESS

#### 3.1 Introduction

This chapter presents the results of the flange rotation and gasket contact stress in four different types of flange-to-shell connections for three different flange sizes. These results demonstrate the tight relationship between these parameters in the bolted flange joint analysis.

#### 3.2 Flange Rotation

Flange rotation is an essential parameter that influences gasket integrity and leakage. Excessive flange rotation can generate high local stresses, which can damage sheet gaskets or result in lift-off of certain gaskets, such as spiral wound. Therefore, the ASME code limits rotation to 0.3 degrees for non-hubbed flanges. Figures 3.1 through 3.6 show the finite element flange ring face axial displacements for the different types of shell connections during bolt-up and pressurization. The analysis was performed for three different sizes of flanges: NPS 26, 48, and 60.

The displacements were plotted as a function of the radial position on the flange ring, and the curves obtained were straight lines. It should be noted that the flange ring rotations were determined from the slope of these lines.

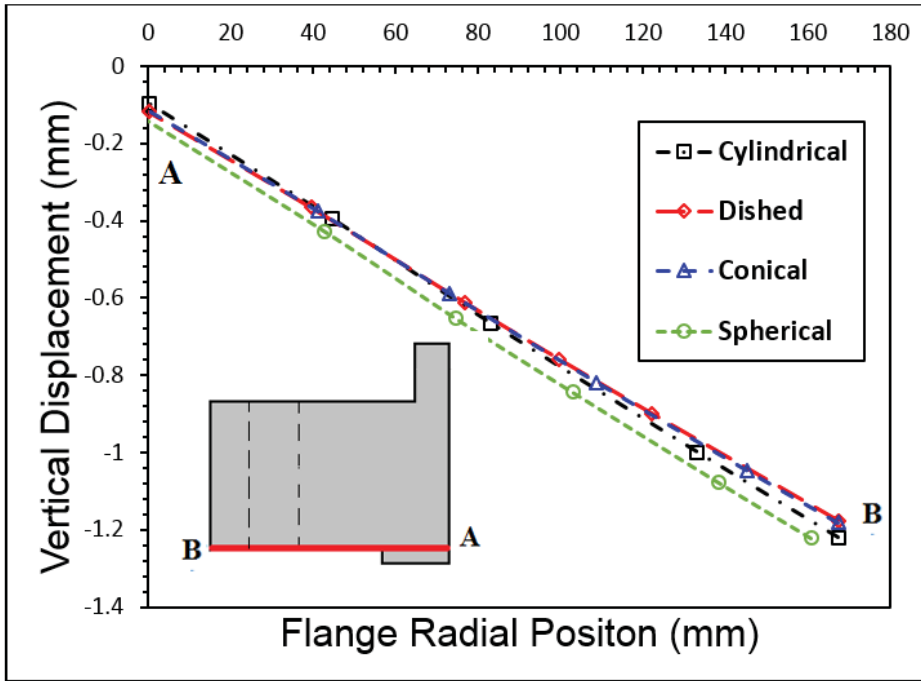


Figure 3.1 Flange rotation for shell connections during bolt-up (NPS 26 class 300)

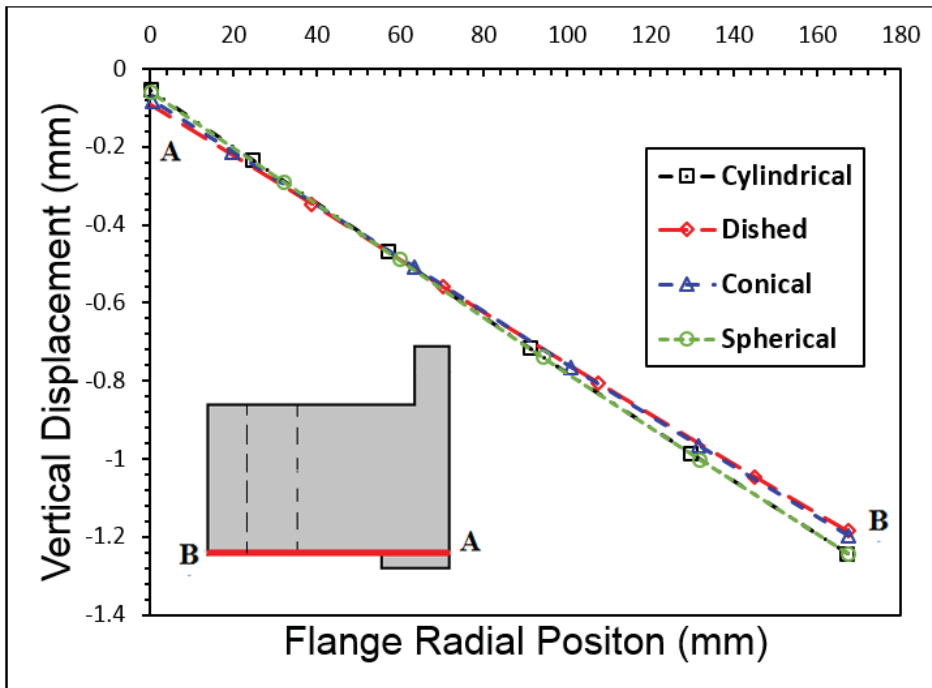


Figure 3.2 Flange rotation for shell connections during pressurization (NPS 26 class 300)

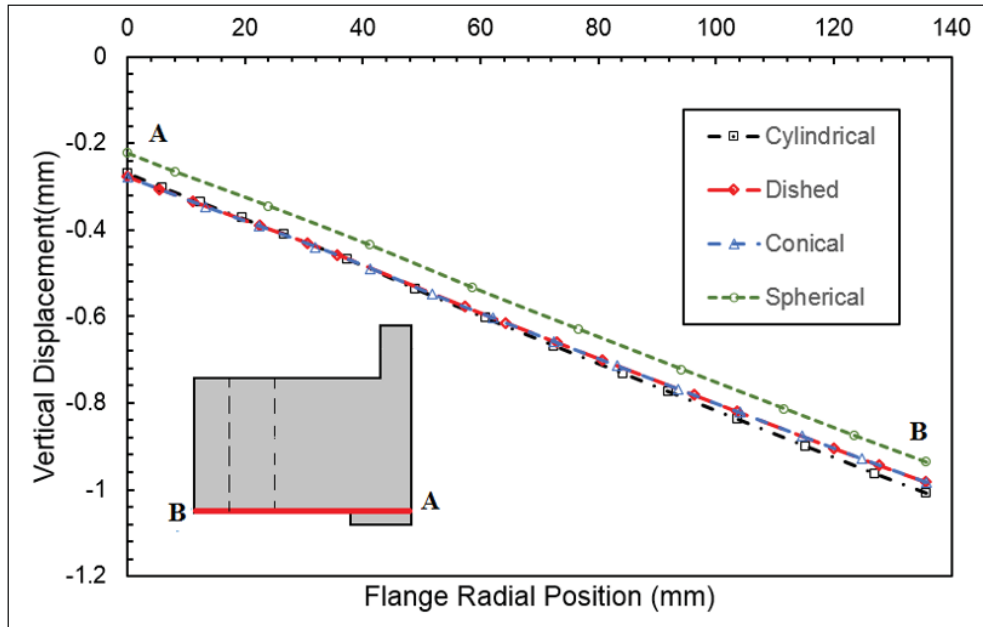


Figure 3.3 Flange rotation for shell connections during bolt-up (NPS 48 class 300)

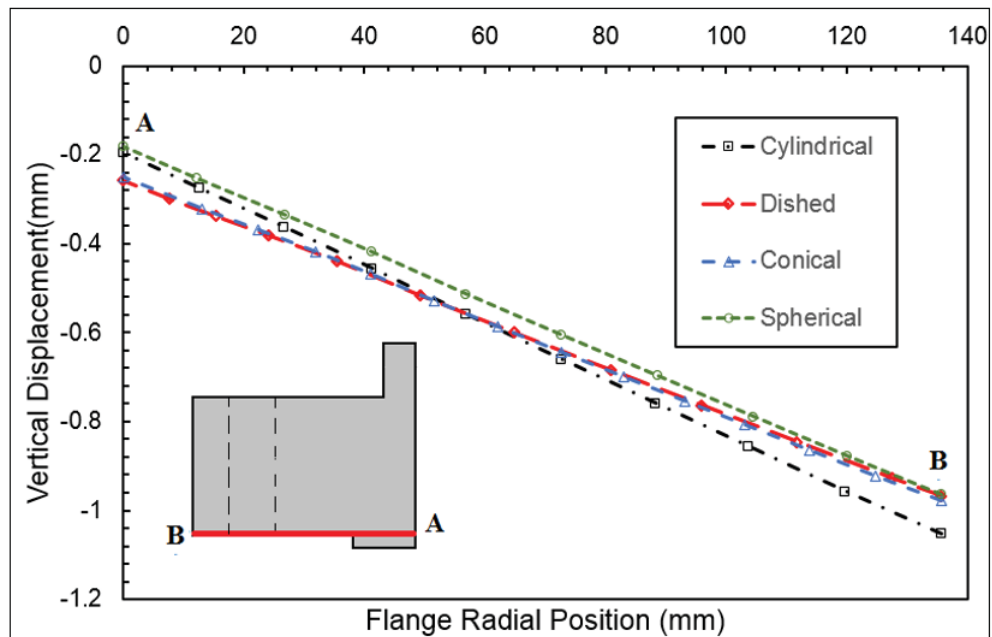


Figure 3.4 Flange rotation for shell connections during pressurization (NPS 48 class 300)

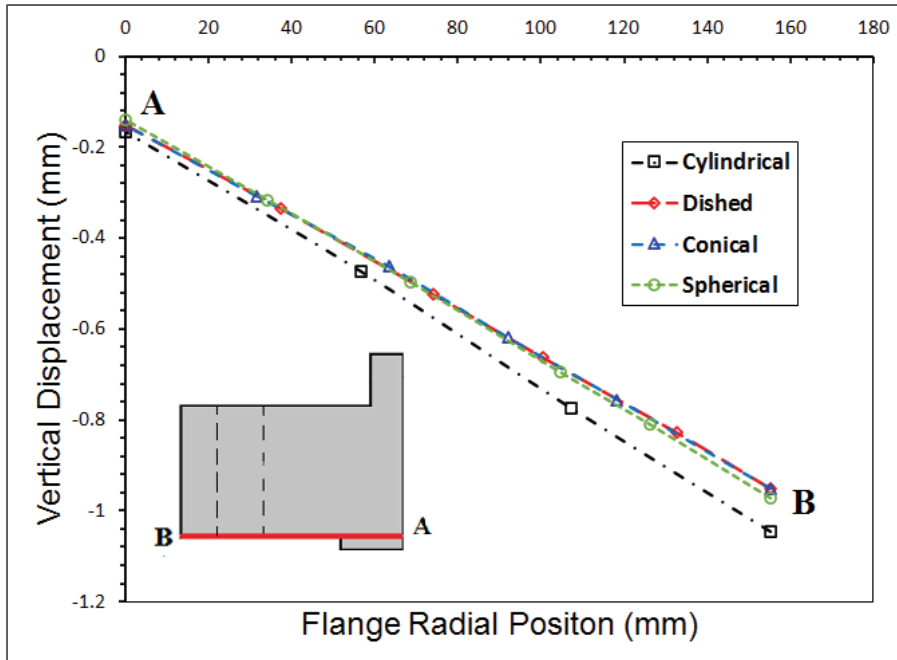


Figure 3.5 Flange rotation for shell connections during bolt-up (NPS 60 class 300)

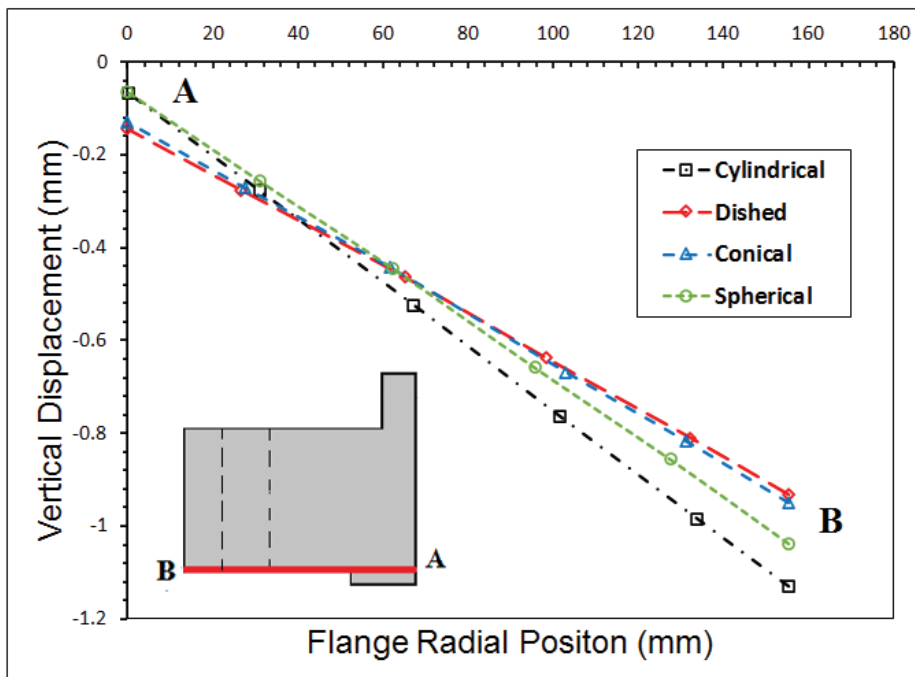


Figure 3.6 Flange rotation for shell connections during pressurization (NPS 60 class 300)

Table 3.1 Analytical and numerical results of flange rotation for four types of shell connections during bolt-up and pressurization

<b>Flange Rotation (deg)</b>					
<b>Flange size (in.)</b>	<b>Shell connection</b>	<b>Bolt-up</b>		<b>Pressurization</b>	
		<b>FEM</b>	<b>Anal.</b>	<b>FEM</b>	<b>Anal.</b>
26	Cylindrical	0.384	0.384	0.407	0.392
	Dished	0.367	0.349	0.372	0.357
	Conical	0.367	0.364	0.384	0.372
	Spherical	0.384	0.384	0.407	0.392
48	Cylindrical	0.315	0.309	0.367	0.338
	Dished	0.298	0.281	0.304	0.286
	Conical	0.298	0.298	0.309	0.304
	Spherical	0.304	0.309	0.332	0.332
60	Cylindrical	0.327	0.318	0.395	0.373
	Dished	0.292	0.297	0.292	0.298
	Conical	0.298	0.311	0.304	0.325
	Spherical	0.309	0.318	0.361	0.365

During bolt-up, all flanges rotated at nearly the same rate, except the cylindrical configuration, which rotated slightly more. More rotation was also observed with the cylindrical shell during pressurization, which was likely because the barreling effect due to side pressure was more significant in this case. The application of pressure had almost no effect on the dished configuration. Table 3.1 provides a comparison of the flange rotations obtained by the finite element and analytical models. As shown, there was good agreement between the two methods.

### 3.3 Gasket Contact Stress

Another important parameter to evaluate is gasket contact stress distribution because it pertains to the flange rotation and directly controls the leak rate in bolted flange joints. Generally, the amount of contact stress of the gasket is not uniform across the gasket width, but increases gradually from the inside to the outside radius. Figures 3.7 through 3.12 illustrate the distribution of gasket contact stress with respect to the gasket width for three sizes of flanges

and four different types of head connections during bolt-up and pressurization. As shown, contact stress during pressurization was always lower than during bolt-up. This was due to hydrostatic end thrust, which can unload the gasket. The gasket stress distribution during the bolt-up was also slightly more pronounced in the spherical shell case. All the other shell type curves are superimposed during bolt-up, which was confirmed by the fact that their rotations were the same.

It should be noted that after applying internal pressure, the average amounts of gasket stress in the dished shell and conical shell were higher than in the spherical and cylindrical shell cases. In fact, gasket stress may be affected by a variety of head geometries. In the cylindrical and spherical shell, the pressure acts on a larger lateral surface, creating more of a barreling effect, which can unload the gasket.

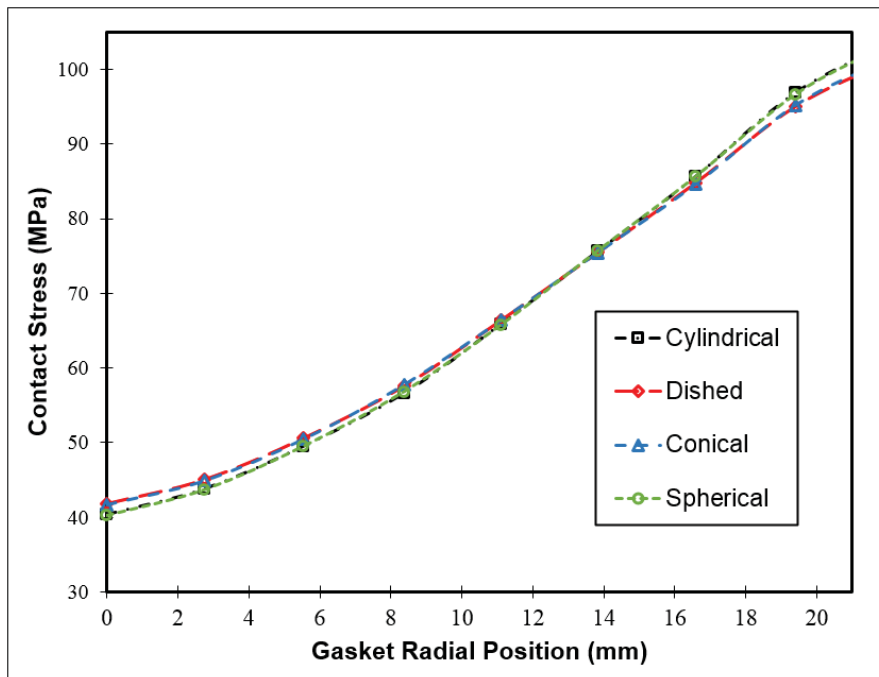


Figure 3.7 Gasket stress for shell connections during bolt-up (NPS 26 class 300)

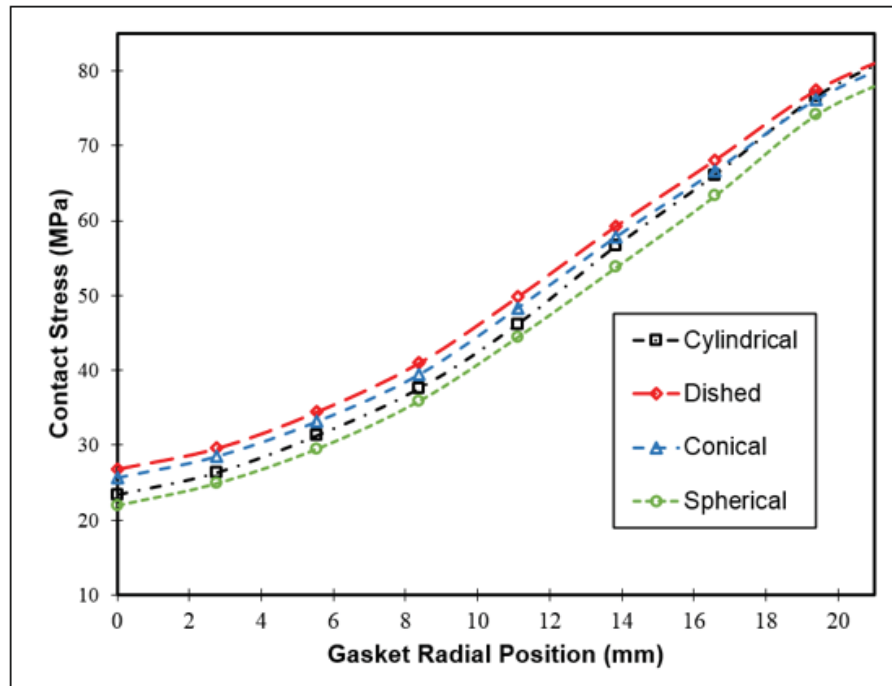


Figure 3.8 Gasket stress for shell connections during pressurization (NPS 26 class 300)

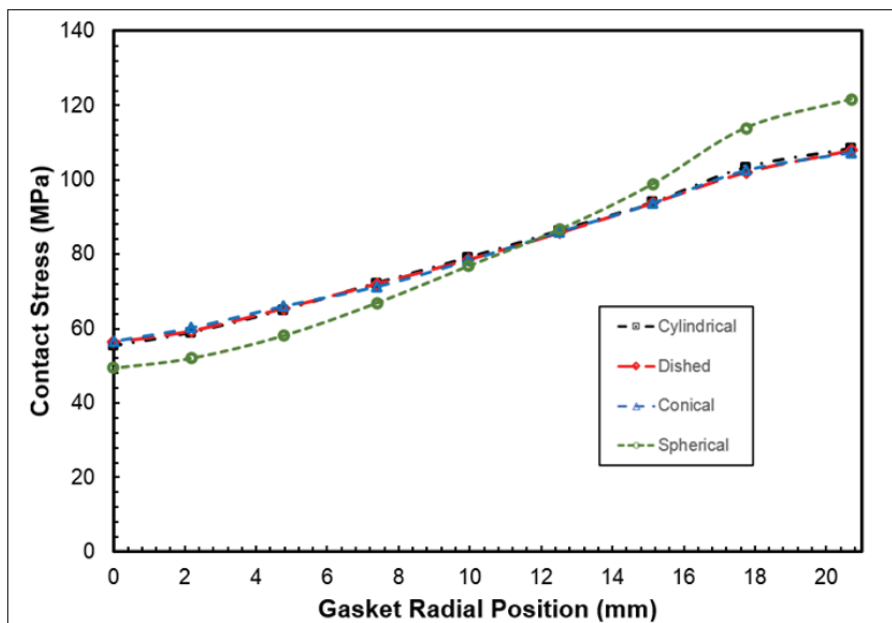


Figure 3.9 Gasket stress for shell connections during bolt-up (NPS 48 class 300)

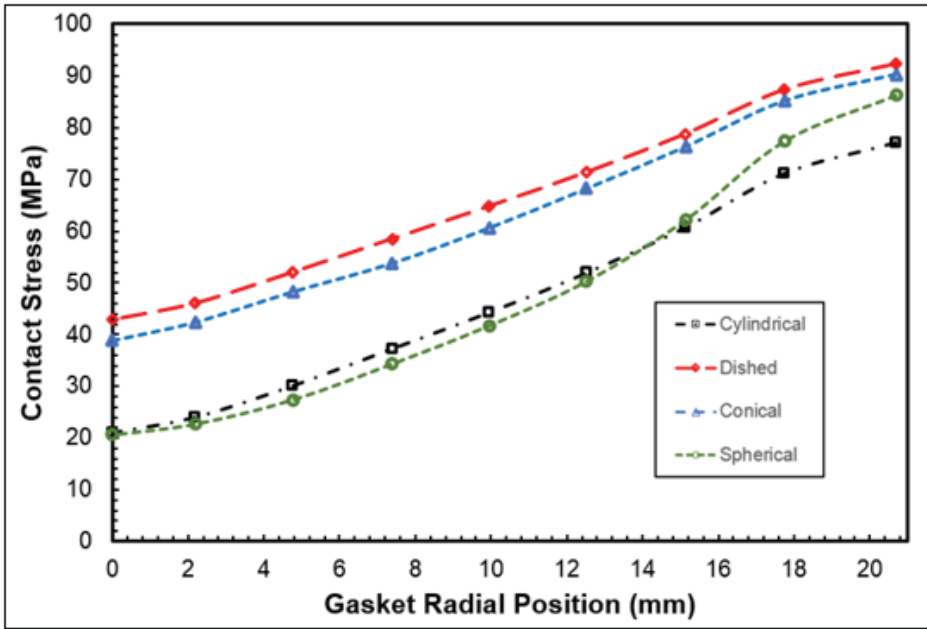


Figure 3.10 Gasket stress for shell connections during pressurization (NPS 48 class 300)

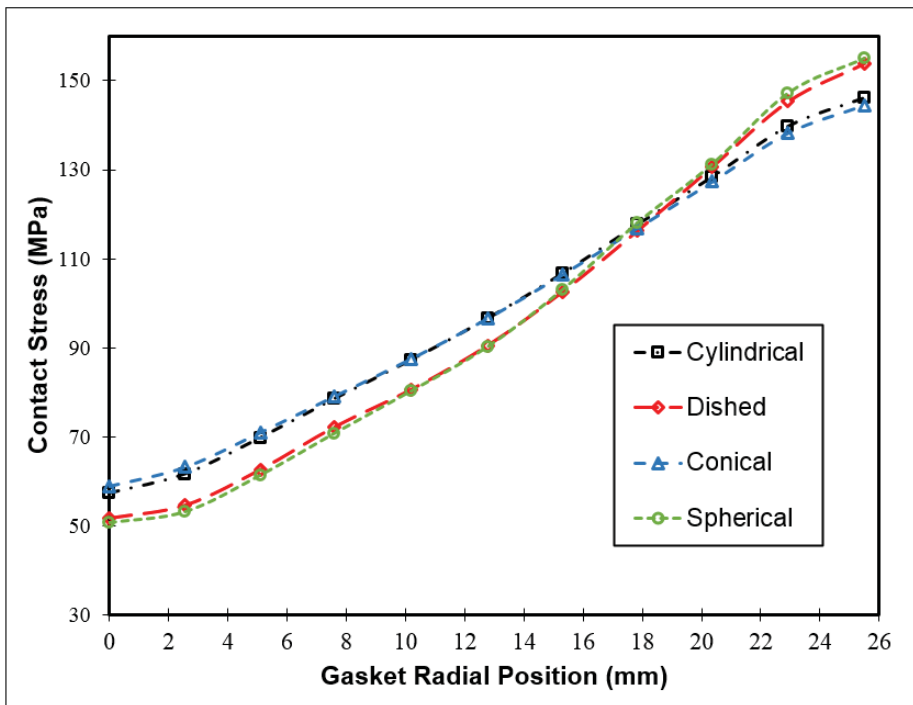


Figure 3.11 Gasket stress for shell connections during bolt-up (NPS 60 class 300)

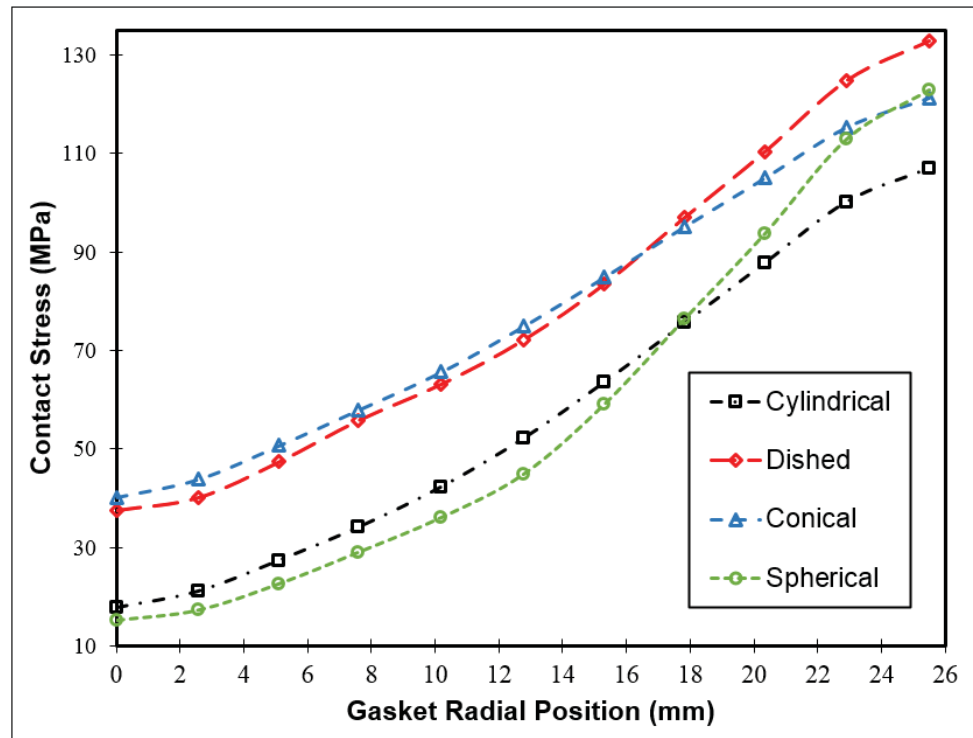


Figure 3.12 Gasket stress for shell connections during pressurization (NPS 60 class 300)

### 3.4 Tightness Criteria of Gasket

It is important to consider gasket compression when designing a bolted joint complex because it plays a crucial role in preventing leakage and avoid loss of revenue maintenance costs and human health and environment consequences. The long-term leak tightness of a bolted flange joint is determined by a number of parameters, including the gasket type, bolt load, flange rotation, internal pressure, external loads temperature and time exposure. However, there is a reliable criterion for evaluating gasket tightness based on internal pressure, such that the minimum amount of gasket contact stress must be at least twice the internal pressure in order to ensure gasket tightness from most gaskets according to the ASME BPV Code. Figures 3.7 through 3.12 show that the smallest amount of gasket contact stress was still sufficient to achieve gasket tightness based on this criterion. It should be noted that the most critical situation occurred during the pressurization process, when the amount of gasket contact stress

was reduced due to excessive flange rotation, especially in spherical and cylindrical heads. Nonetheless, even at flange size 60, the amount of gasket contact stress was sufficient to maintain gasket tightness.

## CHAPTER 4

### EFFECT OF SHELL GEOMETRY ON THE STRESS DISTRIBUTION AT THE JUNCTION WITH BOLTED FLANGE CONNECTIONS

M.Choulaei<sup>a</sup> and A. Bouzid<sup>b</sup>

<sup>a,b</sup> Department of Mechanical Engineering, École de technologie supérieure  
1100, Notre Dame Street West, Montreal, Quebec, Canada, H3C 1K3

Paper submitted to Journal of Pressure Vessel Technology

#### 4.1 Abstract

Due to their ease of installation and operation, bolted flange joints are widely used in a variety of pressure vessel applications across various industries. However, their structural integrity and leakage tightness depend not only on the operating conditions but also on the type of shell to which they are connected. The performance of different flange connection configurations could be considered as a criterion when selecting a movable head design. Unfortunately, the present ASME BPVC flange design does not incorporate a leakage criterion or a flexibility analysis to provide an accurate assessment of the different characteristics.

The purpose of this research was to assess the integrity and leakage tightness of several types of shells connected to a flange ring. The investigation examined crucial factors, such as flange rotation and stress distribution at the flange-shell junction, using various shell theories for three different flange sizes: NPS 26, 48, and 60. It also compared four common types of shell connections: cylindrical, spherical, dish, and conical. All of the shells were directly attached to the raised-face flange ring. Furthermore, these shell connections were simulated using a general-purpose finite element program for comparison with the analytical method and to validate the study. The nonlinear behavior of the gasket was taken into account in the finite element analysis but not in the analytical modeling.

**Keywords:** Bolted flange joints, shell connections, stress analysis, flange rotation, flange and shell stresses.

## 4.2 Introduction

Analyzing the various loading instances is a significant stage of engineering judgment, particularly when a range of components of pressure vessels are examined as feasible solutions. Some complex structures, such as bolted flange joints, may necessitate deep analysis to minimize the risk of failures. For example, discharge of volatile organic compounds owing to leaks can have disastrous implications for health and safety, in addition to industrial plant shutdowns and environmental concerns.

Unexpectedly large stresses in shells of bolted flange connections can sometimes cause shell rupture that results in the discharge of hazardous chemicals into the atmosphere. Furthermore, the shape and geometry of the flange ring and the shell type that form the junction can have a considerable impact on the load redistribution. Shell connections come in a variety of shapes and sizes, including cylindrical, semi-spherical, conical, torispherical, or dished, and they are used in a wide range of industries. Nevertheless, there are few comparisons to optimize the application of the different shell types in the literature (Jawad & Farr, 2019).

The modeling of different loads, including all acting forces and moments in the presence of a variety of shapes and geometries of a bolted flange joint, is a significant task in the design process. Several parameters, namely flange rotation, bolt load, and gasket contact pressure, are fundamental in assessing the correct behavior of the bolted flange joint. Previous research has analyzed various components of bolted joints, including their attachment to pressure vessels, using analytical, experimental, and computational methods under different loading circumstances, such as bolt-up, pressurization, thermal transient, and creep. Waters and Taylor (1927) and Waters et al. (1951) developed the current ASME design method of bolted flange connections, using shell and plate theories, to verify their integrity and leakage tightness. Koves (1996) provided an analytical method for analyzing the behavior of bolted flange joints

subjected to external loads. Other studies were conducted to enrich the research by including the three methods: experimental investigations, analytical modeling, and numerical analysis (Bouزيد, Chaaban & Bazergui, 1995; Mallard, Landry & Birembaut, 2002; Bouزيد & Nechache, 2005; Zhu, Bouزيد, Hong & Zhang, 2018). This triangularization method of validation is often used to support the general findings.

Based on the membrane theory of the shells of revolution, Zingoni (2001) developed a model to estimate the amount of stress and deformation in an egg-shaped sludge digester. He also improved the model to analyze the influence of edge loads on the stresses and deformations in the vicinity of the discontinuities using the bending moment theory (Zingoni, 2001). The results were significantly more accurate when adopting the bending moment theory. A few elaborate models were suggested to investigate the behavior of bolted flange joints using flexibility analysis, but no particular attention was paid to the stress distribution in the shell junction (Dudley, 1961; Murray & Stuart, 1961; Bouزيد & Beghoul, 2003). However, several numerical FEM studies were conducted to evaluate how various mechanical and thermal load scenarios, such as internal pressure, thermal expansion, external loads, and creep phenomena, influenced the leakage rate of the bolted flange joint. Abid and Nash (2006) investigated the performance of gasketed flange joints in the presence of a pressure and temperature combination. They looked at strength and sealing capability factors at the same time. Thermal and creep analysis of bolted flange joints was investigated by Nechache and Bouزيد (2005; 2007; 2008), who used a flange model with linear and rotational spring components to investigate the thermal and creep-relaxation behavior of bolted flange joints. They validated their model using a 3D finite element model, which is a reliable tool to simulate the interaction between the gasket and the bolted flange joint. They used two gasket models (corrugated metal sheet and compressed asbestos) in their research to establish a meaningful comparison between gasket contact stress and displacement. They also proposed an analytical approach to quantify the effect of creep on the amount of tightening load applied to bolted flange joints in increased temperature situations. Finally, they looked at how bolted flange joints relax owing to gasket and bolt material creep, as well as flange and shell creep.

Krishna et al. (2007) used experimental gasket nonlinear characteristic data to conduct a 3D finite element analysis of a bolted flange joint to check its leak tightness. They used three distinct gasket materials, asbestos-filled, graphite-filled, and PTFE-filled spiral-wrapped, to mimic the nonlinear behavior of the gasket during loading and unloading to cover bolt-up and pressurization. They also presented a 3D ANSYS model for analyzing the integrated bolted flange complexity and assessing the influence of the gasket on flange behavior. Of interest was the relationship between flange rotation and axial bolt force as a function of internal pressure. Kobayashi (2014) investigated the viscoelastic behavior of the gasket and its deformation under stress. In his model, he used springs to represent all components of the gasketed flanged connection. In addition, he estimated the bolt force and gasket deflection as a function of time. Kobayashi results were reached by taking the impact of the gasket's short-term creep into consideration. He also showed how gasket compression affects leak rate and how it changes over time.

Luyt et al. (2017) used nonlinear finite element modeling to study the effect of gasket creep-relaxation on circular bolted flange connections. They looked at the contact pressure between the gasket and the flange body as a key factor in determining if the bolted flange joint is tight. They compared the leakage performance of flat-faced and raised-face flanges (class PN10, size DN50) using non-asbestos compressed fiber with aramid and nitrile rubber binder sheet gaskets. They also used ANSYS software to model the integrated bolted flange joint in order to back up their experimental findings. The number of bolt tightening passes and the time interval used to tighten the bolts had a considerable impact on the bolted flange joint creep-relaxation. Several other publications focused on the elastic interaction of bolt tightening, bending flanges, and bolt spacing based on various theories, including bending of ring and plates and beam on elastic foundation (Borak & Marcian, 2014; Choulaei, Bagheri & Khademifar, 2017; Froio & Rizzi, 2017).

Most of the former research focuses on leakage tightness by predicting the forces and stresses in the gasket and bolts. This is because the structural integrity of flanges is rarely considered a significant concern, and if it is, flanges can be reinforced to meet stress requirements. However,

a reinforced flange may become heavier and stiffer, exposing the gasket to relaxation, and eventually, leakage.

An effective way to reduce flange stress and flange rotation is to choose the appropriate flange-to-shell connection design. The type of shell, its geometric form, and the location of the connection to the flange ring all influence the stress distribution in the shell and the rotation of the flange. The goal of this study was to look at variations in shell stresses, flange rotation, and gasket load for different types of shells that could be attached to the flange ring in order to provide insight into the flange-to-shell junction design and minimize flange stresses and rotation. The theoretical and numerical analysis of bolted flange joint efficiency for various configurations during bolt-up and pressurization was performed using FEM. Computational modeling to simulate different scenarios was conducted to validate and verify the different proposed theories for the different shell-to-ring junction designs. The findings of this study will help to improve shell-to-flange designs, lower maintenance costs by reducing the likelihood of unplanned repair and shut down, and avoid negative environmental implications.

### 4.3 Analytical Methods

Numerous theories were used to achieve the mathematical formulation of the stresses in the shell-to-flange ring junction of different types of connections. FEM analysis was used to validate the approach and verify other critical leakage characteristics.

The continuity and equilibrium equations generated from the bolted joint analysis during both bolt-up and pressurization were required to evaluate bolt and gasket load changes, discontinuity edge loads, and stresses. The continuity conditions for radial displacement and tangential rotation at the junction of shell and ring are:

$$w_f = w_s \quad (4.1)$$

And

$$\theta_f = \theta_s \quad (4.2)$$

The gasket force during bolt-up can be determined as follows:

$$H_G^i = H_B^i \quad (4.3)$$

And during pressurization:

$$H_G^f = H_B^f - pA_p \quad (4.4)$$

Linear stiffness springs were used to represent the bolted joint parts, as illustrated in Figure 4.1. The joint is a complex structure and represents a statically undetermined system, which necessitates the use of an additional equation to solve the problem. To overcome this situation, the compatibility of the axial displacement of the components of the flange joints, as described in earlier studies (Bouزيد & Chaaban, 1993; Bouزيد & Nechache, 2005), states that the net traveling axial distance remains the same and is given as follows:

$$u_b^i + u_g^i + u_f^i = u_b^f + u_g^f + u_f^f \quad (4.5)$$

Or in terms of linear stiffnesses and ring rotation:

$$\frac{H_B^i}{K_b} + \frac{H_G^i}{K_g} + 2\theta_f^i(r_b - r_g) = \frac{H_B^f}{K_b} + \frac{H_G^f}{K_g} + 2\theta_f^f(r_b - r_g) \quad (4.6)$$

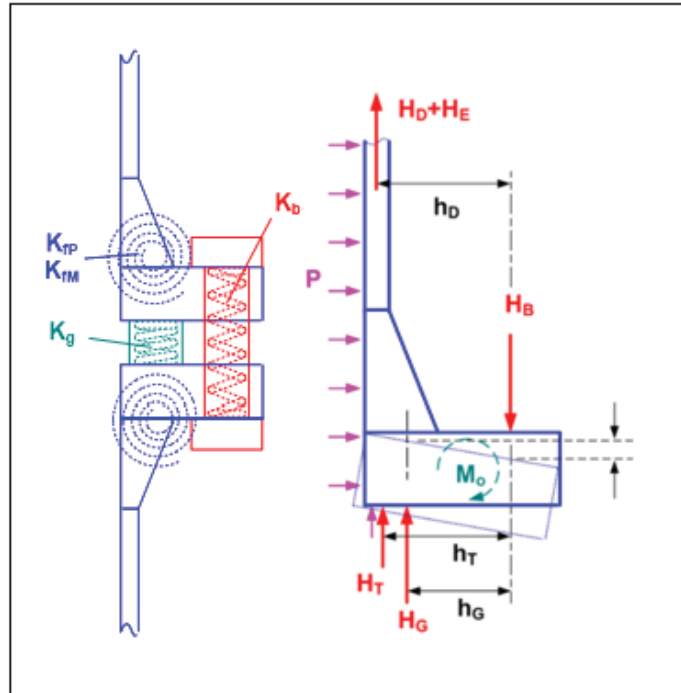


Figure 4.1 Bolted flange model  
Taken from Bouzid and Nechache (2010, p.731)

### 4.3.1 Bolt Stiffness

The stress area  $A_s$  is typically used to determine the practical stiffness of the bolt:

$$K_b = \frac{E_b A_r}{L_b} \quad (4.7)$$

The bolt stress area is given by:

$$A_r = \frac{\pi}{4} (D_b - 1.22687 p_b)^2 \quad (4.8)$$

However, the stress and the bolt pretension are based on the root area of the bolt. The root area of the bolt is given by (Bickford, 2008):

$$A_s = \frac{\pi}{4}(D_b - 0.938p_b)^2 \quad (4.9)$$

By implementing Equation 4.3 for the root area, the bolt load may be obtained as below:

$$H_B = \sigma_b A_s \quad (4.10)$$

Where  $\sigma_b$  is the applied bolt stress and  $H_B$  is the resulting bolt load.

### 4.3.2 Gasket Modeling

The reaction load and contact pressure of the gasket must be anticipated with adequate precision during service, which is a crucial task in the leakage prediction process. To seal the flange connection, the gasket has to be squeezed sufficiently. During the bolt-up or seating stage, gasket material behaves nonlinearly, but it behaves linearly during the unloading or pressurization stage.

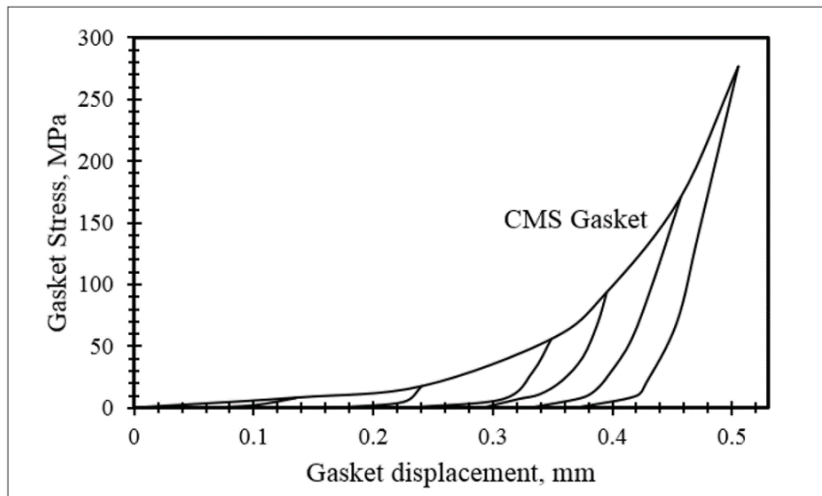


Figure 4.2 Unloading-loading curve for the implemented gasket

Figure 4.2 depicts typical load compression curves of the proposed gasket, which is a corrugated metal sheet with a flexible graphite layer (ASTM F2836, 2018). These curves were produced experimentally in the Static and Dynamic Sealing Laboratory of the ETS University, utilizing the ROTT. The ROTT rig uses a real pair of NPS 4, class 900 flanges (ASME B16.5,

2016). The mechanical behavior was assumed to be similar to the size of the gasket used in this study. The bolted flange connections considered in this study included NPS 26, 48, and 60 (class 300, series A) flanges of ASME B16.47 (ASME B16.47, 2017), for which the hub was ignored for simplicity. The gasket unload was considered to be linear in the analytical model, and the slope of the unloading was used to calculate the gasket compression modulus as follows (Bouزيد & Chaaban, 1993):

$$E_g = \frac{\Delta S_g}{\Delta D_g} \times (t_g - D_s) \quad (4.11)$$

Where  $D_s$  is the displacement that corresponds to the seating stress and  $t_g$  is the initial gasket thickness.

### 4.3.3 Flange Ring

The ASME Code limits flange ring rotation to 0.2 degrees for flanges with a hub and 0.3 degrees for flanges without a hub. The flange generally rises when bolt pretension and internal pressure are applied, and its impact on leakage is well recognized. Excessive rotation has a significant impact on gasket contact stress and can result in lift-off with certain gasket types that have a limit stop to control compression, such as spiral wound gaskets. The applicable theory pertaining to flange ring rotation may be selected based on the width-to-thickness ratio of the flange.

The theory of a circular plate with a central hole can be replaced with ring theory by raising the above-mentioned ratio to determine the rotation (Timoshenko & Woinowsky-Krieger, 1989):

$$\theta_f = \frac{2RY}{Et_f^3} M_f \quad (4.12)$$

Where  $Y$  for a flange assumed as a ring is given by:

$$Y = \frac{6}{\ln k} \quad (4.13)$$

And for a flange considered as a circular plate with a central hole:

$$Y = \frac{3}{k-1} \left[ (1-\nu) + 2(1+\nu) \frac{k^2 \ln k}{k^2 - 1} \right] \quad (4.14)$$

In addition, the following equation shows the radial displacement of the flange at the junction with the shell:

$$w_f = \left( p + Q_o \frac{t_f}{2} \right) \frac{R}{E} \left[ \frac{k^2 + 1}{k^2 - 1} + \nu \right] + \theta_f \frac{t_f}{2} \quad (4.15)$$

#### 4.3.4 Shell Stress Analysis

The assessment of high local shell stress necessitates an examination of the discontinuity's impact at the intersection of the shell and the flange ring in the absence of a hub. Cylindrical, spherical, conical, and dished shells of the same thickness were connected directly to the ring. It should be noted that stress concentration is usually attenuated by introducing a small hub or a fillet.

##### 4.3.4.1 Cylindrical Shell

The various applied forces and moments occurring on the long cylinder, including the discontinuity loads generated at the junction, are shown in Figure 4.3a. The radial displacement and rotation are obtained as follows:

$$w_c = w_p + w_{Q_o} + w_{M_o} \quad (4.16)$$

$$w_c = \frac{pR^2}{Et_s} \left( 1 - \frac{\nu}{2} \right) + \frac{Q_o}{2\beta_s^3 D_s} + \frac{M_o}{2\beta_s^2 D_s} \quad (4.17)$$

And

$$\theta_c = -\theta_{Q_0} - \theta_{M_0} \quad (4.18)$$

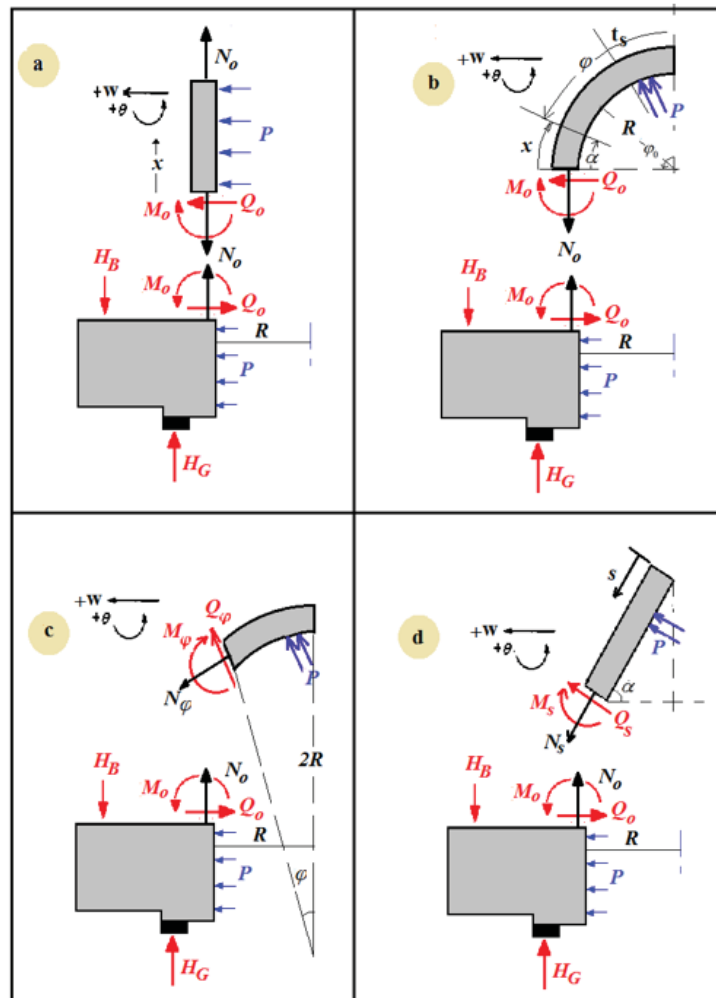


Figure 4.3 Flange rings and different shell types:  
a) cylindrical, b) spherical, c) dished, and d) conical

$$\theta_c = -\frac{2Q_0\beta_s^2}{k_s} - \frac{4M_0\beta_s^3}{k_s} \quad (4.19)$$

Where  $D_s$ ,  $\beta_s$ , and  $k_s$  are determined by:

$$D_s = \frac{Et_s^3}{12(1-\nu^2)}, \quad \beta_s = \frac{\sqrt[4]{3(1-\nu^2)}}{\sqrt{Rt_s}}, \quad k_s = \frac{Et_s}{R^2} \quad (4.20)$$

There is no internal pressure,  $p$ , or hydrostatic force,  $N$ , in the bolt-up process. For each working condition, the bolt and gasket forces  $H_b$  and  $H_g$ , as well as the edge loads,  $M_o$  and  $Q_o$ , may be determined.

To determine the stresses, displacement, rotation, bending moment, and shear force caused by the edge loads,  $M_o$  and  $Q_o$ , as a function of the axial distance, are required:

$$w_s(x) = \frac{Q_0}{2\beta_s^3 D_s} f_1(\beta_s x) + \frac{M_0}{2\beta_s^2 D_s} f_2(\beta_s x) \quad (4.21)$$

$$\theta_s(x) = \frac{-Q_0}{2\beta_s^2 D} f_3(\beta_s x) - \frac{M_0}{\beta_s^3 D_s} f_1(\beta_s x) \quad (4.22)$$

$$M(x) = \frac{Q_0}{\beta_s} f_4(\beta_s x) + M_0 f_3(\beta_s x) \quad (4.23)$$

$$Q(x) = Q_0 f_2(\beta_s x) - 2M_0 \beta_s f_4(\beta_s x) \quad (4.24)$$

Where:

$$f_1(\beta_s x) = e^{-\beta_s x} \cos \beta_s x \quad (4.25)$$

$$f_2(\beta_s x) = e^{-\beta_s x} (\cos \beta_s x - \sin \beta_s x) \quad (4.26)$$

$$f_3(\beta_s x) = e^{-\beta_s x} (\cos \beta_s x + \sin \beta_s x) \quad (4.27)$$

$$f_4(\beta_s x) = e^{-\beta_s x} \sin \beta_s x \quad (4.28)$$

As a result, the cylindrical shell's longitudinal and tangential stresses at the inner and outer surfaces are provided as a function of axial distance from the junction:

$$\sigma_l(x) = \frac{pR}{2t_s} \pm \frac{6M(x)}{t_s^2} \quad (4.29)$$

$$\sigma_t(x) = \frac{pR}{t_s} + \frac{Ew_s(x)}{R} \pm \frac{6\nu M(x)}{t_s^2} \quad (4.30)$$

#### 4.3.4.2 Spherical Shell

Figure 4.3b shows a spherical shell subjected to pressure and edge loads. The displacement and rotation at the junction are as follows (Bouزيد & Nechache, 2005):

$$w_s = \frac{pR^2}{2Et_s} (1-\nu_s) + \frac{Q_0}{2\beta_s^3 D_s} + \frac{M_0}{2\beta_s^2 D_s} \quad (4.31)$$

$$\theta_s = -\frac{2Q_0\beta_s^2}{k_s} - \frac{4M_0\beta_s^3}{k_s} \quad (4.32)$$

Moreover, at any angle  $\phi$  from the junction, the displacement, rotation, moment, and shear force are given by:

$$w_s(x) = \frac{Q_0 \sin^2 \phi}{2\beta_s^3 D_s} f_1(\beta_s x) + \frac{M_0 \sin \phi}{2\beta_s^2 D_s} f_2(\beta_s x) \quad (4.33)$$

$$\theta_s(x) = \frac{Q_0 \sin \phi}{2\beta_s^2 D} f_3(\beta_s x) + \frac{M_0}{\beta_s D} f_1(\beta_s x) \quad (4.34)$$

$$M(x) = \frac{Q_0 \sin \phi}{\beta} f_4(\beta x) + M_0 f_3(\beta x) \quad (4.35)$$

$$Q(x) = Q_0 \sin \phi f_2(\beta x) - 2\beta M_0 f_4(\beta x) \quad (4.36)$$

Where:

$$x = \alpha R = \left(\frac{\pi}{2} - \phi\right)R \quad (4.37)$$

Equations 4.25 through 4.28 define the  $f$  functions. The longitudinal and tangential stresses for the spherical shell can be deduced from:

$$\sigma_l(x) = \frac{pR}{2t_s} \pm \frac{6M(x)}{t_s^2} \quad (4.38)$$

$$\sigma_t(x) = \frac{pR}{2t_s} + \frac{Ew_s(x)}{R} \pm \frac{6\nu M(x)}{t_s^2} \quad (4.39)$$

#### 4.3.4.3 Dished Shell

The displacement and rotation at an angle  $\phi$  from the dished shell axis shown in Figure 4.3c can be obtained as follows (Flugge, 1973):

$$\begin{aligned} w_s &= \frac{R\zeta\sqrt{2}}{Et_s} [A_1(\text{beix} + x^{-1}(1+\nu)\text{ber}'x) \\ &\quad - A_2(\text{berx} + x^{-1}(1+\nu)\text{bei}'x) + B_1(\text{keix} + x^{-1}(1+\nu)\text{ker}'x) \\ &\quad - B_2(\text{kerx} + x^{-1}(1+\nu)\text{kei}'x)] \end{aligned} \quad (4.40)$$

And

$$\begin{aligned} \lambda_s(1-\nu^2)\theta_s &= A_1(2\zeta^2\text{bei}'x - \nu\text{ber}'x) \\ &\quad - A_2(2\zeta^2\text{ber}'x + \nu\text{bei}'x) + B_1(2\zeta^2\text{kei}'x - \nu\text{ker}'x) \\ &\quad - B_2(2\zeta^2\text{ker}'x + \nu\text{kei}'x) \end{aligned} \quad (4.41)$$

Where:

$$x = \zeta_s \phi \sqrt{2} \quad (4.42)$$

$$\zeta_s = \left[ 3(1-\nu^2) \frac{R^2}{t_s^2} - \frac{\nu^2}{4} \right]^{1/4} \quad (4.43)$$

$$\lambda_s = \frac{Et_s}{1-\nu^2} \quad (4.44)$$

The shear forces,  $Q_\phi$ , normal forces ( $N_\phi$ ,  $N_\theta$ ), and bending moments ( $M_\phi$ ,  $M_\theta$ ) are given by:

$$Q_\phi = A_1 \text{ber}'x + A_2 \text{bei}'x + B_1 \text{ker}'x + B_2 \text{kei}'x \quad (4.45)$$

$$N_\phi = -\phi^{-1} Q_\phi \quad (4.46)$$

$$\begin{aligned} N_\theta = \zeta_s \sqrt{2} [ & A_1 (\text{beix} + x^{-1} \text{ber}'x) \\ & - A_2 (\text{berx} - x^{-1} \text{bei}'x) + B_1 (\text{keix} + x^{-1} \text{ker}'x) \\ & - B_2 (\text{kerx} - x^{-1} \text{kei}'x) ] \end{aligned} \quad (4.47)$$

$$\begin{aligned} M_\phi = \frac{D_s \zeta_s \sqrt{2}}{\lambda R (1-\nu^2)} \{ & A_1 [2\zeta_s^2 (\text{berx} - \frac{1-\nu}{x} \text{bei}'x) + \nu (\text{beix} + \frac{1-\nu}{x} \text{ber}'x)] \\ & + A_2 [2\zeta_s^2 (\text{beix} + \frac{1-\nu}{x} \text{ber}'x) - \nu (\text{berx} - \frac{1-\nu}{x} \text{bei}'x)] \\ & + B_1 [2\zeta_s^2 (\text{kerx} - \frac{1-\nu}{x} \text{kei}'x) + \nu (\text{keix} + \frac{1-\nu}{x} \text{ker}'x)] \\ & + B_2 [2\zeta_s^2 (\text{keix} + \frac{1-\nu}{x} \text{ker}'x) - \nu (\text{kerx} - \frac{1-\nu}{x} \text{kei}'x)] \} \end{aligned} \quad (4.48)$$

$$\begin{aligned} M_\theta = \frac{D_s \zeta_s \sqrt{2}}{\lambda_s a (1-\nu^2)} \{ & A_1 [2\zeta_s^2 \nu \text{berx} + \frac{1-\nu}{x} \text{bei}'x) + \nu (\nu \text{beix} - \frac{1-\nu}{x} \text{ber}'x)] \\ & + A_2 [2\zeta_s^2 (\nu \text{beix} - \frac{1-\nu}{x} \text{ber}'x) - \nu (\nu \text{berx} + \frac{1-\nu}{x} \text{bei}'x)] \\ & + B_1 [2\zeta_s^2 (\nu \text{kerx} + \frac{1-\nu}{x} \text{kei}'x) + \nu (\nu \text{keix} - \frac{1-\nu}{x} \text{ker}'x)] \\ & + B_2 [2\zeta_s^2 (\nu \text{keix} - \frac{1-\nu}{x} \text{ker}'x) - \nu (\nu \text{kerx} + \frac{1-\nu}{x} \text{kei}'x)] \} \end{aligned} \quad (4.49)$$

It should be noted that when the shell extends from the junction to  $\phi = 0$  in Equations 4.40 through 4.49,  $A_2$  and  $B_2$  are equal to zero. The longitudinal and tangential stresses are calculated as follows:

$$\sigma_l(x) = \frac{pR}{2t_s} + \frac{N_\phi(x)}{t_s} \pm \frac{6M_\phi(x)}{t_s^2} \quad (4.50)$$

$$\sigma_\theta(x) = \frac{pR}{2t_s} + \frac{N_\theta(x)}{t_s} \pm \frac{6M_\theta(x)}{t_s^2} \quad (4.51)$$

#### 4.3.4.4 Conical Shell

Similarly, Figure 4.3d shows the free body diagram of the conical shell junction. The displacement and rotation may be obtained as follows (Flugge, 1973):

$$\begin{aligned} w_s = & -\frac{\sin \alpha \tan \alpha}{2Et_s} [A_1(-x\text{ber}'x + 2(1+\nu)\text{ber}x - 4(1+\nu)x^{-1}\text{bei}'x) \\ & -A_2(x\text{bei}'x - 2(1+\nu)\text{bei}x - 4(1+\nu)x^{-1}\text{ber}'x) \\ & -B_1(x\text{ker}'x - 2(1+\nu)\text{ker}x + 4(1+\nu)x^{-1}\text{kei}'x) \\ & +B_2(x\text{kei}'x - 2(1+\nu)\text{kei}x - 4(1+\nu)x^{-1}\text{ker}'x)] \end{aligned} \quad (4.52)$$

And

$$\begin{aligned} \theta = & \frac{2 \cot \alpha \sqrt{3(1-\nu^2)}}{Et^2} [A_1(\text{beix} + 2x^{-1}\text{ber}'x) \\ & -A_2(\text{ber}x - 2x^{-1}\text{bei}'x) + B_1(\text{keix} + 2x^{-1}\text{ker}'x) \\ & -B_2(\text{ker}x - 2x^{-1}\text{kei}'x)] \end{aligned} \quad (4.53)$$

Where:

$$x = \chi_s \sqrt{s} \quad (4.54)$$

$$\chi_s = 2[3(1-\nu^2)]^{1/4} \sqrt{\frac{2 \cot(\alpha)}{t_s}} \quad (4.55)$$

The following are the general equations for shear forces,  $Q_s$ , membrane forces ( $N_s$ ,  $N_\theta$ ), and bending moments ( $M_s$ ,  $M_\theta$ ):

$$Q_s = \frac{1}{s} [A_1(\text{ber}x - 2x^{-1}\text{bei}'x) + A_2(\text{beix} + 2x^{-1}\text{ber}'x) + B_1(\text{ker}x - 2x^{-1}\text{kei}'x) + B_2(\text{keix} + 2x^{-1}\text{ker}'x)] \quad (4.56)$$

$$N_s = -Q_s \cot \alpha \quad (4.57)$$

$$N_\theta = -\frac{\cot \alpha}{2s} [A_1(x\text{ber}'x - 2\text{ber}x + 4x^{-1}\text{bei}'x) + A_2(x\text{bei}'x - 2\text{beix} - 4x^{-1}\text{ber}'x) + B_1(x\text{ker}'x - 2\text{ker}x + 4x^{-1}\text{kei}'x) + B_2(x\text{kei}'x - 2\text{keix} - 4x^{-1}\text{ker}'x)] \quad (4.58)$$

$$M_s = 2x^{-2} \{A_1[x\text{bei}'x - 2(1-\nu)(\text{beix} + 2x^{-1}\text{ber}'x)] - A_2[x\text{ber}'x - 2(1-\nu)(\text{ber}x - 2x^{-1}\text{bei}'x)] + B_1[x\text{kei}'x - 2(1-\nu)(\text{keix} + 2x^{-1}\text{ker}'x)] - B_2[x\text{ker}'x - 2(1-\nu)(\text{ker}x - 2x^{-1}\text{kei}'x)]\} \quad (4.59)$$

$$M_\theta = 2x^{-2} \{A_1[\nu x\text{bei}'x + 2(1-\nu)(\text{beix} + 2x^{-1}\text{ber}'x)] - A_2[\nu x\text{ber}'x + 2(1-\nu)(\text{ber}x - 2x^{-1}\text{bei}'x)] + B_1[\nu x\text{kei}'x + 2(1-\nu)(\text{keix} + 2x^{-1}\text{ker}'x)] - B_2[\nu x\text{ker}'x + 2(1-\nu)(\text{ker}x - 2x^{-1}\text{kei}'x)]\} \quad (4.60)$$

When the shell extends from the junction to apex of the cone  $s = 0$ , then  $A_2$  and  $B_2$  are equal to zero. Therefore, the longitudinal and tangential stresses of the conical shell can be represented as follows:

$$\sigma_l(x) = \frac{ps \tan \alpha}{2t_s} + \frac{N_s(x)}{t_s} \pm \frac{6M_s(x)}{t_s^2} \quad (4.61)$$

$$\sigma_\theta(x) = \frac{ps \tan \alpha}{t_s} + \frac{N_\theta(x)}{t_s} \pm \frac{6M_\theta(x)}{t_s^2} \quad (4.62)$$

#### 4.4 Finite Element Modeling

The finite element modeling of the bolted flange joint, composed of the shell or head, flange ring, gasket, and bolts, was carried out for the different types of shell connections, namely cylindrical, spherical, dished, and conical, to verify the analytical results. The proposed bolted joint is used in a symmetrical design for simplification. It was also necessary to maintain the same material and geometric specifications of the various elements of the bolted flange joint, such as the flange ring, bolts, and gasket, in order to compare the stresses at the junction under the same conditions. The specifications and data used in the simulation are listed in Table 4.1. In consideration of the effect of flange size variation, three bolted flange joint sizes were modeled and simulated: NPS 26, 48, and 60 (class 300, series A). The hub was ignored in both the analytical and the numerical modeling.

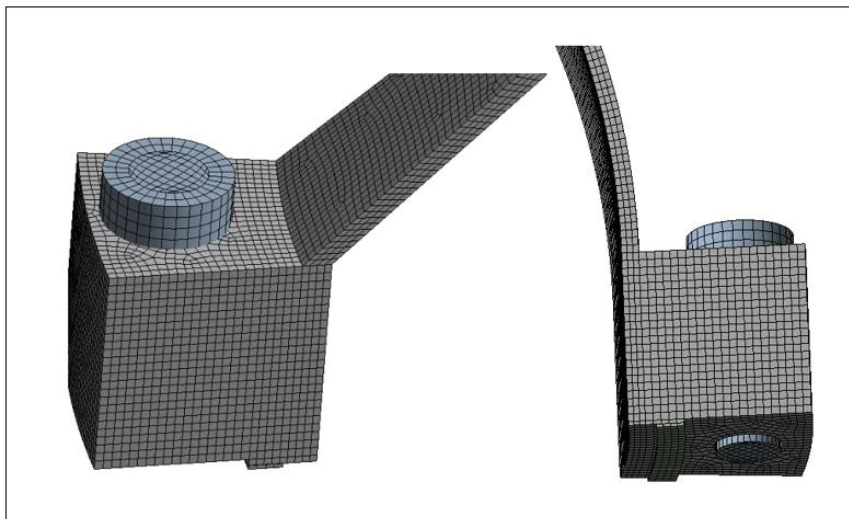


Figure 4.4 FEM bolted flange joint model in ANSYS

Table 4.1 Specifications and data used in the FEM model for different flange sizes

<b>Model Properties</b>			
<b>Flange size (in.)</b>	<b>26</b>	<b>48</b>	<b>60</b>
Outer diameter of flange (mm)	970	1465	1810
Inner diameter of flange (mm)	635	1193.8	1498.6
Bolt circle diameter (mm)	876.3	1371.6	1701.8
Head radius (mm)	317.5	596.9	749.3
Head thickness (mm)	12.7	12.7	12.7
Raised face height (mm)	2	2	2
Flange thickness (mm)	77.8	131.8	162
Bolt diameter (mm)	41.275	47.63	57.15
Number of bolts (mm)	32	32	32
Gasket height (mm)	2	2	2
Gasket width (mm)	22.15	20.7	25.5
Inner diameter of the gasket (mm)	704.7	1235.2	1575
Outer diameter of gasket (mm)	749	1276.6	1626
Bolt preload (kN)	104.6	204.6	380.32
Internal pressure (MPa)	2.07	2.07	2.07
Cone angle (deg)	45	45	45

ANSYS Workbench software was used to simulate detailed models of the different types of shells with the flange ring (Figure 4.4). Due to the axial symmetry, and to simplify the analysis and reduce the simulation CPU time, a half portion model of the bolted flange joint was simulated. It must be emphasized that only part of the attached shell was included in the model. For example, in the case of the cylindrical shell, a sufficient length of the shell was simulated to account for the stress attenuation effects.

Because of the axial symmetry, there was neither axial displacement nor rotation at the gasket mid-plane passing through the mid-length of the bolt. The cyclic boundary condition was investigated at the two cut sections of the simulated bolted joint. To obtain more precise stress measurements, SOLID186 elements (20 nodes per element) were used and the mesh was refined to meet the convergence criterion of less than 1% in the shell equivalent stress at the junction. PRETS179 elements were used to simulate the pretension load of the bolt. Moreover, for each size of flange, a corresponding bolt preload was specified to seat the gasket and maintain sealing during operation. To simulate the contact conditions between the flange ring and the gasket, and between the lubricated bolts and the flange ring, CONTA174 elements were used, with the friction coefficients of 0.7 and 0.15, respectively. Internal pressure of 300 psi was applied to the internal surfaces of the connected shells. In the case of the cylinder, to simulate the hydrostatic end effect, an axial surface load was applied to the cylindrical shell end in addition to the lateral pressure. This pressure load was determined based on the internal radius and shell thickness for each size of flange. The flanges were made of ASTM A105, whereas the bolts were made of ASTM A193 B7. Young's Modulus and Poisson's ratio were 207 GPa, 0.3, and yield stress was 400 Mpa.

## **4.5 Results and Discussion**

The bolted flange joint simulation results are broken down into two categories: the flange rotation and the distribution of the tangential and longitudinal stresses at the inside and outside surfaces of the flange during bolt-up and pressurization for three different flange sizes (NPS 26, 48, and 60) and the four types of shell connections (cylindrical, dished, conical, and spherical).

### **4.5.1 Flange Rotation**

The rotation of the flange has a significant impact on gasket integrity and leakage. Excessive flange rotation can cause high localized stresses, leading to sheet gasket crushing or gasket lift-off, especially in gaskets with outer rings such as spiral wound gaskets. As a result, the ASME

restricts the non-hubbed flange rotation to 0.2 degrees and the hubbed flanges to 0.3. Figures 4.5 through 4.10 illustrate the axial displacements of the finite element flange ring face during bolt-up and pressurization for the four types of shell connections for the three different flange sizes.

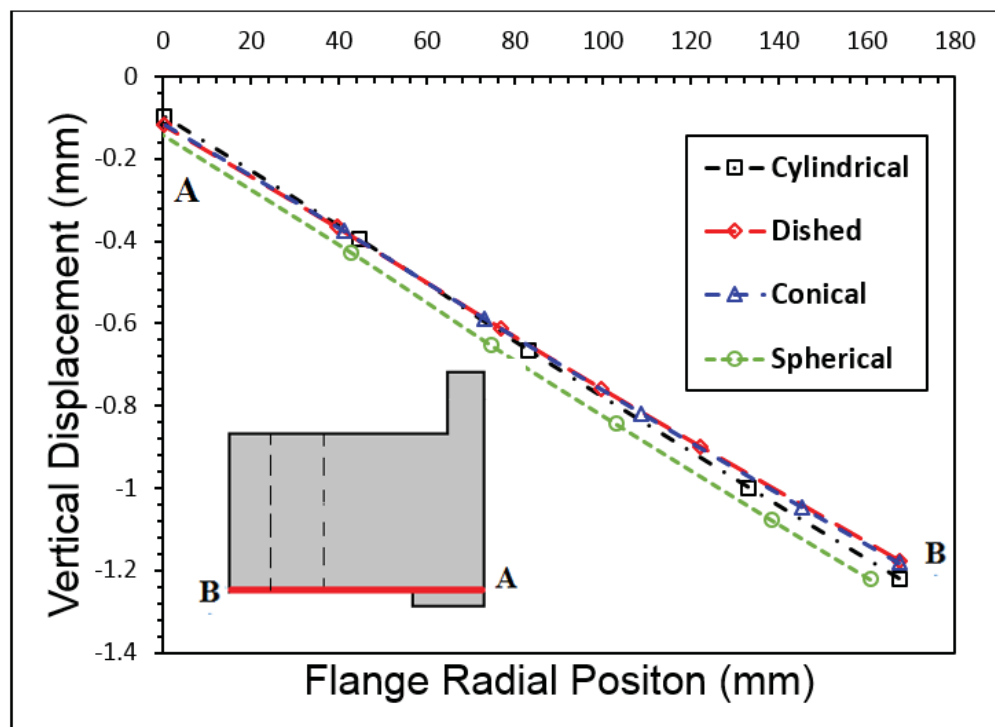


Figure 4.5 Flange rotation of shell connections during bolt-up (NPS 26 class 300)

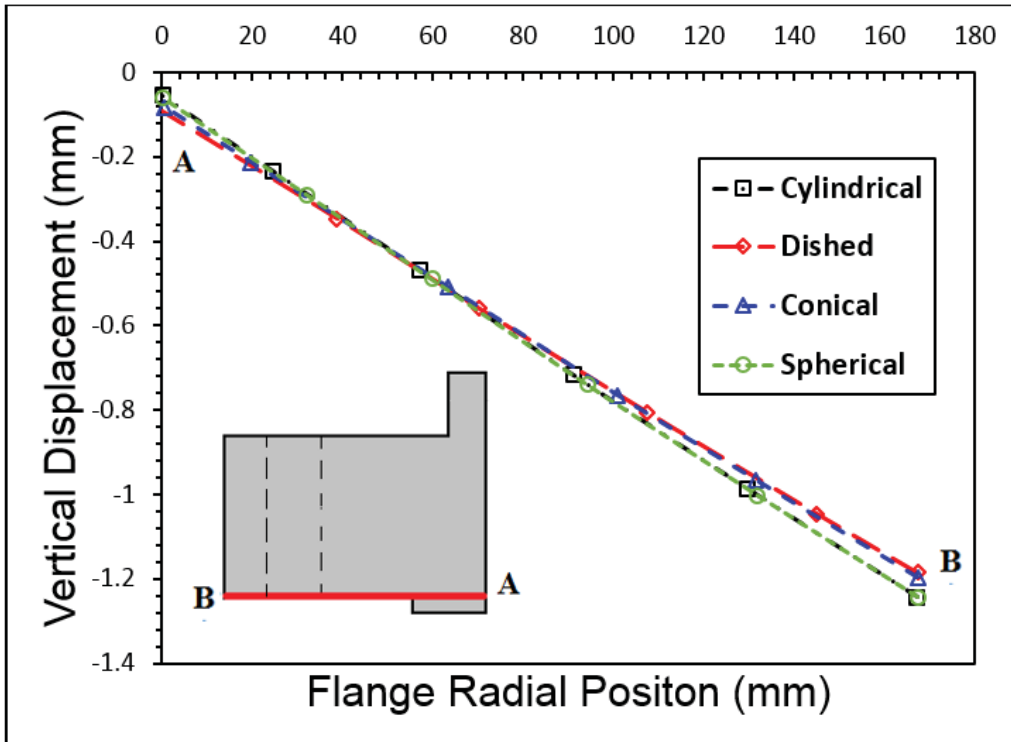


Figure 4.6 Flange rotation of shell connections during pressurization (NPS 26 class 300)

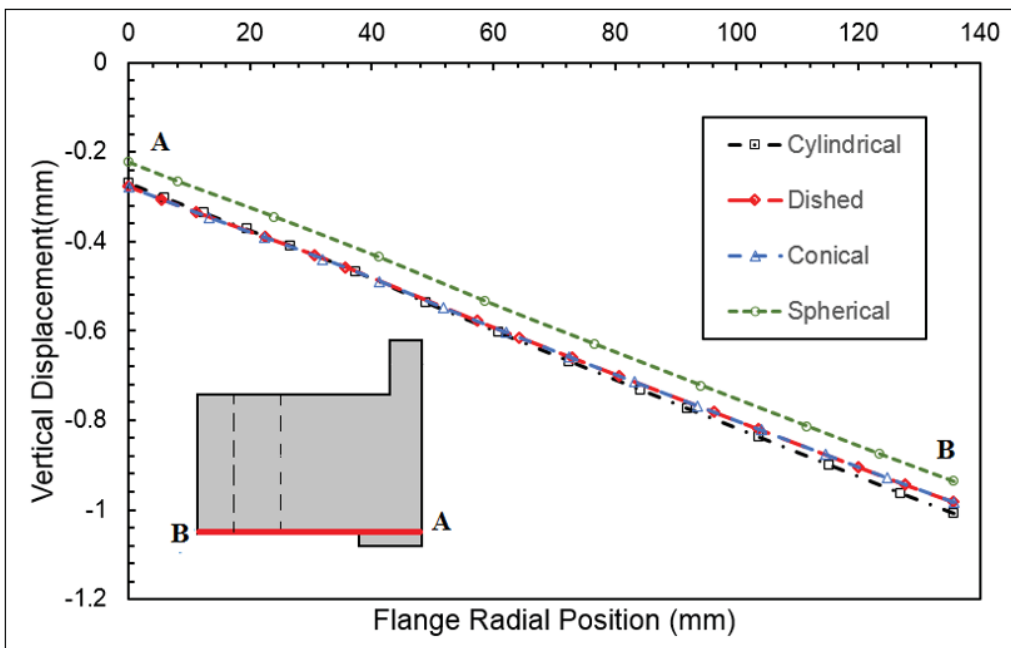


Figure 4.7 Flange rotation of shell connections during bolt-up (NPS 48 class 300)

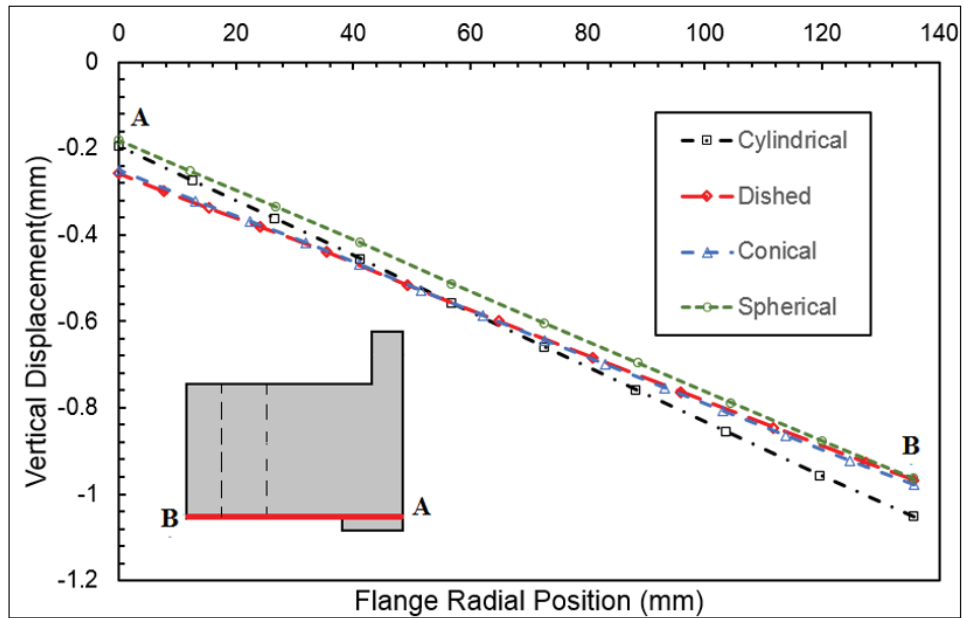


Figure 4.8 Flange rotation of shell connections during pressurization (NPS 48 class 300)

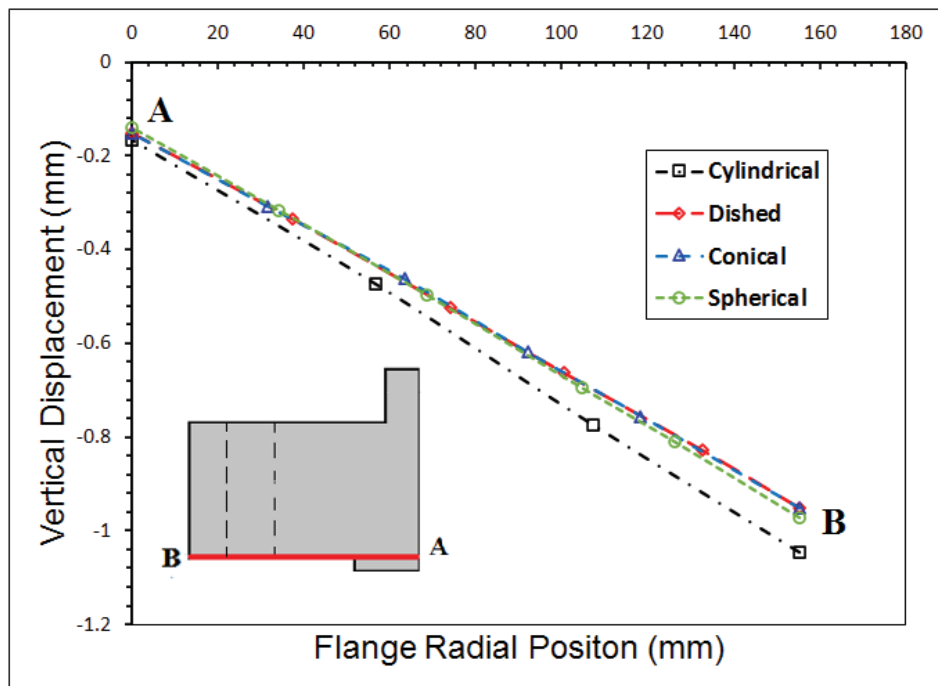


Figure 4.9 Flange rotation of shell connections during bolt-up (NPS 60 class 300)

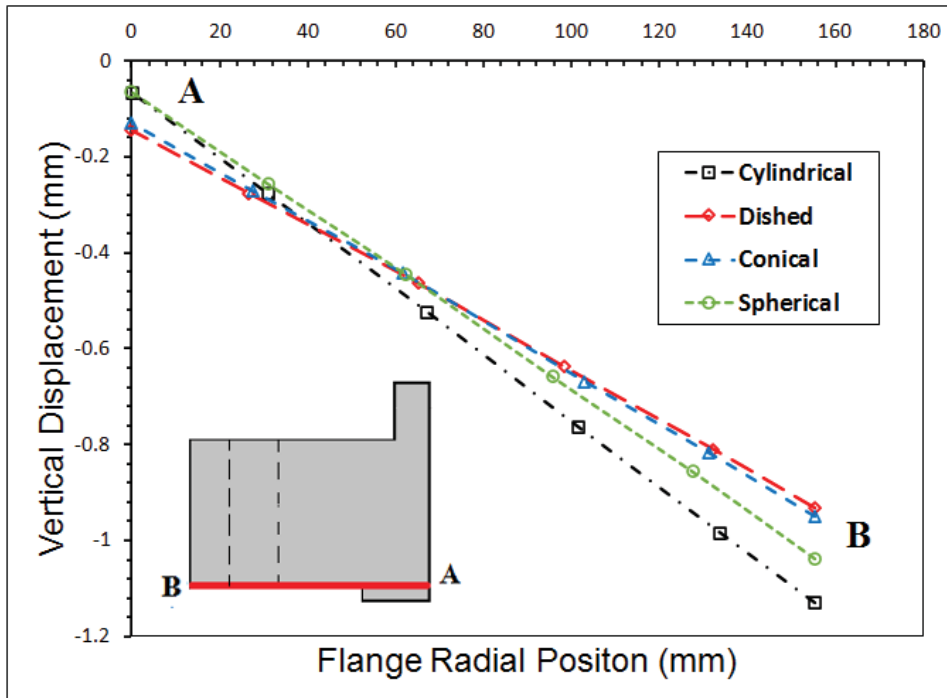


Figure 4.10 Flange rotation of shell connections during pressurization (NPS 60 class 300)

Table 4.2 Analytical and numerical results of flange rotation for four types of shell connections during bolt-up and pressurization

Flange Rotation (deg)					
Flange size (in.)	Shell connection	Bolt-up		Pressurization	
		FEM	Anal.	FEM	Anal.
26	Cylindrical	0.384	0.384	0.407	0.392
	Dished	0.367	0.349	0.372	0.357
	Conical	0.367	0.364	0.384	0.372
	Spherical	0.384	0.384	0.407	0.392
48	Cylindrical	0.315	0.309	0.367	0.338
	Dished	0.298	0.281	0.304	0.286
	Conical	0.298	0.298	0.309	0.304
	Spherical	0.304	0.309	0.332	0.332
60	Cylindrical	0.327	0.318	0.395	0.373
	Dished	0.292	0.297	0.292	0.298
	Conical	0.298	0.311	0.304	0.325
	Spherical	0.309	0.318	0.361	0.365

The displacements are presented in Figures 4.5 through 4.10 as a function of radial location on the flange ring. It should be noted that the slopes of these straight lines determine the flange ring rotations. During bolt-up, all flanges rotate at nearly the same rate, with the cylindrical configuration turning a slightly more.

The cylindrical shell configuration also rotates more during pressurization, which is likely because the barreling effect caused by side pressure is more substantial in this case. The application of pressure has almost no effect on the dished configuration. Table 4.2 presents a comparison of the flange rotations obtained by the finite element and analytical models for the different flange sizes and shell connections. As shown, there is good agreement between the two methods.

#### **4.5.2 Stress Distribution in the Different Shells**

The stress distributions in the different shells at the flange ring junction generated during bolt-up and pressurization are presented in Figures 4.11 through 4.34, which compare the longitudinal and tangential stress distributions as well as the maximum stresses at the inner (IR) and outer (OR) surfaces of the shells during bolt-up and pressurization for the three flange sizes and the four shell connection types.

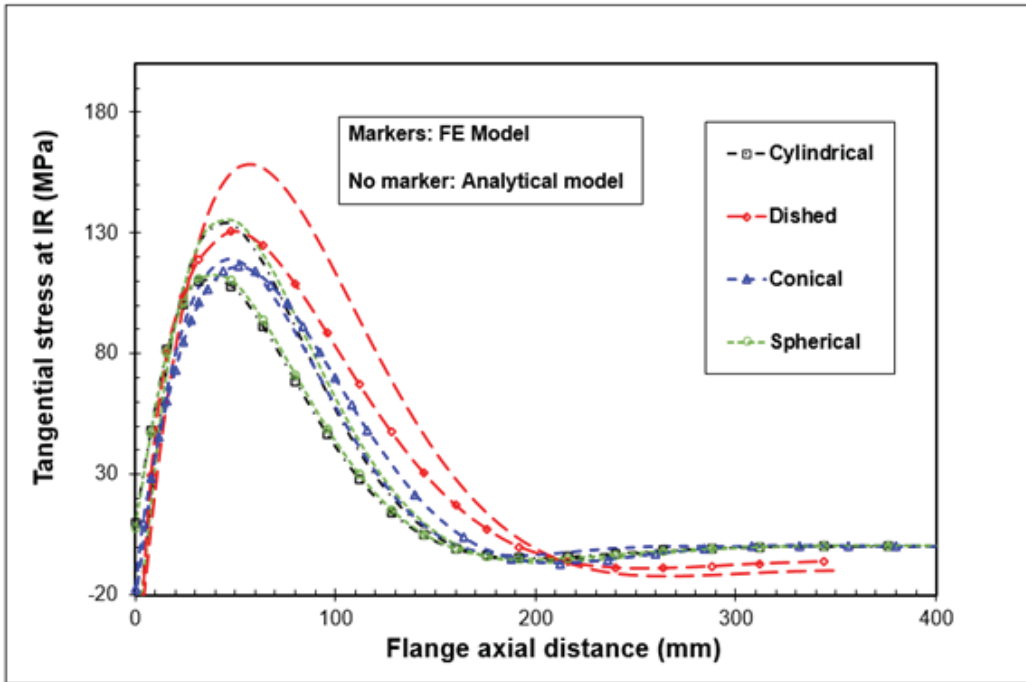


Figure 4.11 Tangential stress at IR of shell connections during bolt-up (NPS 26 class 300)

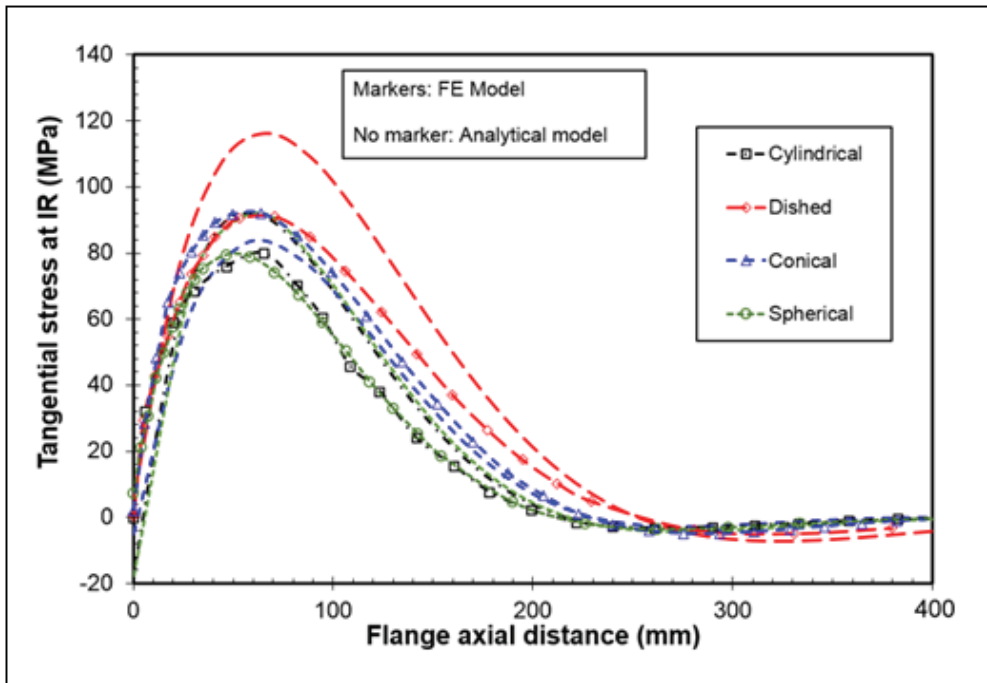


Figure 4.12 Tangential stress at IR of shell connections during bolt-up (NPS 48 class 300)

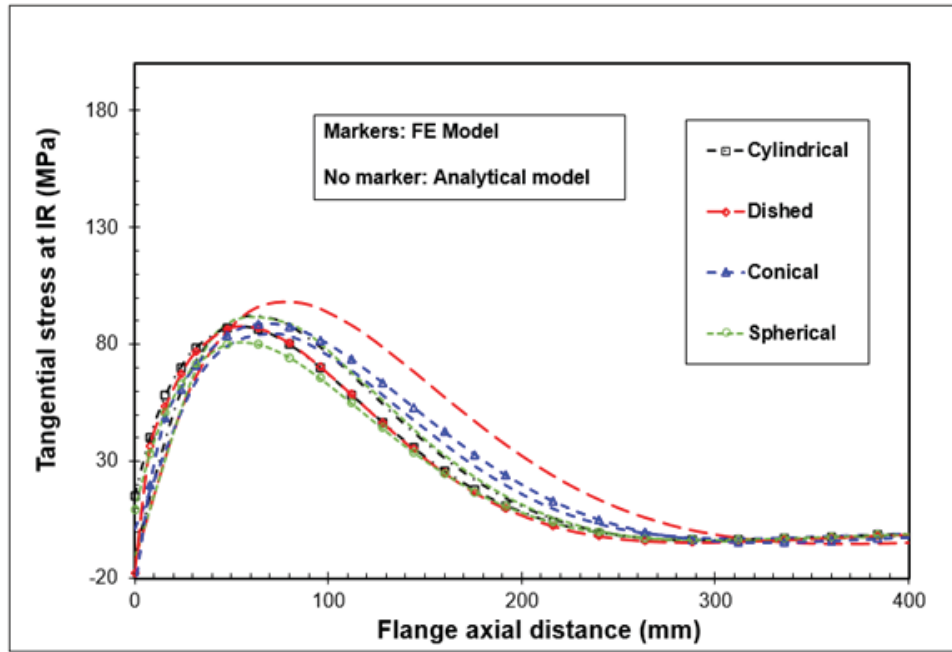


Figure 4.13 Tangential stress at IR of shell connections during bolt-up (NPS 60 class 300)

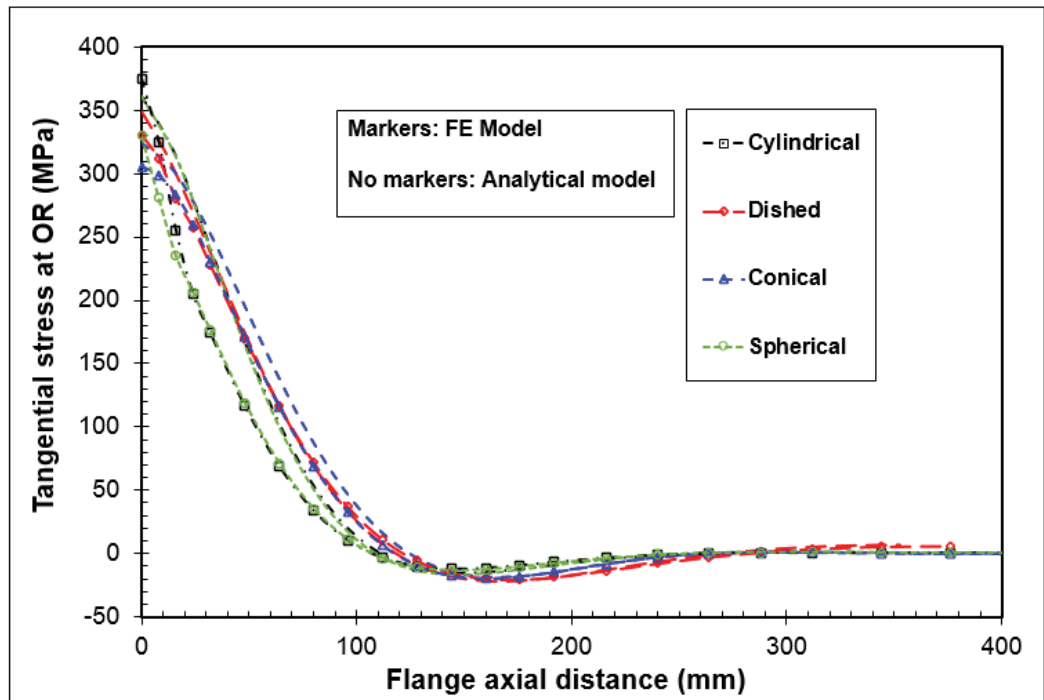


Figure 4.14 Tangential stress at OR of shell connections during bolt-up (NPS 26 class 300)

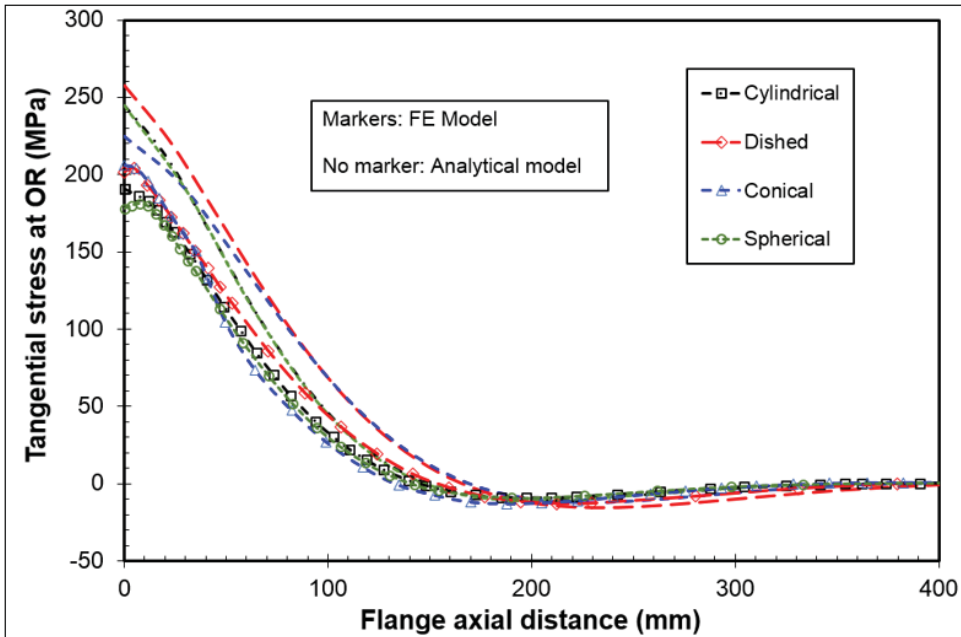


Figure 4.15 Tangential stress at OR of shell connections during bolt-up (NPS 48 class 300)

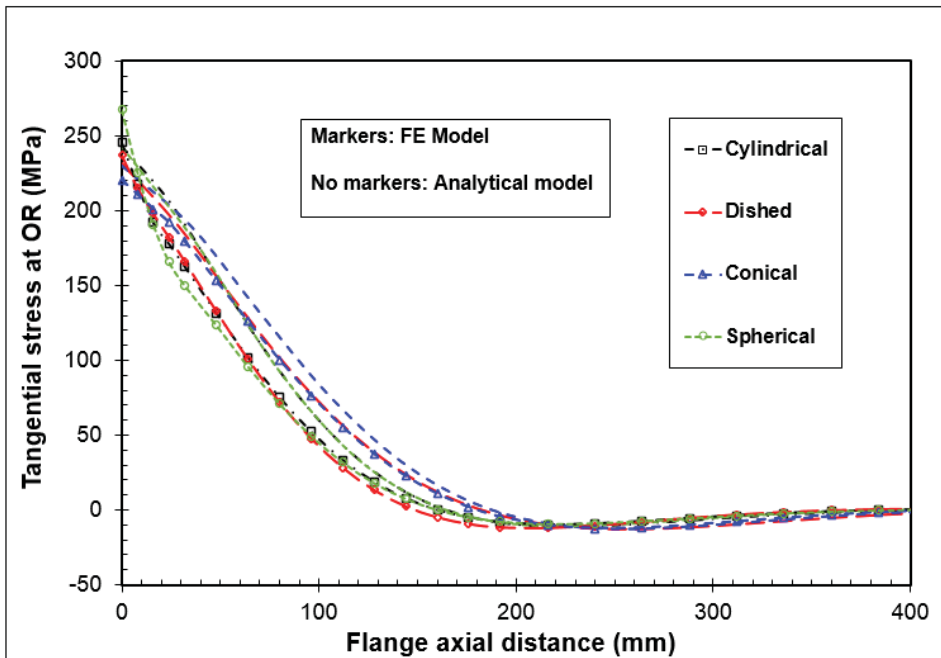


Figure 4.16 Tangential stress at OR of shell connections during bolt-up (NPS 60 class 300)

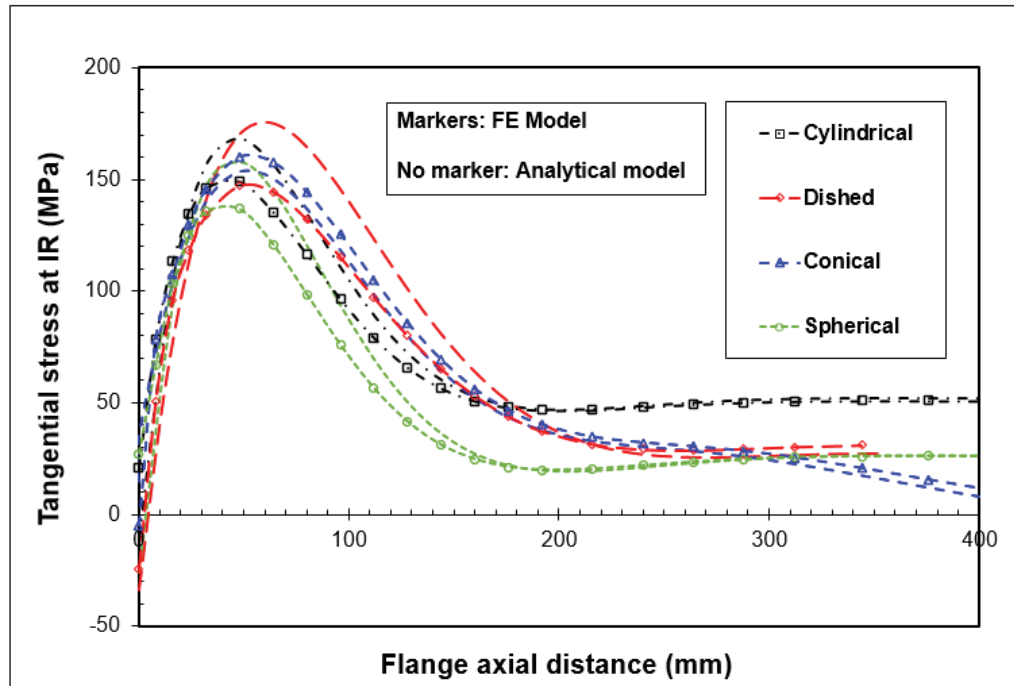


Figure 4.17 Tangential stress at IR of shell connections during pressurization (NPS 26 class 300)

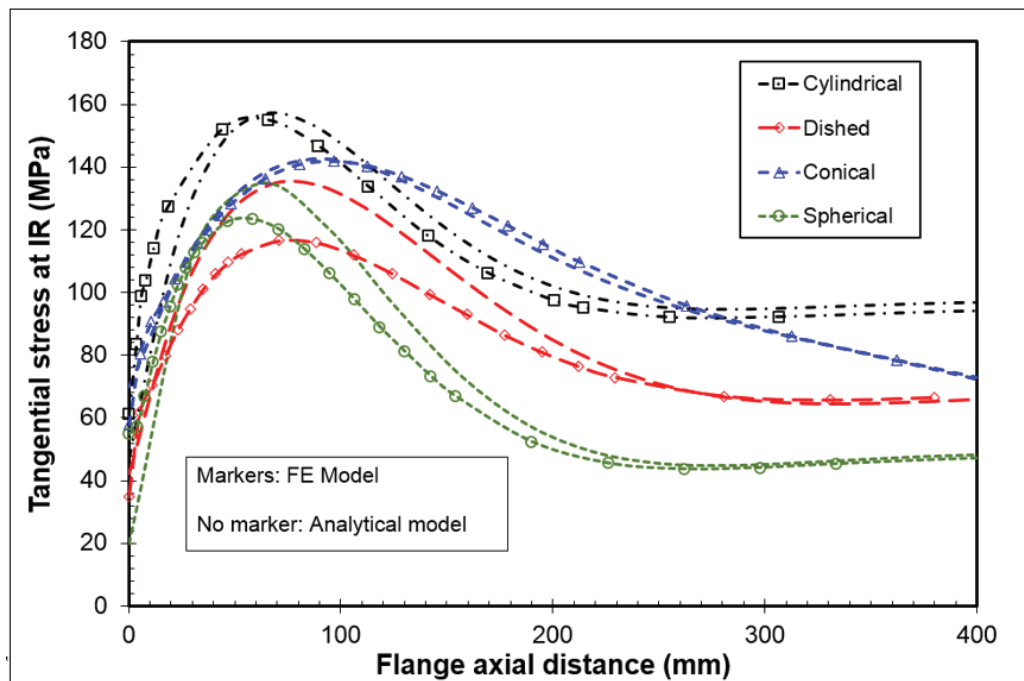


Figure 4.18 Tangential stress at IR of shell connections during pressurization (NPS 48 class 300)

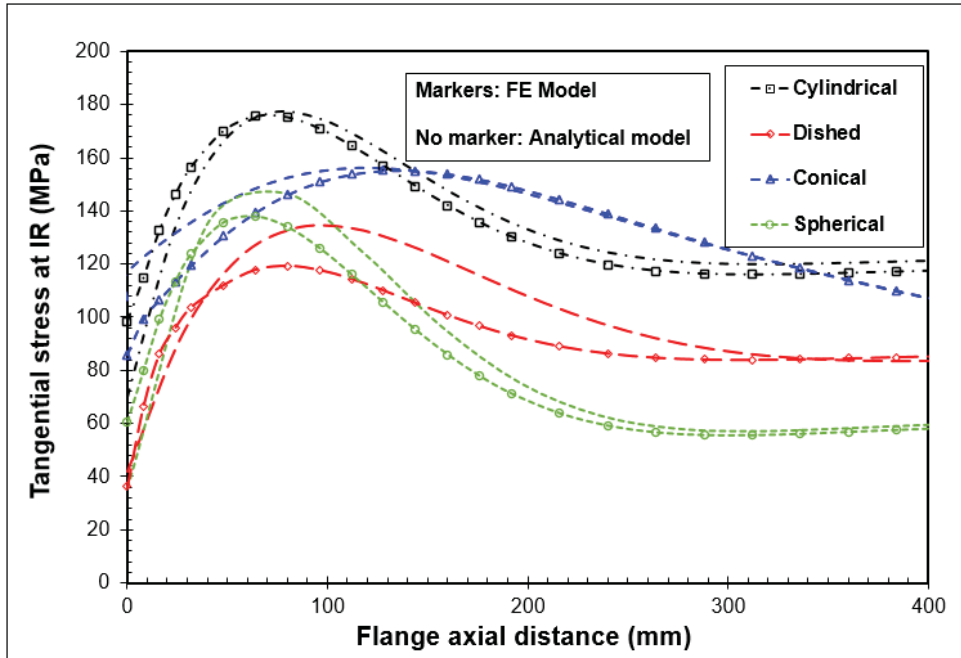


Figure 4.19 Tangential stress at IR of shell connections during pressurization (NPS 60 class 300)

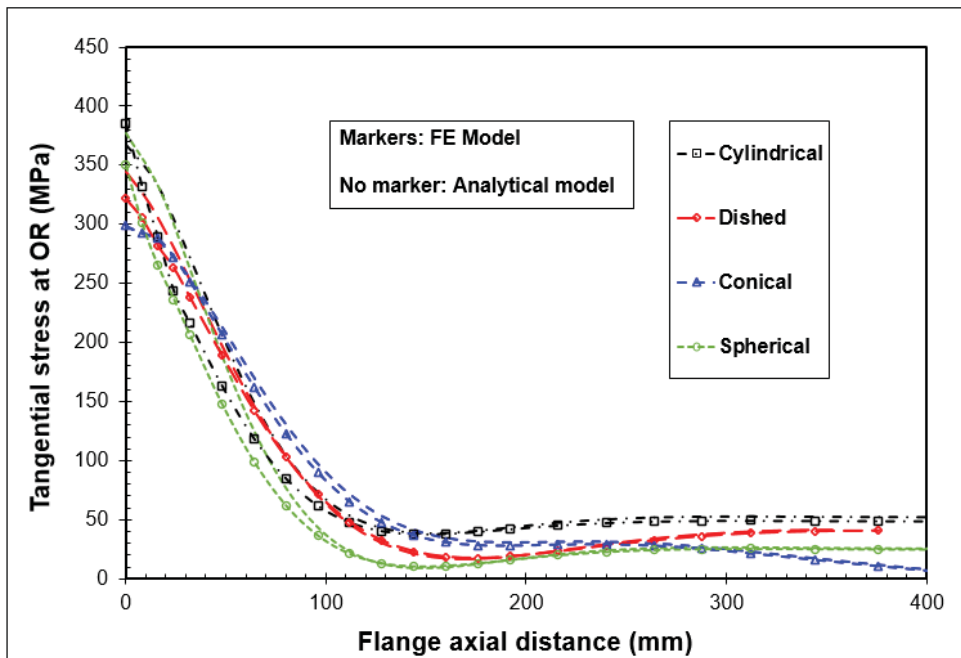


Figure 4.20 Tangential stress at OR of shell connections during pressurization (NPS 26 class 300)

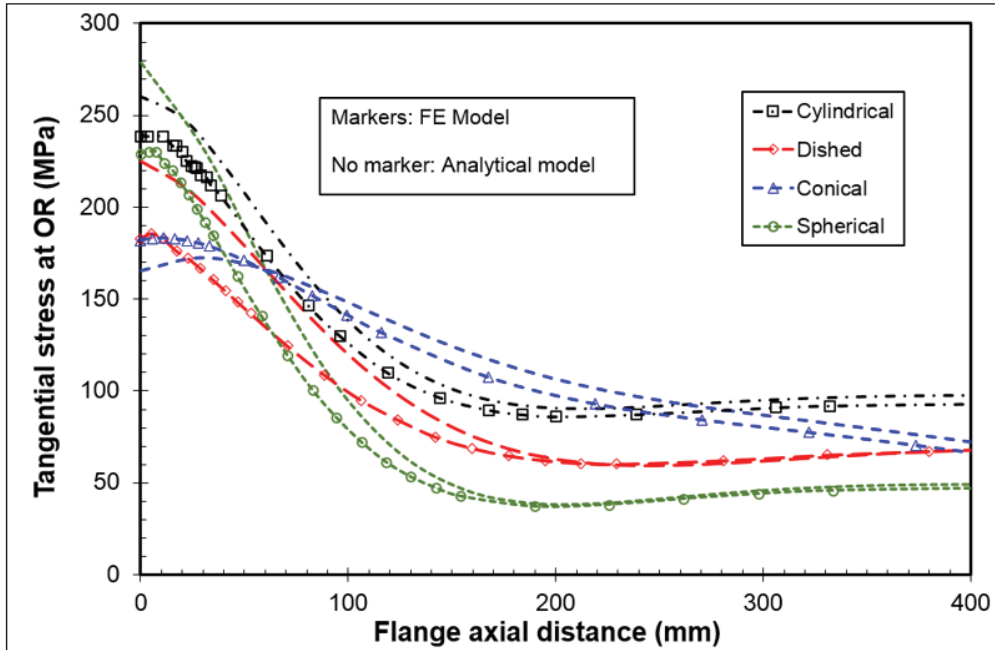


Figure 4.21 Tangential stress at OR of shell connections during pressurization (NPS 48 class 300)

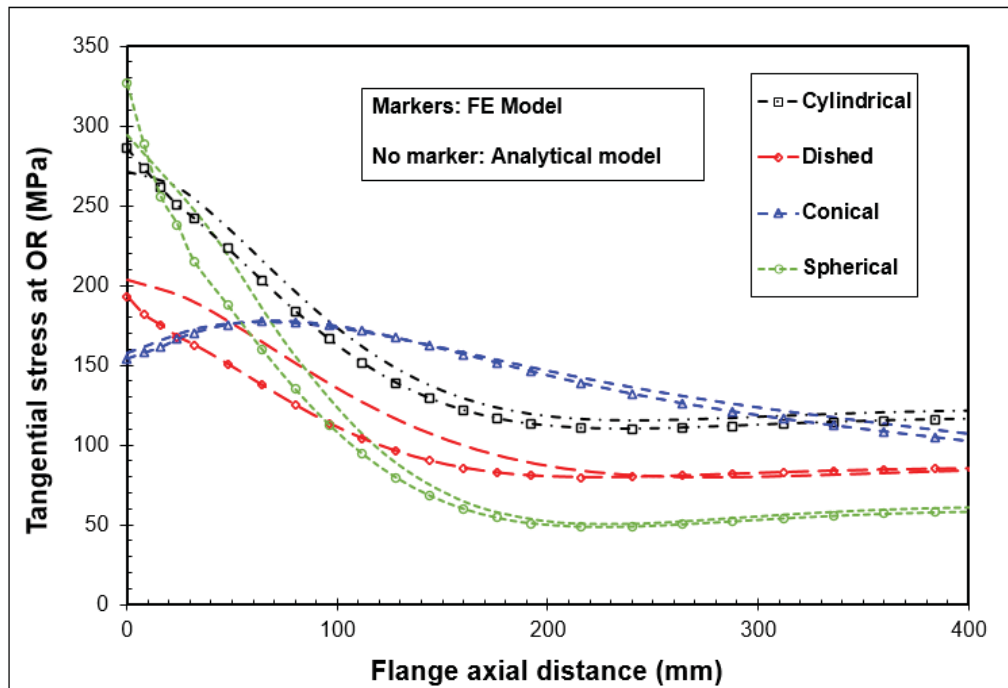


Figure 4.22 Tangential stress at OR of shell connections during pressurization (NPS 60 class 300)

The tangential stress at the inner and outer surfaces of the dished and conical shells has higher values during bolt-up (Figures 4.11 to 4.16). However, when pressure is applied, the cylindrical and spherical shells display greater tangential stresses (Figures 4.17 to 4.22), which is likely due to the barreling effect produced by the radial component of the pressure acting on the shell. The highest tangential stress in the shell outer surface is located exactly at the junction for all connections, whereas the maximum value at the inside is located roughly at one-quarter of the attenuation length of  $2.45\sqrt{Rt}$  from the junction with the ring. Moreover, the tangential stresses are eventually attenuated away from the junction in all cases, with the cylindrical shell showing larger values during pressurization. It should be noted that the analytical and numerical results show similar trends and are in relatively good agreement.

Figures 4.23 through 4.28 show the distribution of longitudinal stresses at the inner and outer surfaces of the different types and sizes of shell connections during bolt-up, while Figures 4.29 through 4.34 depict the distribution of longitudinal stresses during pressurization. In general, the cylindrical and spherical shells show slightly larger longitudinal stresses than the conical and dished shells. The greatest stresses are located at the intersection with the flange ring, with the inner and outer surfaces showing the same level of stress. In all cases, most of the longitudinal and tangential stresses remain below the yield stress, although the presence of the hub and the fillet radius at the junction with the ring will attenuate the stresses. Nevertheless, in all types of shell connections, applying pressure decreases the longitudinal stress at the junction, especially in the conical and dished connections, but stress increases to a stable value away from the junction.

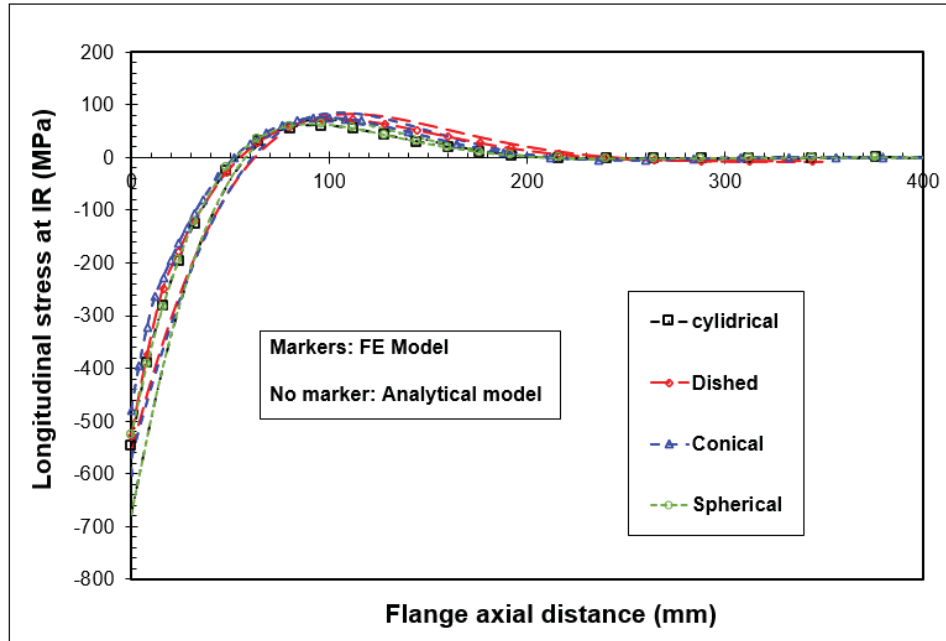


Figure 4.23 Longitudinal stress at IR of shell connections during bolt-up (NPS 26 class 300)

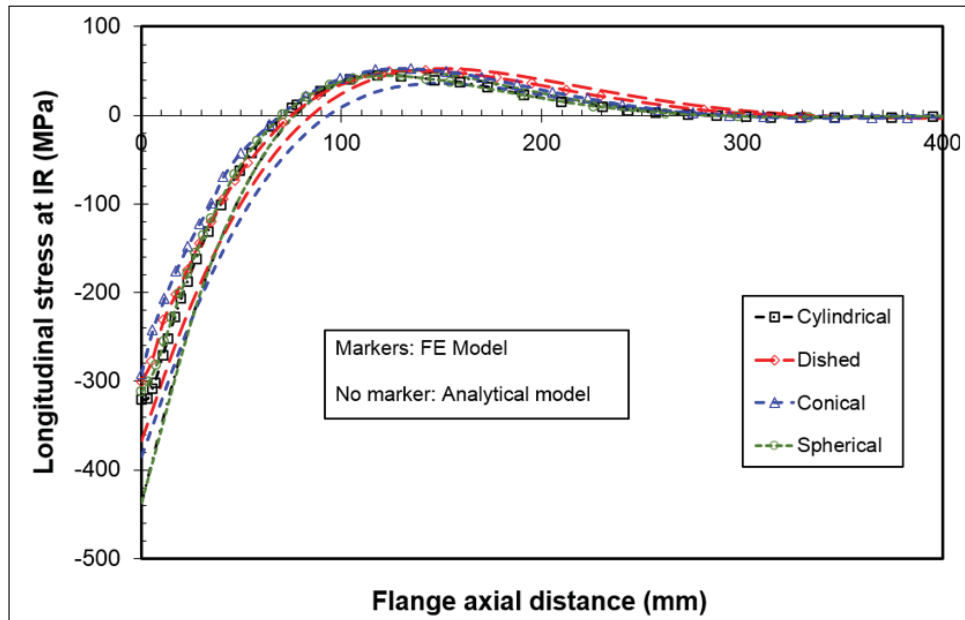


Figure 4.24 Longitudinal stress at IR of shell connections during bolt-up (NPS 48 class 300)

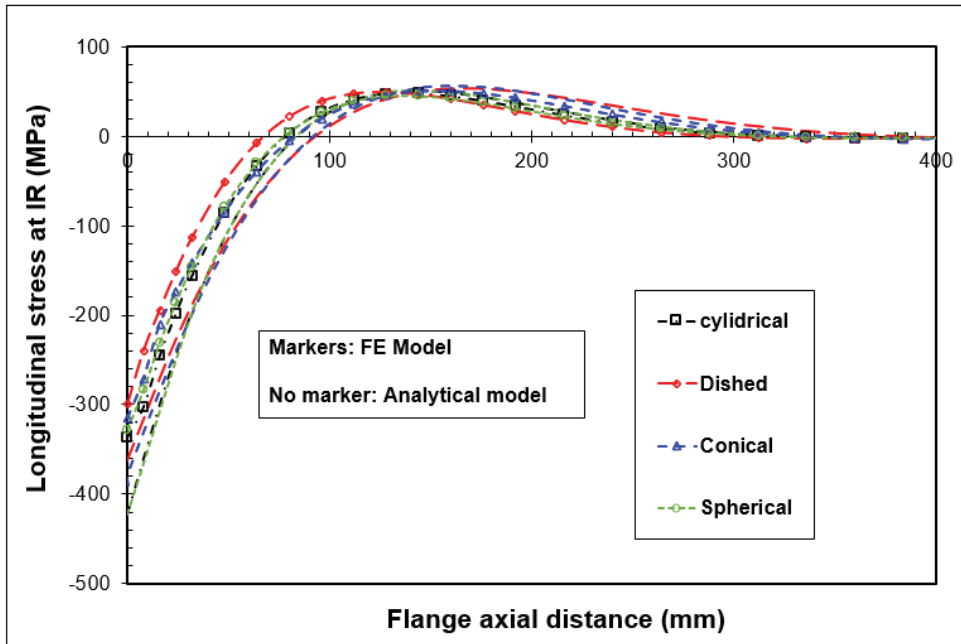


Figure 4.25 Longitudinal stress at IR of shell connections during bolt-up (NPS 60 class 300)

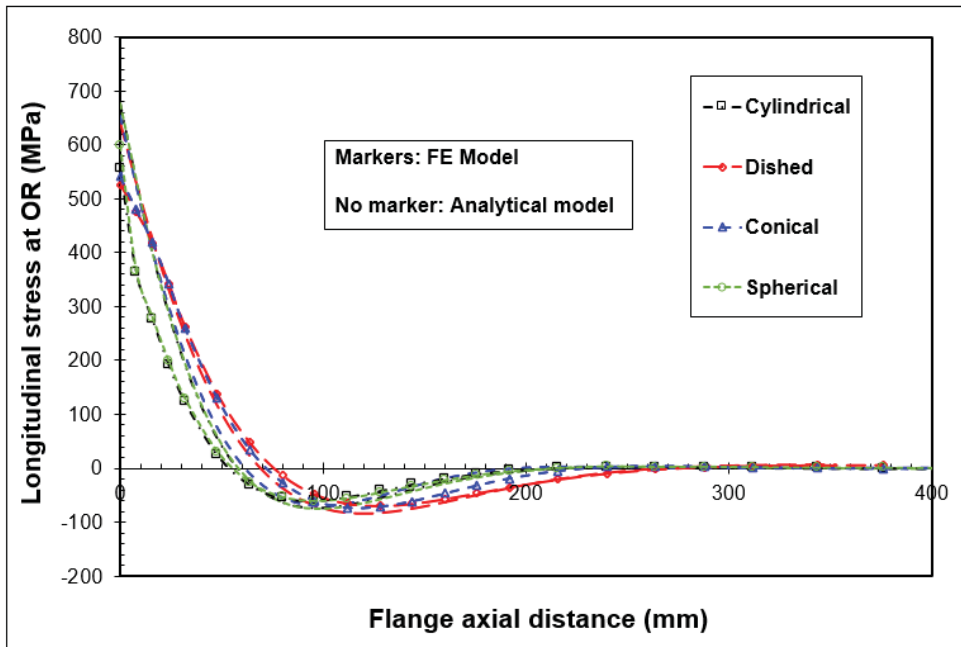


Figure 4.26 Longitudinal stress at OR of shell connections during bolt-up (NPS 26 class 300)

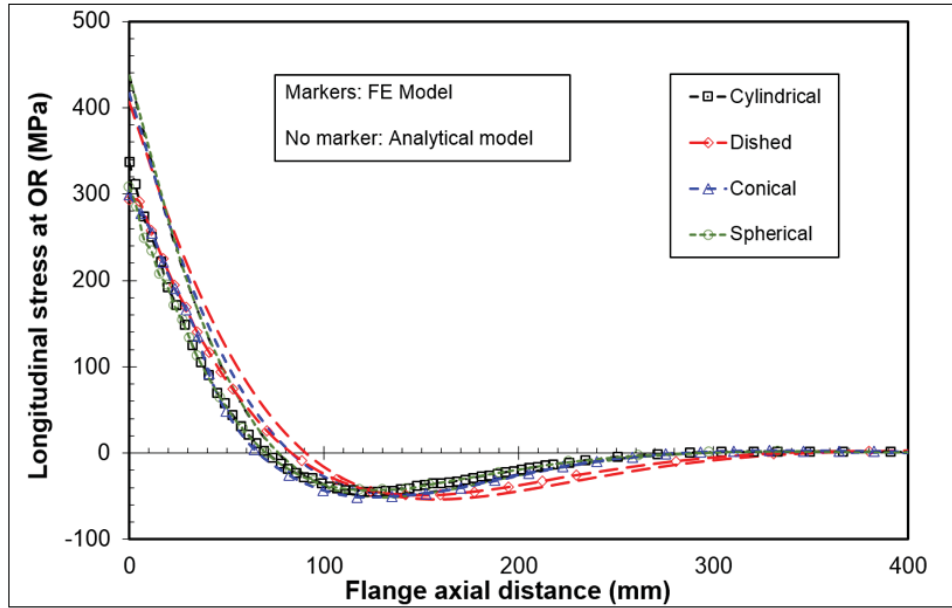


Figure 4.27 Longitudinal stress at OR of shell connections during bolt-up (NPS 48 class 300)

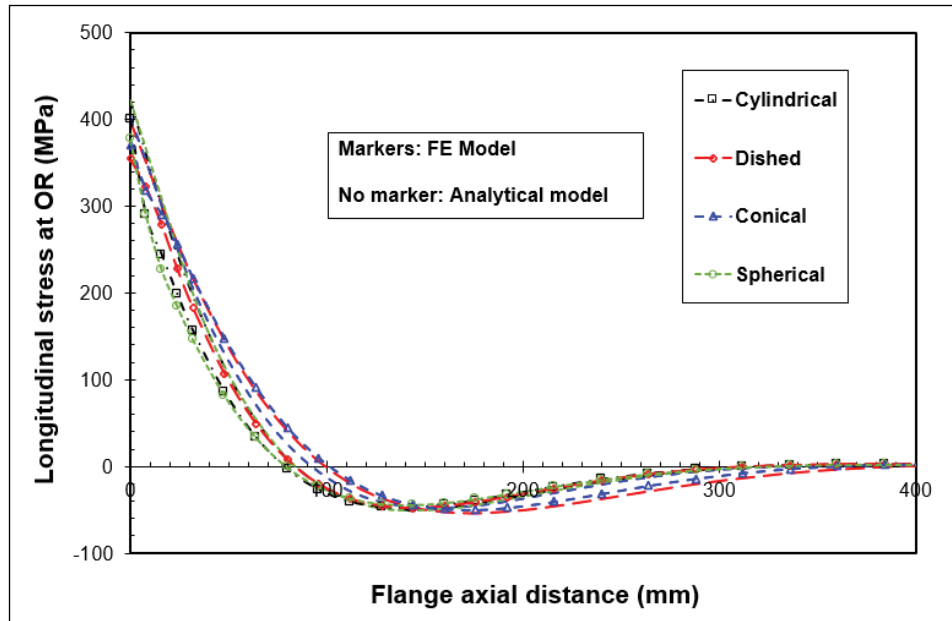


Figure 4.28 Longitudinal stress at OR of shell connections during bolt-up (NPS 60 class 300)

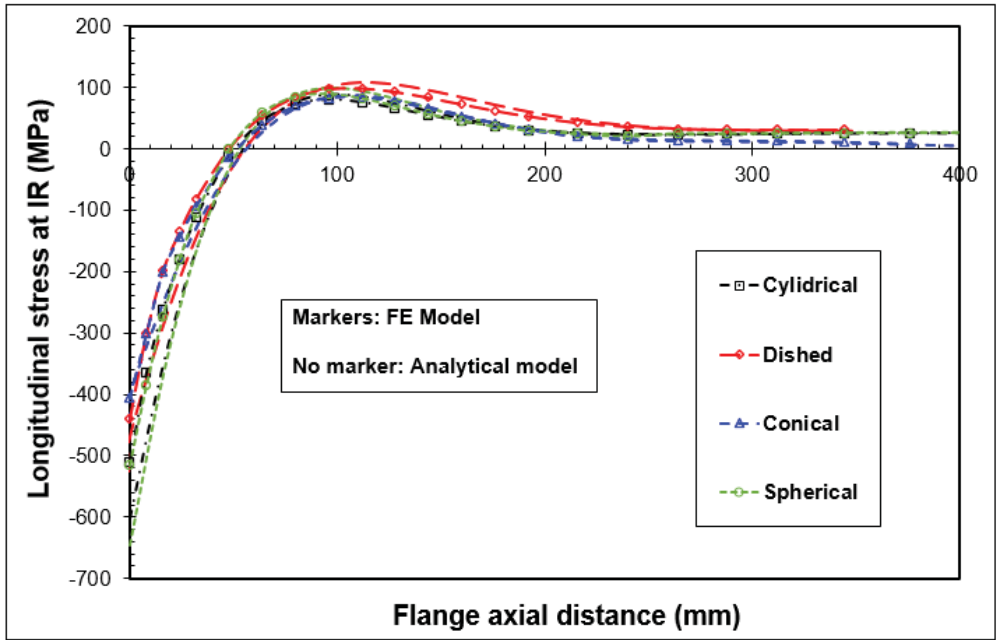


Figure 4.29 Longitudinal stress at IR of shell connections during pressurization (NPS 26 class 300)

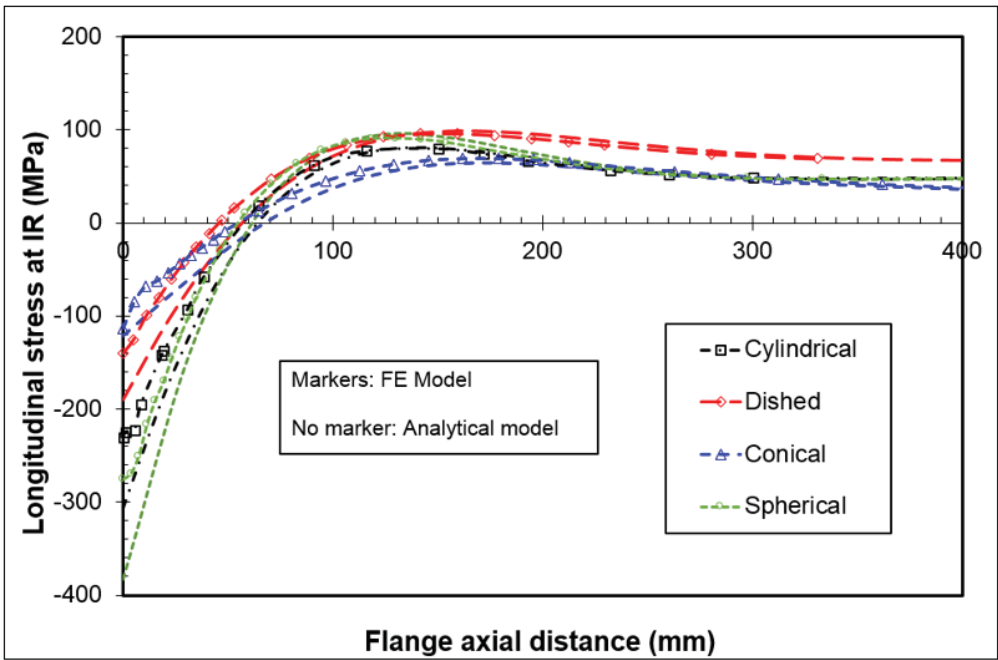


Figure 4.30 Longitudinal stress at IR of shell connections during pressurization (NPS 48 class 300)

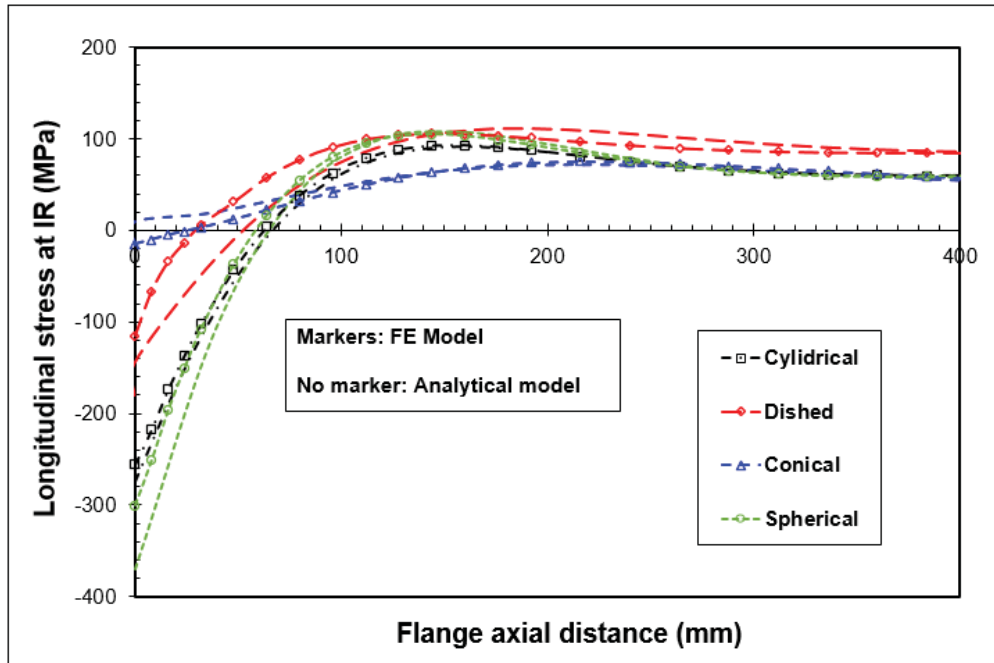


Figure 4.31 Longitudinal stress at IR of shell connections during pressurization (NPS 60 class 300)

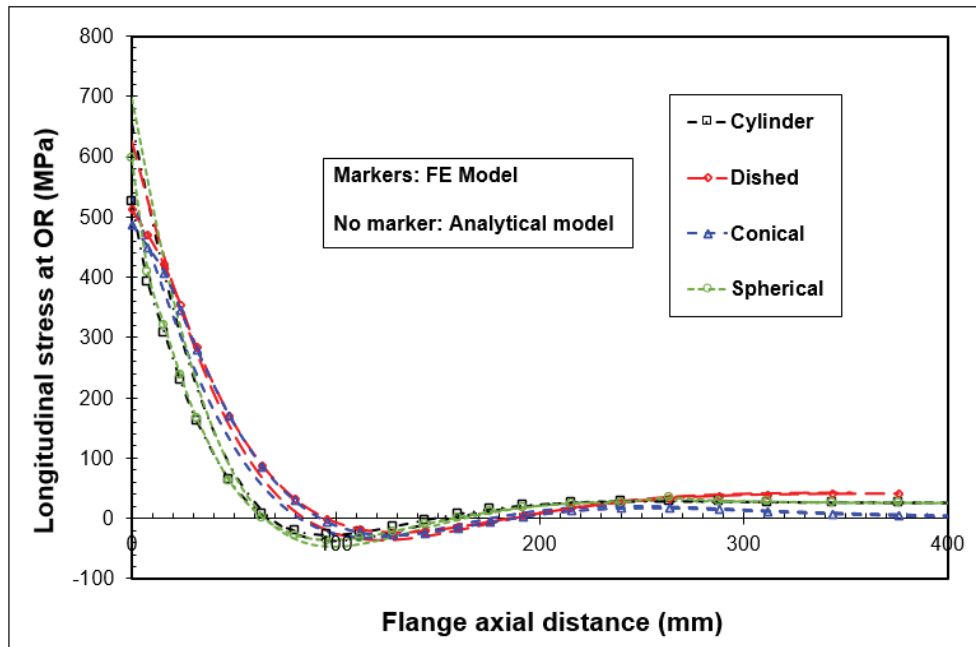


Figure 4.32 Longitudinal stress at OR of shell connections during pressurization (NPS 26 class 300)

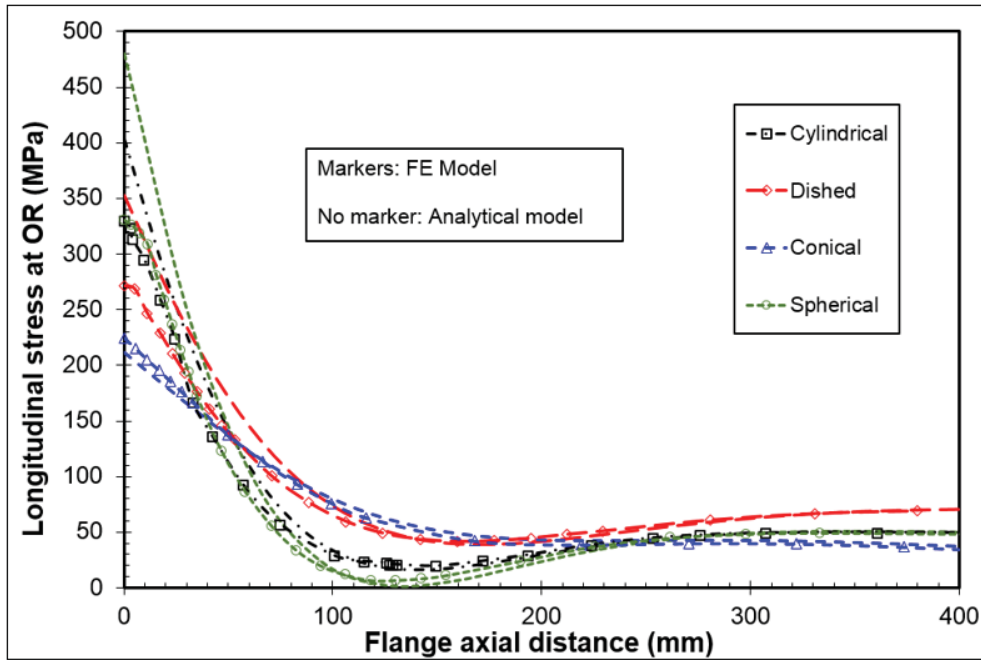


Figure 4.33 Longitudinal stress at OR of shell connections during pressurization (NPS 48 class 300)

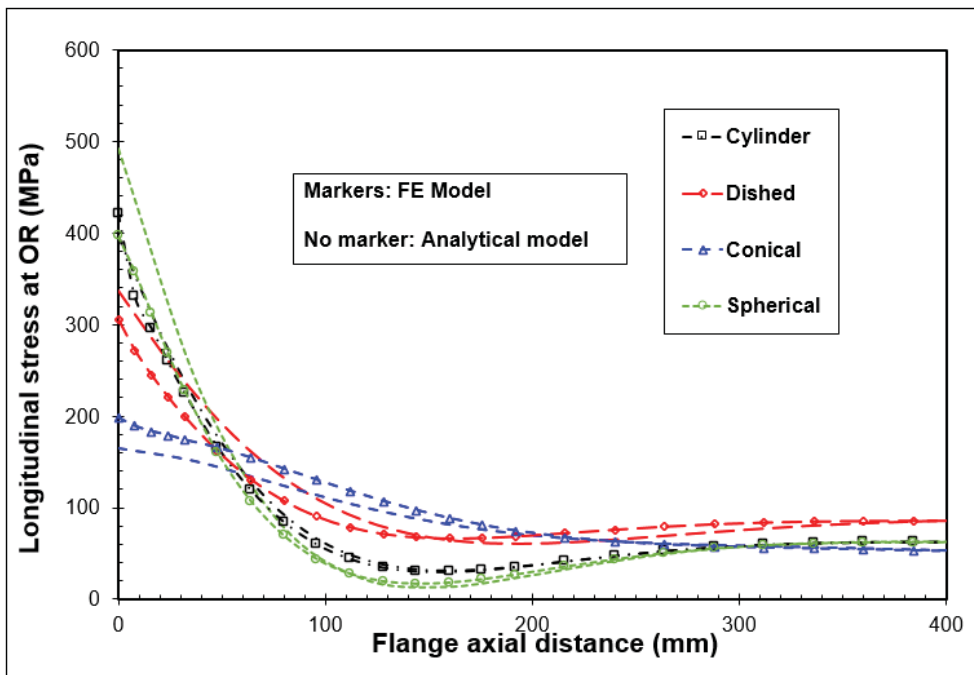


Figure 4.34 Longitudinal stress at OR of shell connections during pressurization (NPS 60 class 300)

Figures 4.35 through 4.40 compare the absolute maximum stresses and the equivalent von Mises stresses of the different shell types during bolt-up and pressurization. The graphs show the maximum longitudinal and tangential stresses at the inner and outer surfaces. Longitudinal stress is found to be larger than tangential stress in most cases, with the cylindrical and spherical shells showing the highest values. Furthermore, compared to the inner surface, the outer surface showed higher stresses.

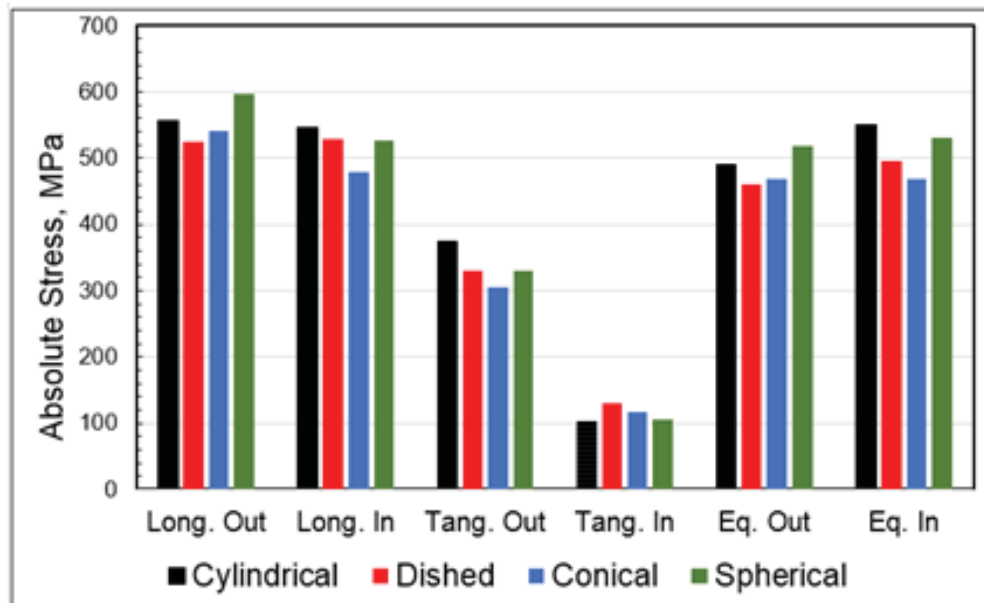


Figure 4.35 Comparison of maximum stresses of shells during bolt-up (NPS 26 class 300)

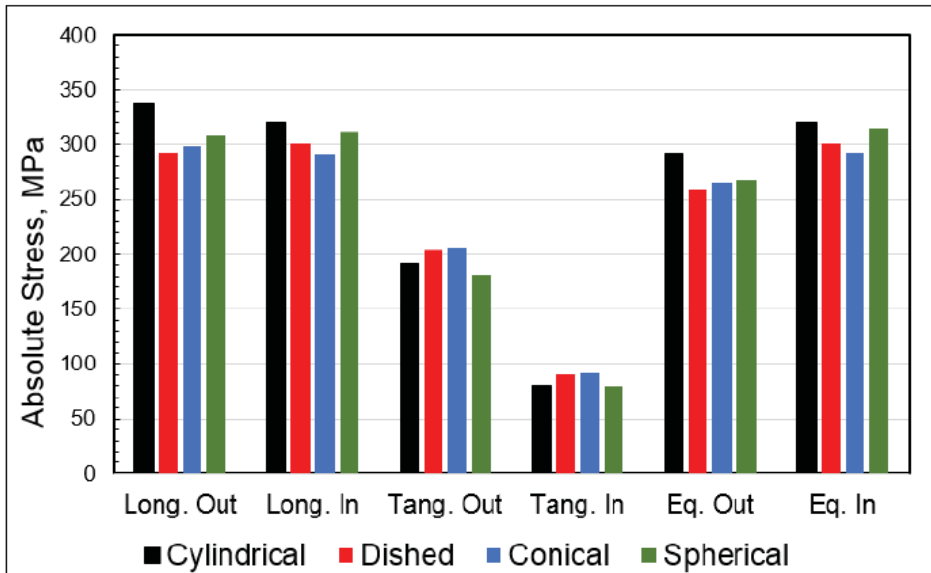


Figure 4.36 Comparison of maximum stresses of shells during bolt-up (NPS 48 class 300)

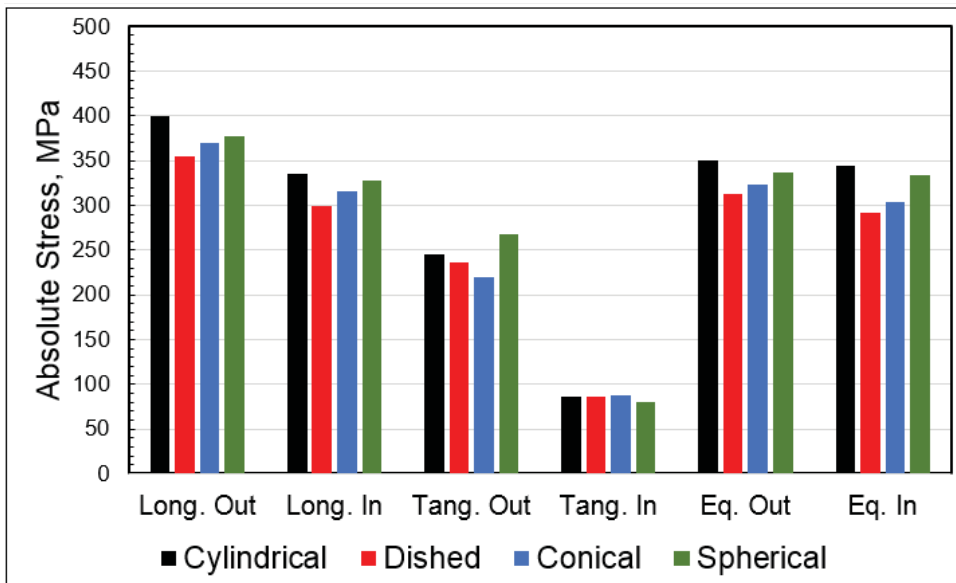


Figure 4.37 Comparison of maximum stresses of shells during bolt-up (NPS 60 class 300)

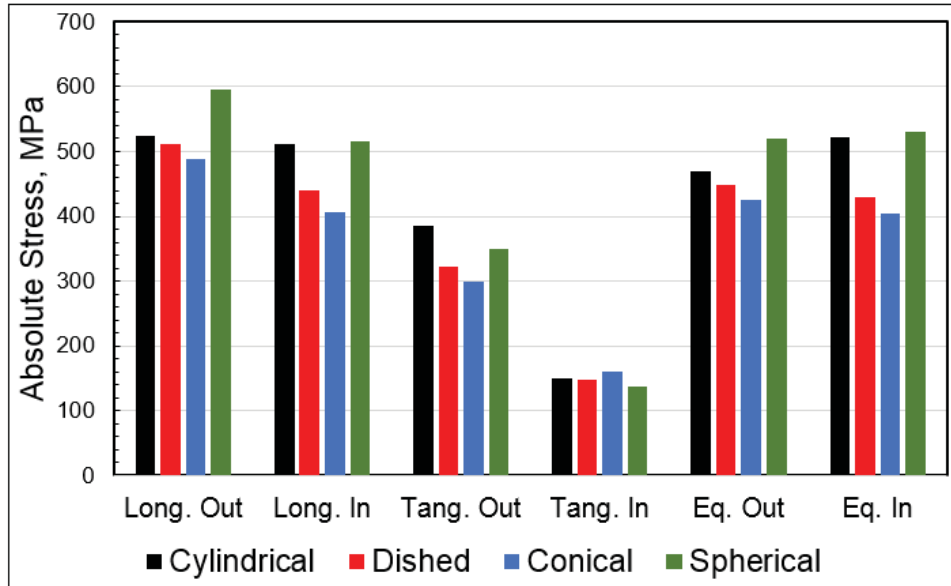


Figure 4.38 Comparison of maximum stresses of shells during pressurization (NPS 26 class 300)

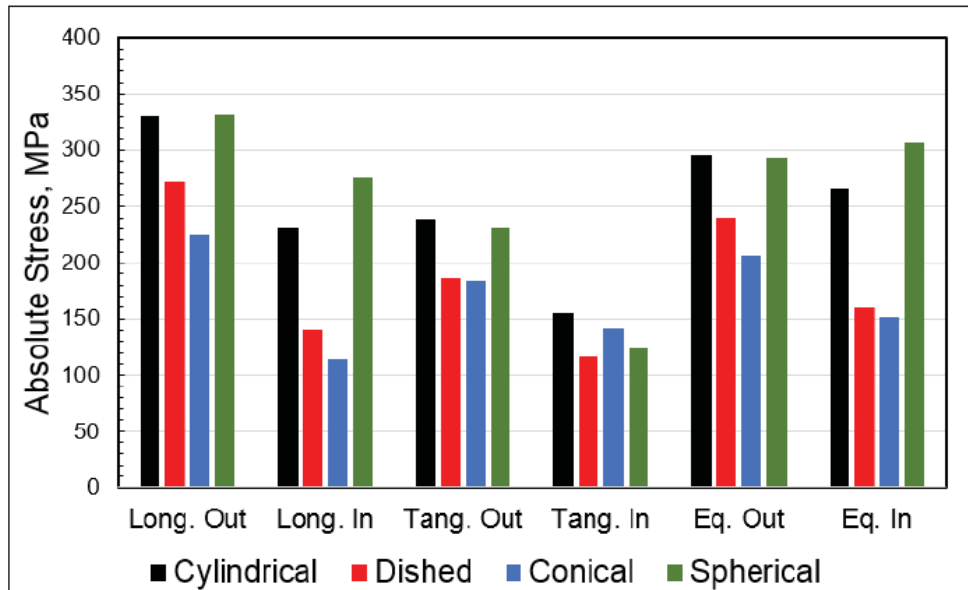


Figure 4.39 Comparison of maximum stresses of shells during pressurization (NPS 48 class 300)

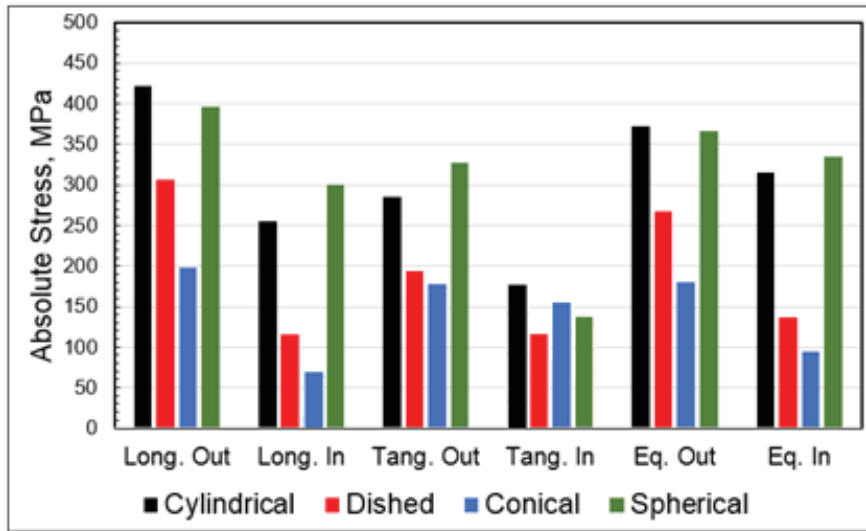


Figure 4.40 Comparison of maximum stresses of shells during pressurization (NPS 60 class 300)

## 4.6 Conclusion

Discontinuity stresses can play an important role in selecting which shell type to use to connect a flange ring. An investigation of the effect of different shell configurations on the flange rotation, loads and stresses was carried out both analytically and numerically, using the finite element method. Four shell connection types (cylindrical, conical, dished, and spherical) were used with three different flange sizes (NPS 26, 48, and 60) for this investigation. The results demonstrated that due to the pressure barreling effect, the cylindrical shell has a greater flange ring rotation than the other three shell attachments. The results also showed that the cylindrical and spherical shells produce larger stresses, whereas the dished and conical shells generate lower stresses, particularly during pressurization.

Additionally, comparing different shell connections showed that the dished and conical shells are less affected by the barreling effect. Furthermore, the results revealed that omitting the hub and the fillet radius produced higher stress values at the junction with the flange ring. While the hub can relieve stresses for cylindrical and spherical connections, other configurations should be investigated. Finally, the results of the analytical models were in agreement with those of the numerical finite element simulations.

## CONCLUSION

The main goal of this research was to determine the integrity of a bolted flange joint under realistic operating conditions by considering various geometries of the shell connection during the bolt-up and pressurization phases. At the beginning of the study, the essential parameters of the bolted flange joint, including flange rotation, longitudinal and tangential stresses at the junction and across the shell, and gasket contact stress, were evaluated using four different shell connections (cylindrical, spherical, conical, and dished) with the same flange sizes NPS 48, class 300). During both bolt-up and pressurization, the stresses at the junction for the cylindrical and spherical shells were much higher than in the dished and conical shells, as described in Chapter 3. In addition, the flange rotation was significantly greater in the cylindrical and spherical shells compared to the conical and dished shells. This was attributed to the barreling effect, which occurred when pressure was applied to a larger area in the case of cylindrical and spherical shells. Moreover, gasket contact stress was not uniform over the width of the gasket and gradually increased from the inner to the outer radius. Furthermore, the contact stress was always lower during pressurization than during bolt-up due to hydrostatic end thrust, which can cause the gasket to unload.

Another goal of this study was to investigate the influence of flange size on the behavior of the bolted flange joint. To that end, the same analysis was carried out comparing three flange sizes (NPS 26, 48, and 60 class 300), as described in Chapter 4. Due to the barreling effect, the flange rotation for the cylindrical and spherical shells was larger than for the dished and conical shells for all flange sizes, as predicted. In terms of stresses, the longitudinal stress was greater than the tangential stress in most circumstances, with cylindrical and spherical shells having the greatest amounts. The outer surface was also more stressed than the inner surface. Furthermore, the results showed that omitting the hub and fillet radius resulted in greater stress values at the flange ring junction. While the hub can significantly reduce stress in cylindrical and spherical connections, other configurations should also be investigated.

All in all, the investigation shows that the cylindrical configuration is more critical to use without hub while the dished configuration is more appropriate to consider in the non-hubbed applications. Finally, the study found agreement between the analytical results and the results from the numerical finite element analysis.

## RECOMMENDATIONS

To further support and confirm the reliability and robustness of the proposed analytical and numerical models of the bolted flange joints, future experimental testing on at least one size and type of shell connection could be undertaken.

The same study could be performed to determine the influence and benefit of the hub to reduce the stresses and rotational characteristics of the bolted flange joint by comparing the new results with the non-hubbed flange results presented in this study.

Long-term creep-relaxation behavior of bolted flange joints is another key problem that requires further research. The load relaxation produced by flange creep could be incorporated into the analytical model proposed in this thesis. The presence of the hub has an important effect on the creep behavior of the flange because it makes the flange more rigid. The effects of ratcheting and thermal ratcheting, produced by bolt load change and thermal cycling could also be investigated.

Finally, certain operational parameters, such as harsh environment, temperature, humidity, corrosion, and fluid characteristics, may affect the behavior of materials. Future research could investigate bolted flange joints subjected to one or more of these parameters. The current study examined the integrity and leak tightness of bolted flange joints using a combination of analytical and computational methodologies. Future research could be carried out using the Fitness-for-Service approach based on the ASME FFS-1/API 579 standards.



## BIBLIOGRAPHY

- Abid, M. (2006). Determination of safe operating conditions for gasketed flange joint under combined internal pressure and temperature: A finite element approach. *International Journal of Pressure Vessels and Piping*, V83, pp.433-441. <https://doi.org/10.1016/j.ijpvp.2006.02.029>
- Abid, M., & Nash, D. H. (2006). Structural strength: Gasketed vs non-gasketed flange joint under bolt up and operating condition. *International Journal of Solids and Structures*, Vol. 43, issues 14-15, pp. 4616-4629. <https://doi.org/10.1016/j.ijsolstr.2005.06.078>
- ASME B16.5. (2017). Pipe flanges and flanged fittings. Revision of ASME B16.5-2013.
- ASME B16.21. (2016). Nonmetallic flat gaskets for pipe flanges. Revision of ASME B16.21-2011.
- ASME B16.47. (2017). Large diameter steel flanges. Revision of ASME B16.47-2011.
- ASME, Boiler and Pressure Vessel Code, Section VIII (2017). Div. 1, Appendix 4, ASME, NY, USA.
- ASTM F2836. (2018). Standard practice for gasket constants for bolted joint design. ASTM International, West Conshohocken, PA, USA.
- Beghoul, H. (2003). Development of a method for the design of bolted flange joints based on flexibility and tightness. Master Thesis, ETS university.
- Bickford, J. H. (2008). Introduction to the design and behavior of bolted joints. CRC press, Taylor & Francis Group, Fourth edition
- Borák, L., & Marcián, P. (2014). Beams on elastic foundation using modified Betti's theorem. *International Journal of Mechanical Sciences* 88, pp. 17-24. <https://doi.org/10.1016/j.ijmecsci.2014.06.014>
- Bouزيد, A., & Beghoul, H. (2003). The design of the flanges based on flexibility and tightness. *Journal of Pressure Vessel Technology*, PVP2003-1870, pp. 31-38. <https://doi.org/10.1115/PVP2003-1870>
- Bouزيد, A., & Chaaban, A. (1993). Flanged joints analysis: A simplified method based on elastic interaction. *CSME Transactions*, 17 (2), pp. 181-196. <https://doi.org/10.1139/tcsme-1993-0011>

- Bouزيد, A., & Derenne, A. (2001). Analytical modeling of the contact stress with nonlinear gaskets. *Journal of Pressure Vessel Technology*, 124(1), pp. 47-53. <https://doi.org/10.1115/1.1426084>
- Bouزيد, A., & Nechache, A. (2005). An analytical solution for evaluating gasket stress change in bolted flange connections subjected to high temperature loading. *ASME Journal of Pressure Vessel Technology*, 127 (4), pp. 414-427. <https://doi.org/10.1115/1.2042480>
- Budynas, R.G. & Nisbett, J.K. (2011). Shigley's mechanical engineering design. Ninth edition, Published by McGraw-Hill Inc.
- Cao, J.J & Bell, A.J. (1992). General solutions for a circular flat plate with a central hole loaded by transverse force or bending moment uniformly distributed along a circumference. *V51, Issue 2*, pp.155-173. [https://doi.org/10.1016/0308-0161\(92\)90078-T](https://doi.org/10.1016/0308-0161(92)90078-T)
- Choulaei, M., Bagheri, A., & Khademifar, A. (2017). Nonlinear vibration and stability analysis of beam on the variable viscoelastic foundation. *Journal of computational applied mechanics* 48(1) pp. 99-110. <https://doi.org/10.22059/JCAMECH.2017.233687.145>
- Choulaei, M., & Bouزيد, A. (2021). Stress analysis of bolted flange joints with different shell connections. *ASME International Mechanical Engineering Congress and Exposition, Proceedings (IMECE), V.12*, <https://doi.org/10.1115/IMECE2021-72063>
- Diany, M., Bouزيد, A., & Derenne, A. (2005). On the validity and limits of the gasket effective width concept. *Pressure vessel and piping conference, PVP 2005-71082*, pp. 15-20. <https://doi.org/10.1115/PVP2005-71082>
- Do, T.D. (2012). The effect of bolt spacing on the tightness behaviour of bolted flange joints. Master Thesis, École de technologie supérieure, Montreal, Quebec, Canada.
- Dudley, W. M. (1961). Deflection of heat exchanger flanged joints as affected by barreling and warping. *Trans. ASME, Ser. B*, 83(4), pp. 460–466.
- Flugge, W. (1973). *Stresses in shells*. Springer-Verlag Berlin Heidelberg, Second edition.
- Froio, D., & Rizzi, E. (2016). Analytical solution for the elastic bending of beams lying on a variable winkler support. *Acta Mechanica*, 227 pp.1157-1179. <https://doi.org/10.1007/s00707-015-1508-y>
- Froio, D., & Rizzi E. (2017). Analytical solution for the elastic bending of beams lying on a linearly variable winkler support. *International Journal of Mechanical Sciences*, 128 pp.680-694. <https://doi.org/10.1016/j.ijmecsci.2017.04.021>
- Gibson, J.E. (1965). *Linear elastic theory of thin shells*. New York, NY: Pergamon Press.

- Harvey, J.F. (1980). Pressure component construction. Reinhold Company, Van Nostmnd.
- Hetenyi, M. (1979). Beams on elastic foundation. The University of Michigan Press, Ann Arbor, USA.
- Huang, F.Y, & Shi, G.L. (1998). Finite element analysis of pressure vessel using beam on elastic foundation analysis. Finite Element in Analysis and Design journal, V. 28, pp.293-302. [https://doi.org/10.1016/S0168-874X\(97\)00041-3](https://doi.org/10.1016/S0168-874X(97)00041-3)
- Jawad, M. H. (2017). Stress in ASME Pressure Vessels, Boilers, and Nuclear Components. John Wiley & Sons.
- Jawad, M. H., & Farr, J. R. (2019). Structural analysis and design of process equipment. Wiley Press, Third edition.
- Kobayashi, T. (2014). Study on the deflection of gaskets and its effects on residual bolt forces and tightness of bolted flanged connections. Pressure Vessels and Piping Conference, American Society of Mechanical Engineers. <https://doi.org/10.1115/PVP2014-28514>
- Kobayashi, T. (2008). Characterization of sealing behaviors of gaskets for the leak rate based design of gasketed bolted flanged connections. ASME PVP200861465, CD-ROM. <https://doi.org/10.1115/PVP2008-61465>
- Kobayashi, T., Hagiri, T., Nishiura, K., Hiratshuka, M., & Itoi, K. (2012). The residual bolt force and the sealing performance of flanged connections with expanded PTFE gaskets (Based on test results for one year). ASME PVP201278694, CD-ROM. <https://doi.org/10.1115/PVP2012-78694>
- Kobayashi, T., & Hamano, K. (2004). The reduction of bolt load in bolted flange joints due to gasket creep-relaxation characteristics. ASME PVP-Vol. 478, pp.97-104. <https://doi.org/10.1115/PVP2004-2627>
- Koves, W.J. (1996). Analysis of flange joints under external loads. ASME Journal of Pressure Vessel Technology, 118, pp. 59-63. <https://citeseerx.ist.psu.edu/viewdoc/download?doi=10.1.1.1083.5891&rep=rep1&type=pdf>
- Krishna, M.M., Shunmugam, M., & Prasad, N.S. (2007). A study on the sealing performance of bolted flange joints with gaskets using finite element analysis. International Journal of Pressure Vessels and Piping 84, pp. 349–357. <https://doi.org/10.1016/j.ijpvp.2007.02.001>
- Luyt, P., Theron, N., & Pietra, F. (2017). Nonlinear finite element modelling and analysis of the effect of gasket creep-relaxation on circular bolted flange connections. International Journal of Pressure Vessels and Piping 150, pp.52-61.

<https://doi.org/10.1016/j.ijpvp.2016.12.001>

Madsen, C.A., Kragh-Poulsen, J-C., Thage, K.J., & Andreassen, M.J. (2017). Analytical and numerical investigation of bolted steel ring flange connection for offshore wind monopile foundations. IOP Conf. Series: Materials Science and Engineering 276 012034. <https://doi.org/10.1088/1757-899X/276/1/012034>

Murray, N. W., & Stuart, D. G., (1961). Behaviour of large taper hub flanges. Proceedings, Symposium on Pressure Vessel Research Towards Better Design, Institution of Mechanical Engineers, pp.133-147.

Naser, K. (1995). Bolted flanged connections with full face gaskets. Master thesis, Concordia University, Quebec, Canada.

Nechache, A., & Bouzid, A. (2007). Creep analysis of bolted flange joints. International Journal of Pressure Vessels and Piping, 84(3), pp. 185-194. <https://doi.org/10.1016/j.ijpvp.2006.06.004>

Nechache, A., & Bouzid A. (2008). On the use of plate theory to evaluate the load relaxation in bolted flanged joints subjected to creep. International Journal of Pressure Vessels and Piping, 85(7), pp. 486-497. <https://doi.org/10.1016/j.ijpvp.2008.01.005>

Mallard, H., Landry, C., Birembaut, Y. (2002). Mechanical analysis of glass reinforced plastics bolt flanged connection with elastomeric seals. Pressure Vessel and Piping Conference, pp. 129-138, PVP 2002-1090, <https://doi.org/10.1115/PVP2002-1090>

Megyesy, E.F. (1972). Pressure vessel handbook. Fourteenth edition, PV Publishing Inc.

Moss, D. (2004). Pressure vessel design manual. Elsevier, Gulf Professional Publishing, Third Edition.

NASA SP-8083. (1971). Discontinuity stresses in metallic pressure vessels. NASA Space Vehicle Design Criteria (Structures), National Aeronautics and Space Administration, USA.

Szilard, R. (1974). Theory and analysis of plates, classical and numerical methods. Prentice-Hall.

Szilard, R. (2004). Theories and applications of plate analysis: Classical, numerical and engineering methods. John Wiley and Sons, Inc, New York. 2004. 1056 pp. ISBN 0-471-42989-9.

Timoshenko, S. (1927). Flat ring and hubbed flanges. Mech. Eng. V49, n12, pp. 1343-1345.

- Timoshenko, S., & Woinowsky-Krieger, S. (1989). *Theory of plates and shells*. McGraw-Hill Book Company, Second edition
- Uddin, M. W. (1986). Large deflection analysis of spherical head pressure vessels. *Nuclear Engineering and Design* 96(1), pp.47-61.
- Uddin, M. W. (1986). Large deformation analysis of ellipsoidal head pressure vessels. *Computers & structures* 23(4), pp. 487-495.
- Uddin, M. W. (1986). Large deflection analysis of conical head pressure vessels. *Forschung im Ingenieurwesen A* 52(5), pp.146-152.
- Wagner, H.N.R., Huehne, C., & Niemann S. (2018). Robust knockdown factors for the design of spherical shells under external pressure: Development and validation. *International Journal of Mechanical Sciences*, 141, pp.58–77. <https://doi.org/10.1016/j.ijmecsci.2018.03.029>
- Waters, E.O., & Taylor, J.H. (1927). The strength of pipe flanges. *Mech. Eng.* V 49, n 5a, pp 531-542.
- Waters, E. B., Rossheim, D. B., Westrom, D. B., & Williams, F. S. G. (1951). *Development of general formulas for bolted flanges*. Taylor Forge and Pipe Works Publication.
- Watts, G.W., & Burrows, W.R. (1949). The basic elastic theory of vessel heads under internal pressure. *Trans. ASME* 71, pp. 55-73.
- Watts, G.W., & Lange, H.A. (1952). The stresses in a pressure vessel with a conical head. *Trans. ASME* 74, pp. 315-326.
- Watts, G.W., & Lange H.A. (1952). The stress in a pressure vessel with a flat head closure. *Trans. ASME* 74, pp. 1083-1091.
- Watts, G.W., & Lange, H.A. (1953). The stresses in a pressure vessel with a hemispherical head. *Trans. ASME* 75, pp. 83-89.
- Zhu, L., Bouzid, A.H., Hong, J. & Zhang, Z. (2018). Elastic interaction in bolted flange joints: An analytical model to predict and optimize bolt load. *Journal of Pressure Vessel Technology*. V140 (4). <https://doi.org/10.1115/1.4040421>
- Zingoni, A. (2001). Stresses and deformations in egg-shaped sludge digestors: Membrane effects. *Journal of Engineering Structures*, 23(11), pp.1365–72. [https://doi.org/10.1016/S0141-0296\(01\)00055-4](https://doi.org/10.1016/S0141-0296(01)00055-4)
- Zingoni, A. (2001). Stresses and deformations in egg-shaped sludge digestors: Discontinuity effects. *Journal of Engineering Structures*, 23(11), pp.1373–82.

[https://doi.org/10.1016/S0141-0296\(01\)00056-6](https://doi.org/10.1016/S0141-0296(01)00056-6)

Zingoni, A. (2015). A theoretical formulation for the stress analysis of multi-segmented spherical shells for high-volume liquid containment. *Journal of Engineering Structures*, 87(11), pp.21–31. <http://dx.doi.org/10.1016/j.engstruct.2015.01.002>